University of São Paulo
Institute of Geosciences

Fossilized melanosomes in the Crato Formation (Araripe Basin, Cretaceous), Brazil: Taphonomy and palaeobiological implications

Melanossomos fossilizados na Formação Crato (Bacia do Araripe, Cretáceo), Brasil: Tafonomia e implicações paleobiológicas

Gustavo Marcondes Evangelista Martins Prado

Supervisor: Prof. Dr. Luiz Eduardo Anelli (University of São Paulo)

VERSÃO CORRIGIDA

São Paulo
2023

University of São Paulo
Institute of Geosciences

Fossilized melanosomes in the Crato Formation (Araripe Basin, Cretaceous), Brazil: Taphonomy and palaeobiological implications

Melanossomos fossilizados na Formação Crato (Bacia do Araripe, Cretáceo), Brasil: Tafonomia e implicações paleobiológicas

Gustavo Marcondes Evangelista Martins Prado

Thesis submitted in partial fulfilment of the requirements for the degree of Doctor in Sciences in the Graduate Program of Geochemistry and Geotectonics in the Institute of Geosciences in the University of São Paulo.

Supervisor: Prof. Dr. Luiz Eduardo Anelli

São Paulo
2023

Serviço de Biblioteca e Documentação do IGc/USP
Ficha catalográfica gerada automaticamente com dados fornecidos pelo(a) autor(a)
via programa desenvolvido pela Seção Técnica de Informática do ICMC/USP

Bibliotecários responsáveis pela estrutura de catalogação da publicação:
Sonia Regina Yole Guerra - CRB-8/4208 | Anderson de Santana - CRB-8/6658

Prado, Gustavo M. E. M.
Fossilized melanosomes in the Crato Formation (Araripe Basin, Cretaceous), Brazil: Taphonomy and palaeobiological implications / Gustavo M. E. M. Prado; orientador Luiz Eduardo Anelli. -- São Paulo, 2023.
284 p.

Tese (Doutorado - Programa de Pós-Graduação em Geoquímica e Geotectônica) -- Instituto de Geociências, Universidade de São Paulo, 2023.

1. Melanin. 2. Melanosomes. 3. Palaeocolour. 4. Taphonomy. 5. Crato Formation. I. Anelli, Luiz Eduardo, orient. II. Título.

University of São Paulo
Institute of Geosciences

Fossilized melanosomes in the Crato Formation (Araripe Basin, Cretaceous), Brazil: Taphonomy and palaeobiological implications

"Melanossomos fossilizados na Formação Crato (Bacia do Araripe, Cretáceo), Brasil: Tafonomia e implicações paleobiológicas"

Gustavo Marcondes Evangelista Martins Prado

Supervisor: Prof. Dr. Luiz Eduardo Anelli

DOCTORATE THESIS

N° 659

EXAMINATION COMMITTEE MEMBERS

Dr. Luiz Eduardo Anelli

Dr. Lorian Cobra Straker

Dr. Ismar de Souza Carvalho

Dra. Evelyn Aparecida Mecenero Sanchez Bizan

Dr. Fábio Rodrigues

São Paulo
2023

DEDICATION

I would like to dedicate this thesis to my father and mother, Alcindo M. P. Filho and Maria Auxiliadora M. E. M. Prado, for all the support and strength given throughout the development of this doctorate. I thank you for their patience and ears for listening to me explain recently read papers, getting insights, mumbling when trying to sort something out, or simply by thinking out loud. I owe a lot to you both and I deeply love you.

ACKNOWLEDGEMENTS

Foremost of all, I thank my supervisor Prof. Dr. Luis Eduardo Anelli (IGc/USP) who taught me so much in addition to everything that he had done to support me, giving me the opportunity to develop this doctorate (as well as other projects), and for being a real source of inspiration and professionalism. I am also immensely grateful to my supervisor Prof. Dr. Felipe L. Pinheiro (UNIPAMPA) for all the discussions and teachings, apart from being a great friend, who without his support, it wouldn't be possible to develop this project. Finally, I thank my abroad supervisor, Dr. Jakob Vinther (University of Bristol) for all the teachings and discussions, and for being my mentor during my welcoming stay in Bristol.

For all the discussions and sheer company, I deeply thank my "brothers" from the 'Mocó Research Group' (Room 103, Ground Floor, IGc/USP): Dr. Bruno Becker-Kerber (IGc/USP, LNLS/CNPEM), Dr. Lucas Martins Lino (IGc/USP), MSc. Francy R. Quiroz-Valle (IGc/USP), and Dr. Rafael Casati (IGc/USP). I also thank my esteemed friends Dr. Gabriel L. Osés (IF-USP), Dr. Guilherme R. Romero (IGc/USP), Dr. Luana P. C. Morais (IAG/USP), Dr. Rudney A. Santos (UFC), Dr. Mírian L.A.F. Pacheco (UFSCar), Dr. Paula A. Sucerquia Rendón (UFPE), Dr. Silvio Y. Onary (FFLCRP/USP), Dr. Cibele P. Voltani (IGc/USP), MSc. Victor B. D. Campo (BSCPG, Germany), MSc. Fellipe P. Muniz (FFLCRP/USP), MSc. Julian (FFLCRP/USP), MSc. Jorge C. L. Arthuzzi (KIT, Germany), MSc. Jaime J. Dias (IGc/UFRJ), Biol. Raphaella Paula D. Silva (IGc/USP), Dr. Yumi Asakura (UFPE), and my oldest friend of all, who finally became my collaborator, MSc. Rafael C. J. P. S. Salvato (School of Engineering of Lorena/USP). I would like to thank Alcindo M. Prado Filho for all the help provided by organizing and reviewing the references the present document.

I am greatly indebted to the people from the Chemosphere Laboratory of the Institute of Chemistry of the University of São Paulo (LC-IQ/USP), especially MSc. Evandro P. Silva, Dr. Ana Carolina Carvalho, Prof. Dr. Fábio Rodrigues (IQ-USP), and Dr. Douglas Galante (LNLS/CNPEM), due to their invaluable support, without it this work would not be possible.

I thank all my University of Bristol schoolmates/flatmates/friends that taught me the British ways and gave me company during the COVID-19 lockdown while in my sojourn in Bristol: Katy Hancox, Amber Rothera, Tochi Ejimofo, Rebecca Pugh, Annabelle Eccleshall, Megan Hopkins, Larica Tsang, Emily Goddard, Molly Fulford-Knibbs, Barney Williams, Ciarán Dawson, and Jacob Virchis. I also thank my dear friend Hortência Meechan and her husband

Prof. Dave Meechan for the hospitality during my stay in Solihull (Birmingham). I miss them all and hope to meet again, somewhere, someday. I thank Dr. Yang Zhang (Yunnan University, China) for the everyday company and discussions on taphonomy while in the Building of Life Sciences. I also thank Dr. Evan T. Saitta (Field Museum of Natural History) for the invaluable discussions on many many papers, and on taphonomy of vertebrate soft tissues.

I would like to thank Dr. Carlos Pérez (LNLS/CNPEM) and Mr. Jackson L. Silva (LNLS/CNPEM) for supporting the experiments at the D09BXRF-XRF beamline of the UVX-LNLS; I thank Dr. Raul O. Freitas and Dr. Lucyano J. A. Macedo for the support in FTIR experiments performed in the IMBUIA Beamline of LNLS. I also thank Fabiano Montoro, João Marcos da Silva, and Dr. Élcio L. Pires (LNNano-CNPEM) for their invaluable support on the SEM-EDS analysis at the LNNano.

I am deeply thankful to the IGc/USP staff for their support in this project, especially Henrique Martins, Ivone C. Gonzales, Ubiratan C. S. Lima, Katherine K. Hummel, Alexandre B. Bezerra, Luciana N. P. Souza, and Tadeu Caggiano. Finally, I also thank the IGc/USP professors, mainly Prof. Dr. Thomas R. Fairchild, Prof. Dr. Juliana de Moraes L. Basso (IGc-USP), Prof. Dr. Paulo Eduardo de Oliveira (IGc-USP), Prof. Dr. Paulo César Boggiani (IGc-USP), and Prof. Dr. Paulo César F. Giannini, for all the teachings, support, and discussions during the development of this work. Is also thanked my aunt and uncle, Maria Celia M. E. Picazzio and Prof. Dr. Enos Picazzio (IAG-USP) for heartening me to pursuing this academic dream of mine.

I would like to thank the bands Buzzcocks, Plebe Rude, Bad Religion, NOFX, Lagwagon, Propagandhi, and Dead Fish for giving me all inspiration and strength. Without their music and words, it would not be possible to achieve any goal in life, especially this thesis. As Bad Religion says in ‘There Will Be a Way’ tune, “*[…] March ahead/more enlightened than before/And there's sure to be bump and distractions/But I know we'll get through […] And now it's time to set the agenda/Learn the past, make it last/Share the wealth, hold your fire/Conserve life, make it right/Kill the hate, negotiate/There will be a way!*”.

Finally, I thank the Coordination for the Improvement of Higher Education - Personnel Institutional Internationalization Program of CAPES (CAPES-PrInt), and National Council for Scientific and Technological Development (CNPq) for the scholarships granted both in Brazil as well as in Bristol (Grants: CAPES-PrInt, 88887.466483/2019-00; CNPq, 142246/2019-0).

EPIGRAPH

"Eu nasci tal qual a flor em um jardim,
Foi assim que cresci,
Depois veio a idade e envelheci,
E, quando tive que morrer, feneci,
E morri"

O grande Pachakuti Inca Yupanqui (1346 - 1471)
Governante do império Inca.

ABSTRACT

The preservation of organic compounds is noteworthy in the geologic record as these components usually are lost soon after decay is established. Among these, melanin is a delicate and highly heterogeneous natural pigment, which can be found in virtually all organisms. This pigment, or biochrome, is generally found inside the organelles called melanosomes, which size ranges from 0.1 to 2.0 µm, and whose shape varies in accordance with the melanin produced. Overall, these subcellular particles can be divided into two forms: the spherical phaeomelanosomes that produce the red-yellowish-coloured phaeomelanin; and the rod-shaped eumelanosomes that produce the black-brownish eumelanin. Despite its delicate nature, melanosomes were found in fossils of animals from many deposits around the world, and these organelles allowed inferences about the taphonomy of these (and others) organic molecules, as well as the biological role of colour patterns in addition to their relationship with the palaeoenvironment. In Brazil, the Cretaceous Crato Formation (Araripe Basin, NE) is accounted for most cases of these organelles. However, only a few taxa have been examined, and in a few studies, whilst important palaeobiological, palaeoecological, and taphonomic aspects still remain obscure. In response to this issue, in this thesis, a comprehensive number of fossils (a total of 87 specimens consisting of two fish, one frog, two pterosaurs, and 82 isolated feathers) were analysed focusing on the identification of melanosomes and melanin using multiple analytical and statistical approaches. Overall, it was revealed that most soft tissues exhibited the presence of fossilized oblate to elongated microbodies. These occur as solid or external moulds and are preserved as kerogen/eumelanin, calcium phosphate, and iron oxyhydroxide, (i.e., limonite). Eumelanin was only detected in carbonized and phosphatized specimens, whereas the limonite-rich fossils only showed their mineral signature with no signal of melanin or other pigments (e.g., carotenoids). Therefore, due to dimensions and chemistry, in addition to the remarkable similarities with melanosomes from tissues of modern animals, the microbodies observed in these fossils were then identified as the fossilized analogues of these organelles. Chemical analysis indicated that the microbody's physical integrity and eumelanin retention inside varied according to its composition/mineralogy. While the kerogeneous and phosphatized microbodies remained physically pristine, those limonite-rich ones exhibited signatures of mineralization, which its extent could lead to their disintegration into scattered single acicular crystals. In kerogenized and phosphatized granules, it was recognized that diagenetic processes (e.g., increase in temperature) were responsible for the degradation of eumelanin into a larger and disordered polymer; whereas, in limonite-rich fossils, this biochrome was totally degraded. In sum, eumelanin and eumelanosomes in these fossils, possibly played a fundamental role in photoprotection, such as in the case of fish eyes and frog skin, and display or camouflage in feathers and pterosaurs. In conclusion, this investigation provided a holistic view of the taphonomy and the possible role of melanin and melanosomes in extinct taxa of the Crato Formation. This thesis also showed that the Palaeocolour studies have great potential to broaden and expand knowledge, which also suggests its applicability to other fields of science, such as astrobiology and geobiology.

Keywords: Melanin, Melanosomes, Palaeocolour, Taphonomy, Crato Formation.

RESUMO

A preservação de compostos orgânicos é notável no registro geológico, pois esses componentes geralmente são perdidos logo após o estabelecimento da decomposição. Dentre estes, a melanina é um pigmento natural delicado e altamente heterogêneo, que pode ser encontrado em praticamente todos os organismos. Esse pigmento, ou biocromo, geralmente se encontra no interior de organelas denominadas melanossomos, cujo tamanho varia de 0.1 a 2.0 µm, e cujo formato varia de acordo com a melanina produzida. Em geral, essas partículas subcelulares podem ser divididas em duas formas: os feomelanossomos esféricos que produzem a feomelanina de cor vermelho-amarelada; e os eumelanossomos em forma de bastonete que produzem a eumelanina preto-acastanhada. Apesar de sua natureza delicada, melanossomos foram encontrados em fósseis de animais de diversos depósitos ao redor do mundo, e essas organelas permitiram inferências sobre a tafonomia dessas (e outras) moléculas orgânicas, bem como o papel biológico dos padrões de cores, além de sua relação com o paleoambiente. No Brasil, o Cretáceo da Formação Crato (Bacia do Araripe, NE) é responsável pela maioria dos casos dessas organelas. No entanto, apenas alguns táxons foram examinados e em poucos estudos, enquanto importantes aspectos paleobiológicos, paleoecológicos e tafonômicos ainda permanecem obscuros. Em resposta a esta questão, nesta tese, um número abrangente de fósseis (um total de 87 espécimes consistindo em dois peixes, uma rã, dois pterossauros e 82 penas isoladas) foi analisado com foco na identificação de melanossomos e melanina usando múltiplos métodos analíticos e abordagens estatísticas. No geral, foi revelado que a maioria dos tecidos moles exibiu a presença de microcorpos oblatos a alongados fossilizados. Estes ocorrem como moldes sólidos ou externos e são preservados como querogênio/eumelanina, fosfato de cálcio e oxihidróxidos de ferro (i.e., limonita). A eumelanina foi detectada apenas em espécimes carbonizados e fosfatizados, enquanto os fósseis ricos em limonita mostraram apenas sua assinatura mineral sem sinal de melanina ou outros pigmentos (e.g., carotenoides). Portanto, devido às dimensões e química, além das notáveis semelhanças com melanossomos de tecidos de animais modernos, os microcorpos observados nesses fósseis puderam ser identificados como os análogos fósseis dessas organelas. A análise química indicou que a integridade física do microcorpo e a retenção de eumelanina em seu interior variaram de acordo com sua composição/mineralogia. Enquanto os microcorpos querogenizados e fosfatizados permaneceram fisicamente intactos, aqueles ricos em limonita exibiram assinaturas de mineralização, cuja extensão poderia levar à sua desintegração em cristais aciculares únicos dispersos. Em grânulos querogenizados e fosfatizados, foi reconhecido que processos diagenéticos (e.g., aumento de temperatura) foram responsáveis pela degradação da eumelanina em um polímero maior e desordenado; ao passo que, nos fósseis ricos em limonita, esse biocromo foi totalmente degradado. Em suma, a eumelanina e os eumelanossomos nestes fósseis, possivelmente, desempenharam um papel fundamental na fotoproteção, como no caso de olhos de peixe e pele de rã, e exibição ou camuflagem em penas e pterossauros. Em conclusão, esta investigação forneceu uma visão holística da tafonomia e o possível papel da melanina e dos melanossomos em táxons extintos da Formação Crato. Esta tese também mostrou que os estudos em Paleocoloração têm grande potencial para ampliar e expandir o conhecimento, o que também sugere sua aplicabilidade a outros campos da ciência, como astrobiologia e geobiologia.

Palavras-Chave: Melanina, Melanossomos, Paleocor, Tafonomia, Formação Crato.

SUMMARY

CHAPTER 1 - INTRODUCTION

1.1. PREAMBLE

The present document is the result of five years of research on the preservation of melanin and melanosomes in fossils from the Cretaceous Crato Formation of the Araripe Basin (SE Brazil). This also encompass the experience that I had during the abroad internship at the University of Bristol, where I was supervised by Dr. Jakob Vinther.

In Brazil, studies on melanosomes in fossils are very limited and, so far, confined to two isolated feathers and two specimens of pterosaur from the same species. As observed, the number of samples analysed remains low ($n<5$), and as a consequence, the presence of melanosomes in other vertebrate groups remains unknown, especially in exceptionally preserved fossils from the Crato Formation. Therefore, the aim of this project can be abridged into the following propositions: (a) the identification of melanosomes in tissues of different vertebrates from the Crato Formation; (b) identify the chemical signatures of these microbodies, and if possible, the molecular alterations that can occur during the diagenesis; (c) recognize the process of fossilization and the taphonomic pathways for the preservation of soft tissues, hence, the melanosomes; and (d) the putative palaeobiological role that melanin had in the Crato Formation animals.

Despite that not all vertebrate were examined as wished (it lacks the lizards, turtles, and crocodiles), experiments were carried out in two fish, one anuran, two Tapejarid pterosaurs, and 82 isolated feathers from Coelurosaur dinosaurs. Not all these investigations produced manuscripts, the exception is the anuran that was studied by an undergraduate student Raphaella Domingues, who was supervised by Prof. Dr. Luiz E. Anelli, and also by me. Additionally, two fish, whose the results of recent performed experiments still requires processing, and hence, they could not be included in the present document.

In Chapter 1, I present an holistic view of the object that are focus of this thesis, i.e., the introduction to main subject (i.e., fossil melanin and melanosomes), followed by the geologic context in which the fossils come from, and the aspect of the pigment of interest. In Chapter 2, I briefly illustrate the general information about the samples and the analytical techniques that all papers share in common. The Chapter 3 is the first paper produced,

where I present the results of the investigation performed on a fish eye. It is concluded that due to the lack of preserved photoreceptors, the capacity of this particular specimen to see colours still remains elusive. However, the presence of eumelanin and melanosomes in the eye, indicates that the animal could discern light to shade, suggesting an adaptation to live in low light conditions. In Chapter 4, I present the results of investigations on the preservation of isolated feathers from the Crato Formation. To this extent, this chapter is somewhat a review of my master's degree, which I was able to review it, re-run some analysis in addition to perform others. It is concluded that the preservation of Crato feathers occurred following the taphonomic model suggested in the literature, where fossils where pyritized and kerogenized. The identification of eumelanin and eumelanosomes allowed us to predict the possible colouration for these feathers, which suggests that colour patterns where similar to modern aquatic birds, where black and iridescent hues predominates. The Chapter 5 is the only published paper of this thesis. This is the results of the investigation of the presence of melanosomes in the headcrest of the Tapejaridae pterosaur *Tupandactylus imperator*. Previous interpretation suggested that the oblate microbodies most likely represented mineralized coccoid bacteria. However, results from chemical analysis indicated that microbodies are in fact, eumelanosomes, enriched with phosphorus and 'aged' eumelanin. This also suggests that the *T. imperator* headcrest had a black to brown colour pattern. Due to the contrasting subspherical morphology and eumelanic chemistry, we raised questions about the colour inferences based only on morphology. In the Chapter 6, I present the results of the preliminary investigation on another Tapejaridae pterosaur, the *Tupandactylus navigans*. In spite that most data remains to be processed (e.g., FTIR, SR-µXRF, ToF-SIMS), in addition to new experiments must be performed, some interpretations can already be drawn from the available evidence. Consequently, the results of microscopic and chemical analysis has revealed that this specimen is exceptionally preserved with presence of integumentary tissues from the headcrest, beak, and nasoantorbital regions. The presence of pyritized oblate melanosomes suggests possible brownish colouration, and hence, it is possible that the headcrest colour may had protective and display role. We also concluded that it is possible that the two *Tupandactylus* species may be synonyms, and the headcrests colour and animals' size may reflect a dimorphic trait. In Chapter 7, I questioned the reliability of the sole use of scanning electron microscopy and Raman spectroscopy on the identification

of melanosomes in kerogenized fossils with numerous pyrite framboids. In fact, this manuscript is a comment (written in 2018) to a paper published in the literature. In this paper, as both compounds (i.e., melanin and kerogen) have similar spectral bands, we discuss the difficulty in distinguishing them. Also, we highlight the remarkable similarity between the pyrite framboids with the melanin granule aggregates. Ergo we suggest that the identification of microbodies must be done together with multiple analytical techniques, such as Fourier-Transform InfraRed Spectroscopy (FTIR) or Mass Spectrometry (MS). Finally, in the Chapter 8, I provide the final considerations about the results obtained in this document, commenting the achievements and problems arisen from these studies.

It is important to note that the supplementary materials produced in each paper is contained in the appropriated chapter. However, I also included in the Annex A images of the fossils studied, in Annex B the abstracts that were produced in this thesis and presented in palaeontological events. Finally, in Annex C, I present a list of papers that I collaborated that were published, under review, or about to be submitted. Although these papers are not related to this project, they were all developed during the period of my doctorate, and each one gave me the opportunity to discuss interpretations, discover new things, and learn or improve the analytical approaches.

1.2. THE PALAEOCOLOUR

The preservation of organic molecules is a rare event in the fossil record compared to most mineralized tissues, and when present, they allow inferences about biochemistry, physiology and behaviour of extinct organisms (Briggs & Summons, 2014; Benton, 2017). Albeit also rare in most sedimentary deposits, the occurrence of vertebrate soft tissue is relatively common in Konservat-Lagerstätten (Allison & Briggs, 1993; Eliason et al., 2017). Nevertheless, both components (i.e. organics and soft tissues) can also give information about the sedimentary environment and diagenesis (Briggs & Mcmahon, 2016; Parry et al., 2018; Purnell et al., 2018). In other words, as soon as death occur and after the final burial, the organic matter generally endures a rapid structural changes by diagenetic processes (Briggs & Summons, 2014; Parry et al., 2018; Purnell et al., 2018). Notably the temperature, pressure and deep time are considered main factors that acts on this phenomenon (Muscente et al., 2018). With the right amount of conditions, the organic matter can become highly crosslinked, transformed into aromatized compounds, or long chains of aliphatic hydrocarbons with varying weight and elemental bonding (Briggs & Summons, 2014; Gupta, 2014; Muscente et al., 2018; Wiemann et al., 2018).

The discovery of fossilized melanin-bearing organelles called melanosomes in 2008 (Vinther et al., 2008) has brought a new area of study to palaeontology, which is now defined as ‘palaeocolour’ (Vinther, 2015). Until that year, the presence of spherical and elongated microbodies in the soft tissue of fossils was considered evidence of fossilized bacteria due to their overall dimension, shape, and occurrence in virtually all environments, including decaying carcasses (Wuttke, 1983; Liebig et al., 1996; Martill & Wilby, 1994). This interpretation was mainly supported by the fact that some microbial strains are able to precipitate minerals onto their cell membranes during their metabolic activity, leading to the formation of a 'sarcophagus-like' structure (Schultze-Lam et al., 1996). As a result, due to the fact that simple cells have been found preserved as minerals in rocks from Archean to the Present, these records led researchers to consider most fossil microbodies as being self-preserved bacteria, or, in other words, 'autolithified bacteria' (Wuttke, 1983; Briggs, 2003). Since then, this interpretation prevailed in all studies of the fossilization of non-recalcitrant

tissues, such as in metazoan embryos (e.g., Raff et al., 2008), plants (e.g., Iniesto et al., 2018), invertebrates (e.g., Briggs et al., 2005), and vertebrates (e.g., Martill, 1987).

Despite the microbial hypothesis was fully adopted by palaeontologists, a reinterpretation only occurred after Vinther et al. (2008) conducted a comparative study between fossil microbodies and extant melanosomes. Subsequent studies with ink sac of fossil cephalopods supported this reinterpretation by finding the presence of slightly altered eumelanin within these microbodies (Glass et al., 2012, 2013; Ito et al., 2013; Košťák et al., 2018; Košťák & Jagt, 2018), suggesting that this pigment is evolutionarily and geologically conservative (Colleary et al., 2015). Interestingly, melanosomes are also present in tissues of many extant and extinct organisms, such as skin and feathers (Fig. 1.1), which dwell in different parts of the globe, under varied climate conditions (d'Ischia et al., 2013). As a consequence, it has been questioned the probability of bacteria becoming fossils under normal conditions, as opposed to melanosomes (Vinther, 2015).

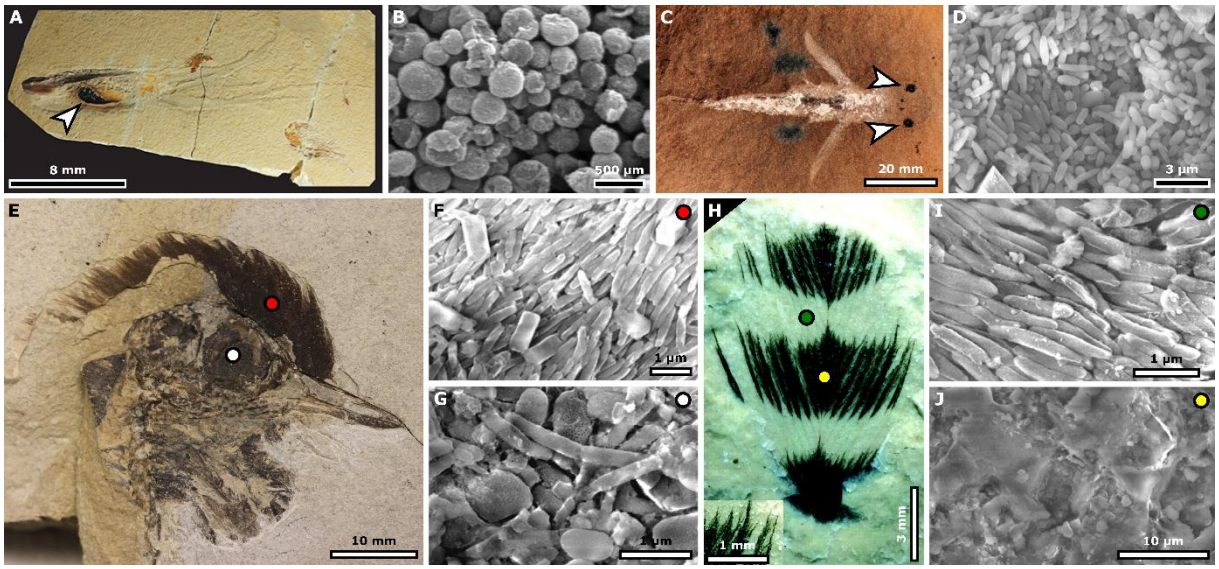

Figure 1.1. Examined fossils and their respectively melanosomes. (**A**) A fossil squid *Glyphiteuthis* (NPL 52123AB) from the Cretaceous Hajoula Formation of Lebanon, with the ink sac preserved (arrowhead), and (**B**) their globular melanosomes. (**C**) The putative lungfish larvae *Esconicthys apopyris* (PF9831) from the Carboniferous of Mazon Creek Formation of USA and (**D**) the melanosome the eyes (arrowheads). (**E**) An undescribed bird (MGUH 28.929) from the Eocene Für Formation of Denmark and melanosomes from the (**F**) feather crest (red circle) and (**G**) eye (white circle). (**H**) An isolated fossil feather from Cretaceous Crato Formation of Brazil, exhibiting the banded pattern coloration, and its (**I-J**) melanosomes. Images extracted and modified from: (A and B) University of Texas at Austin (*http://www.jsg.utexas.edu/npl/outreach/squids-the-cretaceous-ink-well/*), (C and D) from Clements et al. (2016). (E to J) Vinther et al. (2008).

Conversely, advocates of the former hypothesis (i.e., microbes fossils) also started to question the endogenous nature and the possibility of these small and delicate organelles

becoming fossils (Moyer et al., 2014; Lindgren et al., 2015a, 2015b; Schweitzer et al., 2015). In addition, for most of these authors, it was mandatory to perform multiple geochemical analyses, to provide further support for this interpretation, hence, ruling out the microbial hypothesis (Lindgren et al., 2015b). They also evoked the fact that bacteria are also able to produce melanin, though their biosynthesis and molecular precursors greatly differ from those seen in animals (D'Alba & Shawkey, 2019). Therefore, for them, even if a melanin signature is detected in fossils, due to possible bacterial melanin origin, the former hypothesis could not be rejected.

In contrast to these claims, subsequent investigations with experimental maturation of feathers and multivariate statistical approaches thoroughly showed that microbes cells can only be preserved under unique environmental conditions such as those seen in hydrothermal springs (Saitta et al., 2017a, 2017b, 2018a, 2018b; Roy et al., 2020a, 2020b; Zhao et al., 2020). In other words, for microbial preservation to occur, it is necessary that the geochemical conditions are favourable for rapid mineralization before cell apoptosis, with suitable pH, temperature, ions disponible, and appropriate time for this process (Vinther, 2020). On the other hand, it has been suggested that only the basic pH is able to degrade melanosomes and melanins, once both components are regulated by slightly acidic conditions (Slater et al., 2020).

The identification of melanosomes coupled with the application of chemical techniques (Fig. 1.2, A) and multivariate statistical analyses (Fig. 1.2, B) allow scientists to predict the possible colouring patterns of extinct animals (Fig. 1.2, C-G) (Vinther, 2015; Roy et al., 2019; Smithwick & Vinther, 2020; Vinther, 2020). However, their presence is not limited to colour reconstructions. It has been demonstrated that melanosomes were also useful in taxonomic analysis of isolated feathers (Gren et al., 2017), in understanding vertebrate evolution (Gabbott et al., 2016; Clements et al., 2016; Lindgren et al., 2018), and in physiological aspects of these animals (Lindgren et al., 2012; Li et al., 2014; Lindgren et al., 2014; Tanaka et al., 2014; Eliason et al., 2016; Tanaka et al., 2017; Lindgren et al., 2018). Apart from this intrinsic palaeobiological aspect, the identification of ancient biochromes and its ultrastructures have also informed the palaeoenvironmental (Vinther et al., 2016) and taphonomic conditions that acted on fossil preservation (McNamara et al., 2013, Colleary et al., 2015; McNamara et al., 2018a, 2018b; Muscente et al., 2018).

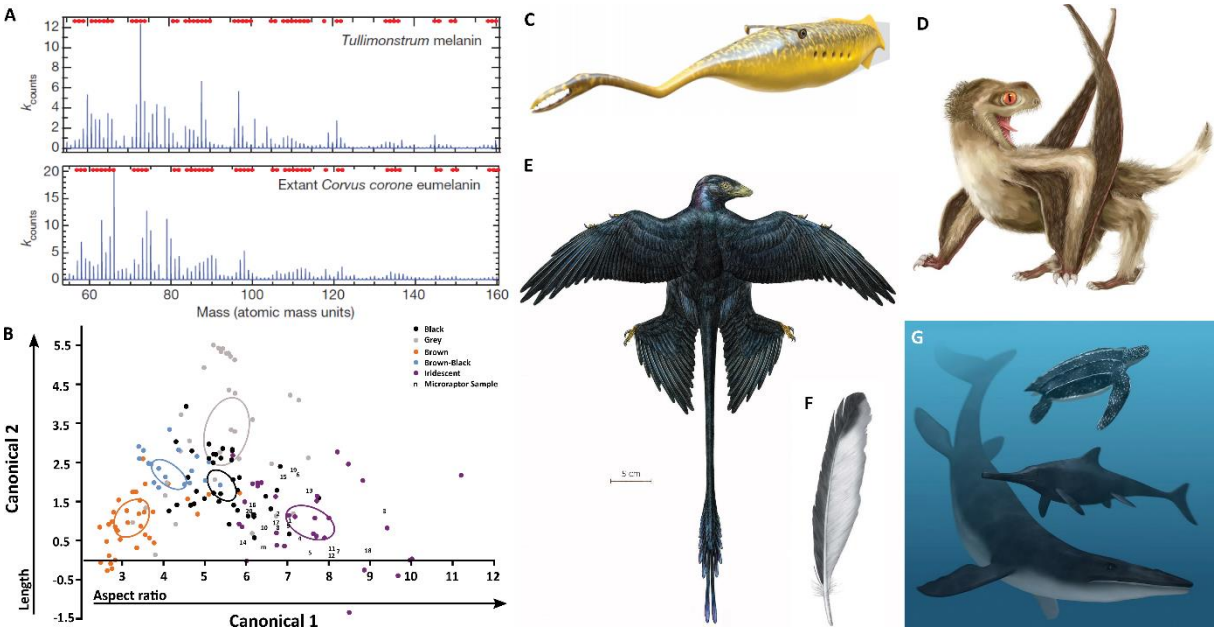

Figure 1.2. The colour inference of extinct animals. (**A**) The ToF-SIMS spectra of the Carboniferous hagfish *Tullimonstrum gregarium* (upper spectra) and a feather of the extant crow (*Corvus corone*) showing they are chemically similar. (**B**) The CQDA from the melanosome dataset to predict the colour pattern of the maniraptoran dinosaur *Microraptor gui* (colour reconstructed in E). (**C**) The aspect of the *T. gregarium* based on melanosome analysis. (**D**) The colour pattern reconstruction of an unspecific Cretaceous Anurognathid pterosaur from China. (**E**) Colour reconstruction of the dinosaur *Microraptor gui*. (**F**) Colour pattern of the isolated feather of *Archaeopteryx lithographica*. (**G**) The predicted countershading pattern in aquatic extinct reptiles from the Cretaceous (Mosasaur and leatherback turtle) and Jurassic (Ichthyosaur). Images extracted from: (A and C) Clements et al. (2016); (D) Yang et al. (2019); (B and E) Li et al. (2012); (F) Manning et al. (2013); (G) Lindgren et al. (2014).

Melanin has proven for being the only type of biochrome that withstand almost unaltered throughout the diagenetic processes (Glass et al., 2012, 2013; Ito et al., 2013; Simpson et al., 2013), and its resilience may be derived from their heterogeneous molecular structure, and localization inside the melanosomes. As a consequence, the study of fossil melanin is of great interest for molecular palaeobiologists as the analysis of these microbodies is able to provide important taphonomic information about the processes that acted on the alteration of their morphology and chemistry, indicating the mechanisms of soft tissue preservation (Mcnamara, 2013; Ito et al., 2013; McNamara et al., 2013, 2018a, 2018b). For instance, the increase in temperature and pressure through a long period of time (i.e. late in diagenesis) is able to alter significantly the melanosome shape, and their dimension can shrink up to 20% of the original size (McNamara et al., 2013; Colleary et al., 2015). In

most cases, microbodies[1] are found preserved as kerogen, but other types of composition can also be found, such as phosphates and iron sulphides (Briggs & Summons, 2014; Muscente et al., 2018). In addition, remains of melanin can be determined as the result of chemical degradation or be identified as small fragments of the original molecule (e.g. indoles and pyrroles) and functional groups (e.g. C=O, C-N) (Roy et al., 2019). Furthermore, physical features observed in melanosomes can also indicate its fossil status (Fig. 1.3), such as the presence of scattered pits, arbitrary breakages, molds and soft-tissue grainy surface (Glass et al., 2012, 2013; Ito et al., 2013).

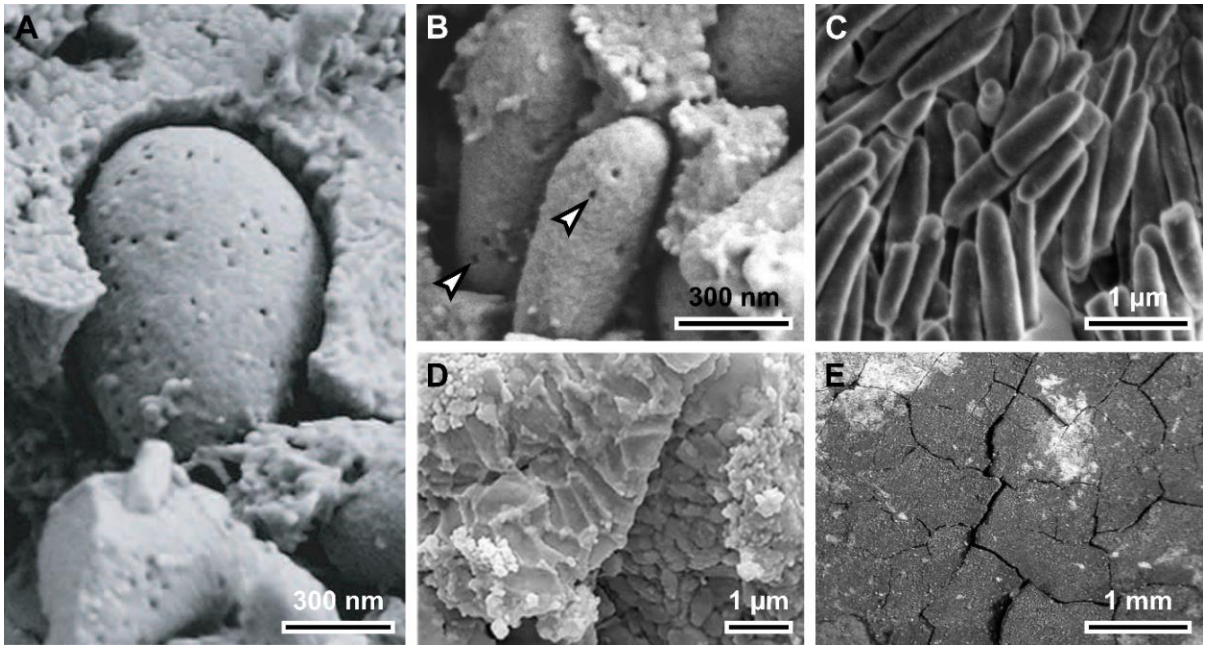

Figure 1.3. Fossil status of melanosomes. (**A** and **B**) The presence of scattered pits (arrowheads in B) onto the surface of granules from two fossil turtles. (**C**) Arbitrary breakages of rods of an isolated feather. (**D**) Casts (external molds) of rods from a pterosaur tissue. (**E**) The grainy texture of the soft-tissue anuran sample, exhibiting a high concentration of microbodies. Images extracted from: (A) Lindgren et al. (2017), (B) Lindgren et al. (2014), (C) Prado (2017), (D) Yang et al. (2019), (E) Mcnamara et al. (2009).

On the other hand, the discovery of β-keratin remnants in fossil feathers indicated their preservation potential (Moyer et al., 2016a, 2016b; Pan et al., 2016; Schweitzer et al., 2018; Pan et al., 2019). However, experiments shows uncertainty, suggesting that keratin could not be preserved even in exceptional conditions (Saitta et al., 2017a, 2017b, 2018a, 2018b; Saitta & Vinther, 2019). As a result, its preservation remains controversial, but face the current body of evidence, it is possible assume that is unlikely that this protein fossilize.

[1] The term 'microbodies', is used to refer microscopic corpuscles, which can be melanosomes, crystals, or small particles. In the present thesis, this term is often used interchangeably — according to their shape and dimensions — with other terms, such as, 'globules', 'spherules', 'particles', 'grains', or 'granules'.

To date, in Brazil, only two units exhibited such structures: the Aptian (ca. 110 Ma) Crato Formation of the Araripe Basin, and the Palaeogene (ca. 25 Ma) Tremembé Formation of the Taubaté Basin (Prado et al., 2015). Both deposits are known for the richest biota of their time, with several groups of animals and plants exquisitely preserved (Martill et al., 2007b; Prado et al., 2015). In these units, melanosomes were observed in isolated feathers, in an anuran, and in a pterosaur headcrest (Prado et al., 2015; Campos et al., 2019; Pinheiro et al., 2019; Cincotta et al., 2022). On the other hand, some other groups of animals (e.g., crocodiles and lizards) remain unexamined, and thus, the presence of melanosomes still unknown. Moreover, only a small number of specimens were examined (n<5; see Chapter 4, Fig. 4.1), requiring that a statistically significant investigation must be performed.

1.3. THE GEOLOGIC SETTING

1.3.1. The Crato Formation

Located in the north-eastern of Brazil (Fig. 1.4, A), the Crato Formation belongs to the Santana Group that represent the Mesozoic sequence of the Araripe Basin. This unit is composed by multiple transgressive-regressive cycles (Fig. 1.4, B and C), that were responsible for the deposition of greeny and bituminous black shales, limestones, sandstones, and layers of evaporitic minerals (Assine et al., 2014). At atop, it is covered by the gypsum layers from the Ipubi Formation, whereas at bottom, it lies concordantly above the greeny shales of the Barbalha Formation (Assine, 1992, 2007; Assine et al., 2014; Fambrini et al., 2015). The Crato Formation consist of several lithologies, but because fossils occur mainly on limestones, this rock-type drew more attention to geologists and palaeontologists. As fossils of this study are preserved in these rocks, their characteristics will be explored in this section. Consequently, the Crato Formation limestones have been widely used as ornamental rock, being sold mainly on the northeastern region of Brazil. For this aspect, the rocks of the Araripe Basin have been subject of intense study and exploitation by mining companies, from at least, the XIX century (Carvalho & Santos, 2005). Although being well studied, there are still much controversy about its depositional environment. According to Rojas (2009), the upper layers of the Crato Formation represents a sabkha depositional

system. This proposition was supported by the geographical distribution of carbonate rocks and the thick beds of gypsum from the upper Ipubi Formation, as both are limited to the NE portion of the Araripe Basin (Assine, 1992). For the bottom layers where most fossils discovered, evidence of freshwater fossils and occasional (cyclic) increase in salinity and reducing conditions undisputedly indicates a lacustrine system (Neumann & Cabrera, 2002). These interpretations were later confirmed by a detailed study conducted by Varejão et al. (2020, 2021), who recognized the sabkha setting at the top, with transitional brackish waters in the middle, and an endorreic freshwater palaeolake at bottom. Moreover, this proposition is also supported by the record of freshwater bivalves: *Cratonaia novaolindensis*, *Monginellopsis bellaradiata*, and *Araripenaia elliptica* (Silva et al. 2020a, 2020b).

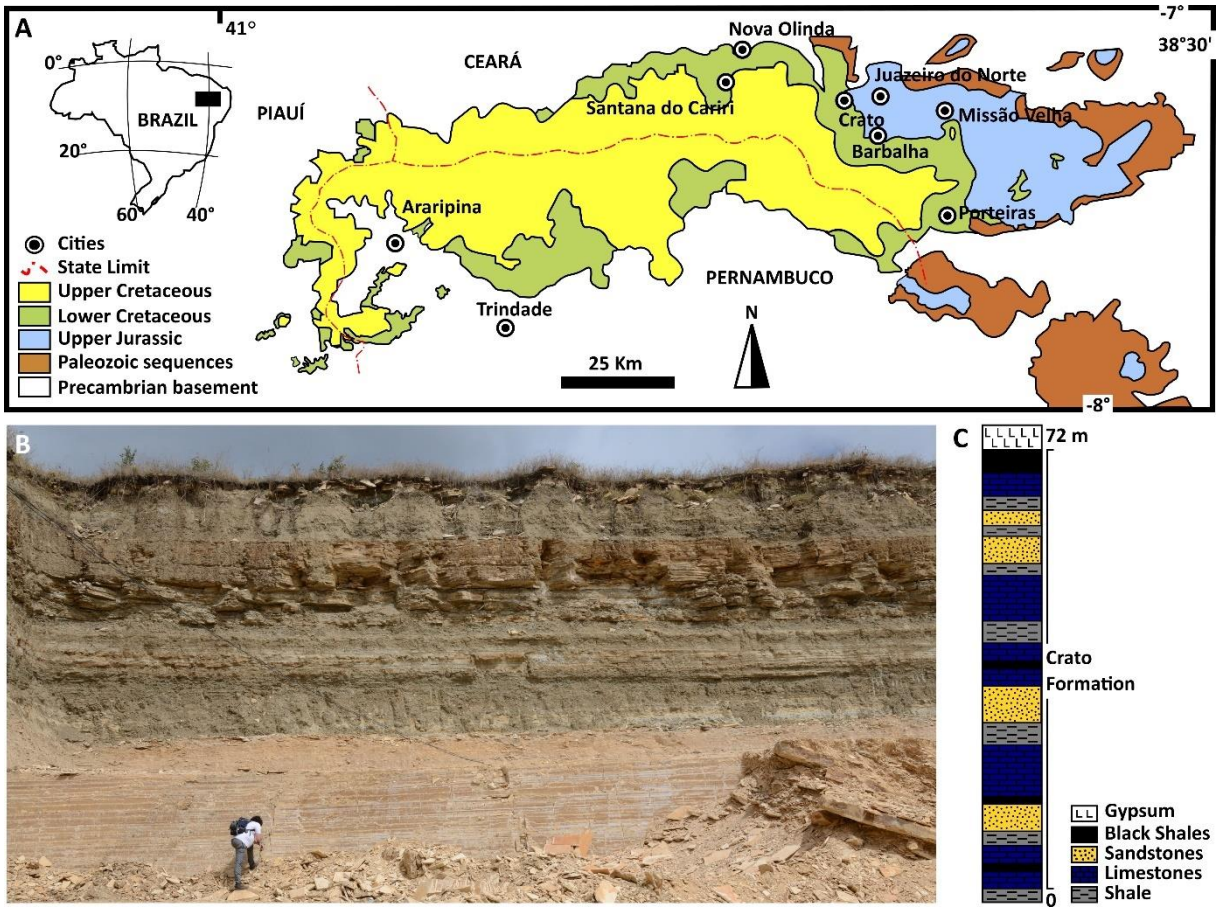

Figure 1.4. The location of the Araripe Basin and the Crato Formation rocks. (**A**) The stratigraphic distribution with a simplified chronostratigraphic sequence. (**B**) The limestones that outcrops at the Pedra do Triunfo quarry in the city of Santana do Cariri-CE. (**C**) The stratigraphic column representing the deepest portion of the Basin, where the Crato Formation is better represented. Figure (A and B) is extracted and modified from Pinheiro et al. (2019) and (B) from Osés et al. (2017). All images are under the Creative Commons International Licence 4.0.

Besides these recent propositions, Neumann (1999) and Neumann & Cabrera (2000) suggested that the Crato Formation sediments were mainly deposited under an endorheic

lacustrine setting with seasonal climatic conditions. Using the Sequence Stratigraphy, these authors also recognized six sedimentary cycles of third order, whose intervals occur between 10^6 to 10^7 Ma. Thus, the high system tract periods would represent the maximum extension and water depth of the palaeolake. As a result, the deposition of sediments varied laterally, as the base level accompanied the variation of palaeolake extension (Neumann & Cabrera, 2000). Moreover, these authors also suggested that a mild but active tectonics was responsible for controlling the base level, palaeodrainage as well as the formation of sin-sedimentary structures (Cabral et al., 2019; Celestino et al., 2021), such as penecontemporaneous deformations (e.g., loop-beddings, flame-structures and microslumps), and micro to macro fractures and veins, which can be seen filled with calcite, and more rarely, by pyrite (Fig. 1.5). Because structures follows the patterns of the Precambrian basement faults, these brittle deformations most likely occurred during the post depositional phase of diagenesis (Neumann et al., 2008; Miranda et al., 2011, 2017, 2018; Celestino et al., 2021).

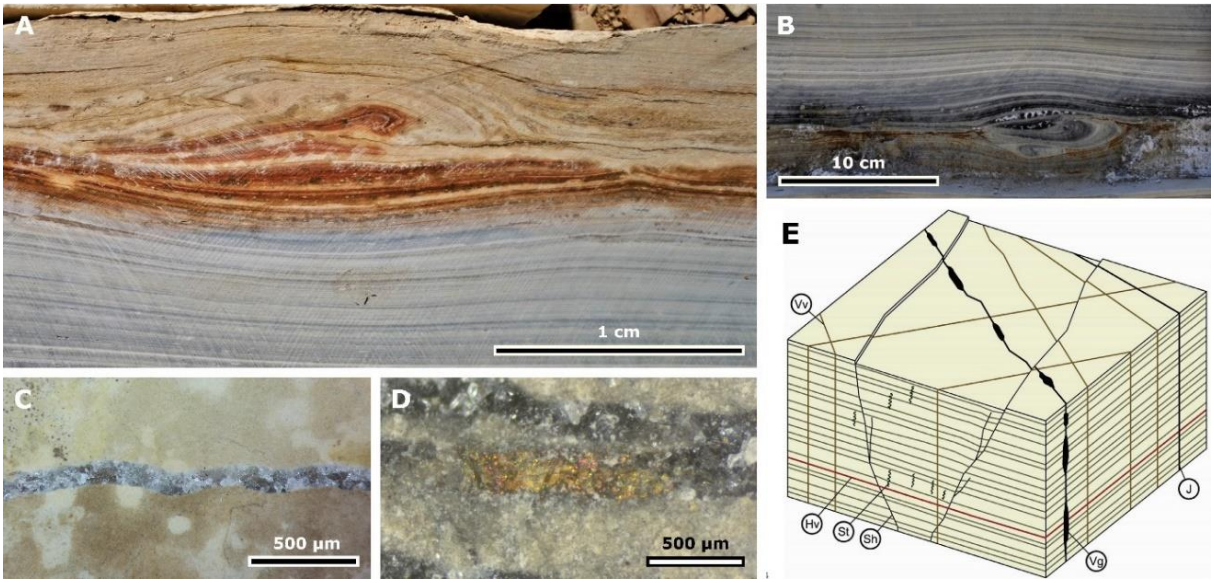

Figure 1.5. Sedimentary structures of the Crato Formation limestones. (**A**) Convoluted limestone layers and (**B**) a slump structure that was firstly interpreted as wrinkled microbial mat, but they may also represent a tectonic-induced deformation. Fractures veins filled with (**C**) calcite and (**D**) pyrite. (**E**) Diagram showing the fracture patterns of the limestones. Legend: (Hv) horizontal vein, (J) joint, (Sh) Shear fracture, (St) stylolite, (Vg) Vuggy fracture, (Vv) – vertical vein. Images extracted and modified from: (A) Varejão et al. (2019); (B) Catto et al. (2016); (E) Miranda et al. (2018).

The tectonics were also influenced by the climate conditions since the transitions from tropical to arid/semi-arid controlled the weathering, erosion, and water feedback rates, (Neumann et al., 2002). This latter process may have also affected the rate of sediment input

into the paleolake. During the warm and humid setting, a higher content of organic matter and ion-rich waters nourished the palaeolake, but in the arid/semi-arid period, evaporation rate was higher than water load (Neumann & Cabrera, 2002). This led to an increase in salinity levels and anoxia at the water-sediment interface (Neumann & Cabrera, 2002; Silva et al., 2002), which eventually caused mass mortalities of fish (Martill et al., 2007b).

1.3.2. The Crato Carbonates

The analysis of the distribution of rocks in the northeastern part of the basin suggested several transgressive-regressive cycles responsible for the formation of six sequences (C1 to C6) of carbonate beds (Fig. 1.6, A), representing different depositional settings (Neumann, 1999; Silva et al., 2002; Castro et al., 2006). Another striking characteristic of the Crato Formation limestone is the presence of two distinct facies (Fig. 1.6, B), the beige (BL) and greyish limestones (GL) (Osés et al., 2017). Albeit both lithotypes are composed by sparry and micrite crystals, the GL is richer in blocky and euhedral micrite, clay minerals, quartz and amorphous organic matter; while the BL is richer in flaky micrite and microspar crystals, halite and iron oxides/iron oxyhydroxides (Neumann et al., 2003).

A

Transgressive Cycle	Litology	Interpreted Palaeoenvironment
C6	Sandstone, Shales Limestones	Deltaic/Lacustrine
C5	Sandstone, Shales Limestones	Fluvio-Estuarine Deltaic, Lacustrine
C3/C4	Sandstone, Shales, Marls Siltites, Limestones	Deltaic Lacustrine
C1/C2	Limestones	Lacustrine

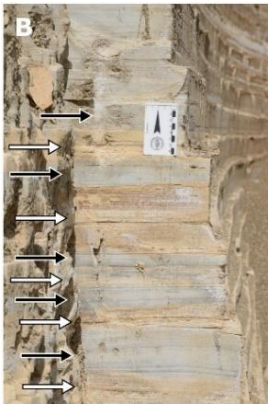

Figure 1.6. The Crato formation carbonatic sequences. (**A**) Cycles of carbonates identified by Neumann (1999). (**B**) The carbonates exhibiting the intercalation of greyish (black arrows) with beige facies (white arrows). Figure (A) is adapted from Osés (2016).

Some authors suggest that Crato limestones were formed during blooms of picoplankton and phytoplankton (Heimhofer & Martill, 2007; Martill et al., 2007b, 2008; Heimhofer et al., 2010), whilst others, by microbial mats (MMs) (Fig. 1.7, A) (Mabesoone, 1986; Srivastava, 1996; Catto et al., 2016; Santos et al., 2017; Cabral et al., 2019).

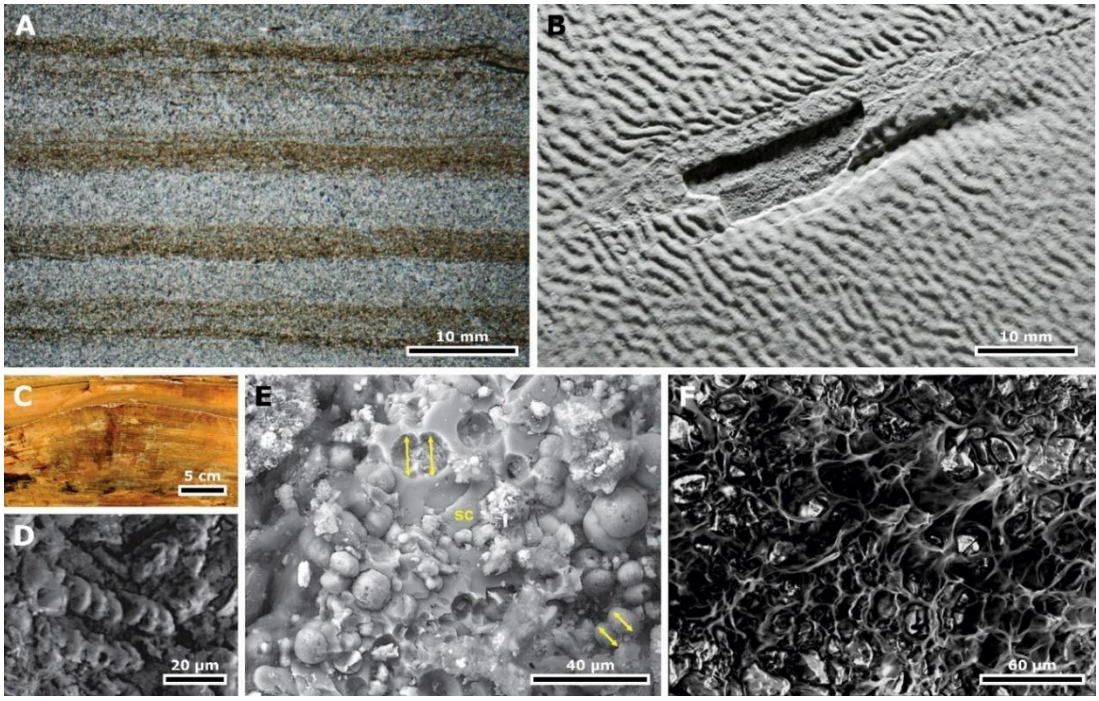

Figure 1.7. The Crato formation microbial structures and fossilized cells. (**A**) Petrographic thin section of the Crato Formation limestone, with the grey and brownish laminae. (**B**) The "*Kinneya*-like" structure (elephant skin) formed when the microbial mat is corrugated by the waves. (**C**) A domical shaped stromatolite. (**D** and **E**) Calcified bacterial cells, (**D**) a putative *Spirulina* sp. and (**E**) several coccoid exhibiting an isolated or in binary-fission, As well as their casts (yellow arrows). (**F**) Honeycomb-shaped EPS devoid of bacterial cells. Images extracted and modified from (A) Varejão et al. (2019), (B and C) Warren et al. (2017), (D-F) Catto et al. (2016).

Not rare, it is possible to observe crystals of pyrolusite (MnO_2) (Fig. 1.8, A), pyrite (FeS_2) (Fig. 1.8, B-C) and filaments of unknown composition (Fig. 1.8, E-F), the latter component most likely is the soot remains caused by occasional wild fires (Pires et al., 2019).

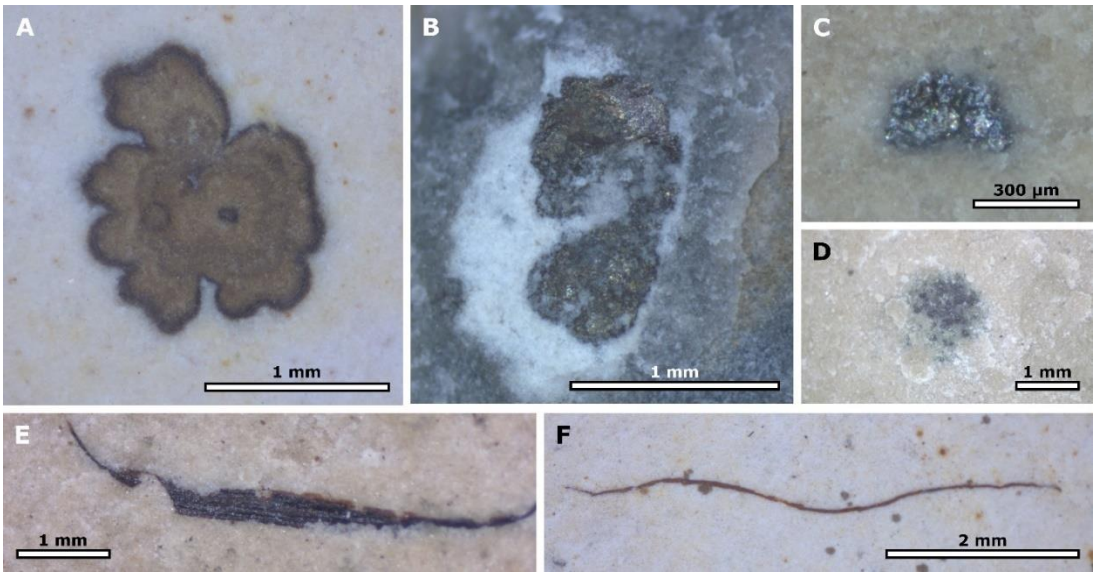

Figure 1.8. Minerals and structures with unknown provenance in the Crato Formation matrix. (**A**) A flower-like crystal of pyrolusite exhibiting a radial growth. (**B**-**D**) Isolated pyrite crystals found disseminated in both facies. (**E** and **F**) Filaments of unknown origin that also occur scattered in the matrix. They most likely are soot from plant remains from wild fires.

This difference in rock colouration was previously explained as the result of the weathering processes that acted onto the exposed surfaces (Martill, 1993; Martill et al., 2007a). According to this hypothesis, the meteoric waters would be responsible for the removal and transport – through sediment pores – of the components (e.g. ion-rich fluids) from the upper (BL) into bottom (GL) layers (Heimhofer & Martill, 2007; Martill & Heimhofer, 2007; Heimhofer et al., 2010). As one expect, this process would result in a richer bed with organic matter and elemental ions on the GL facies. In this scenery, slabs and fossils would exhibit high concentrations of heavy elements brought by this "leaching" from the upper layers. However, using geochemical techniques, recent palaeontological studies have demonstrated that both facies are in fact not so much chemically distinct as expected, and difference of facies may derive mainly by the mineralogical texture and paleontological aspect, such as the type (chemistry) and degree/mode of preservation (Osés et al., 2017; Bezerra et al., 2018).

Due to the absence of reliable isotopes, the absolute dating of the Crato Formation is still lacking (Martill, 2007), but a Lower Cretaceous age (Aptian) is fairly accepted by several authors. This age is established by palaeontological evidence, and provided mainly by palaeobotany, palynology, and microfossils. Altogether, they place this unit at the sub-zone P-270 that is equivalent to the Aptian-Albian Age (an interval of ca. 125 Ma to 100.4 Ma) (Regali, 1989; Coimbra et al., 2002; Rios-Netto et al., 2012).

1.3.3. The Crato Formation fossil preservation

One great aspect of the Crato Formation is the abundance and diversity of fossils that generally exhibit an exceptionally preservation, not rare, with delicate tissues preserved as kerogen or stains of limonite (Fig. 1.9). This latter trait has enabled palaeontologists to classify this unit as both *Konzentrat-Lagerstätte* and *Konservat-Lagerstätte*, a feature held only by few deposits around the world (Martill et al., 2007a). In other words, the sheer number and the presence of exquisite fossils characterize the Crato Formation as a deposit of high concentration and exceptional preservation. As the fossil record indicates, the large and diverse animals suggests that during Crato deposition, a well-established trophic chain like modern environments was already established (Maisey, 1991; Martill, 1993).

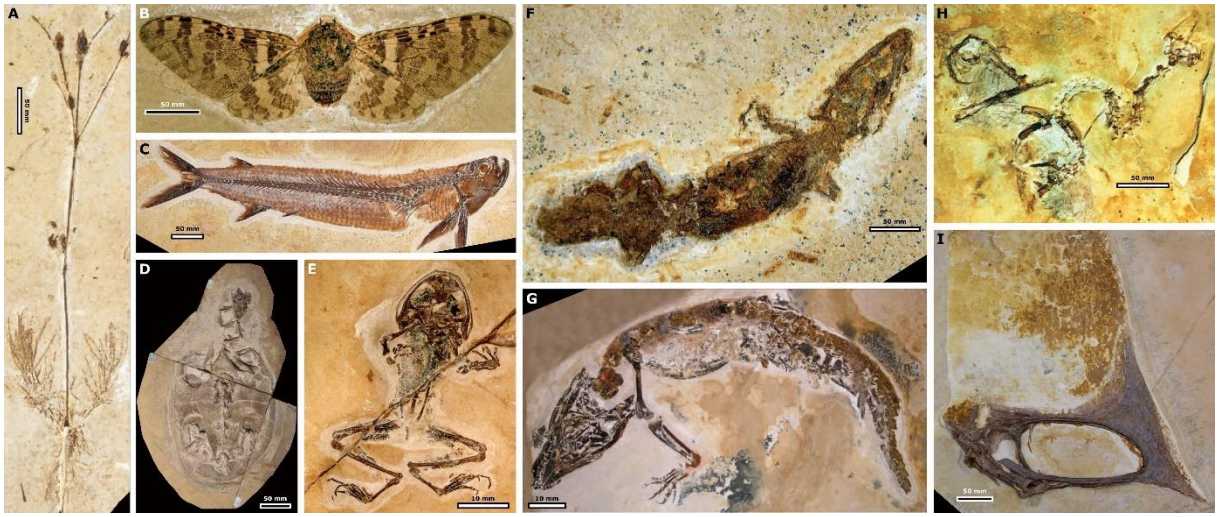

Figure 1.9. Fossils from the Crato Formation. (**A**) A gnetophyte plant exhibiting organic connections with leaves and roots. (**B**) The Cycadomorpha specimen *Baeocossus fortunatus* exhibiting colour pattern of the wings. (**C**) A fossil fish *Cladocyclus garneri* with soft tissues and scales preserved throughout the body. (**D**) A nearly complete Pleurodira turtle Araripemys barretoi (LP-UFC-722). (**E**) An undescribed frog (UFC-NO 004v) with the presence of soft tissues, such as eyes and skin. (**F**) An undescribed lizard specimen exhibiting the presence of soft tissues while the tail is absent. (**G**) The crocodile specimen *Araripesuchus gomesii* (SMNK PAL 6404) with osteoderm and soft tissues. (**H**) Remains of the supposed enantiornithine bird that remain undescribed and is housed at the Collection Masayuki Murata, in Kyoto, Japan. (**I**) The Tapejarid pterosaur *Tupandactylus navigans* (SMNK PAL 2344) exhibiting the headcrest and rhamphotheca tissues. Images extracted from: (A-B, G-I) Martill et al. (2007a), (D) Limaverde et al. (2018), (E) Leite (2013).

Albeit distributed throughout the basin, life seemed to be more active in the paleolake surroundings. If examples of modern animal ecology are taken into consideration, it is possible to suggest a putative niche distribution of the Crato fossils (Fig. 1.10). Some terrestrial vertebrates unequivocally dwelled near the Crato paleolake, such as the case of turtles, crocodiles, and frogs. Few animals may have lived even in the adjacent areas like rocky coasts and shorelines, as extant birds species do (Pereira, 2018), such as the case of pterosaurs. In turn, snakes, lizards, avian and small non-avian dinosaurs may have lived inland (Mendes et al., 2021; Ribeiro et al., 2021) and used the palaeolake waters to drink, or even as a source of relief from an excess of heat (Pough et al., 2013). It is possible that after death, the cadavers reached the lowest portion of the lake, where it was deposited in a euxinic conditions at the bottom. According to Osés et al. (2017), the rapid burial caused by events of great input of sediments, favoured in many cases, the preservation of the animal soft tissues. Furthermore, the low concentration of oxygen and high level of salts prevented a complete decay as well as the activity of scavenging organisms (Martill et al., 2007b). Once the hypersalinity were achieved, it may have surpassed the osmotic tolerance of waterborne animals, leading to mortalities of fish and other animals (Martill et al., 2007a, 2008).

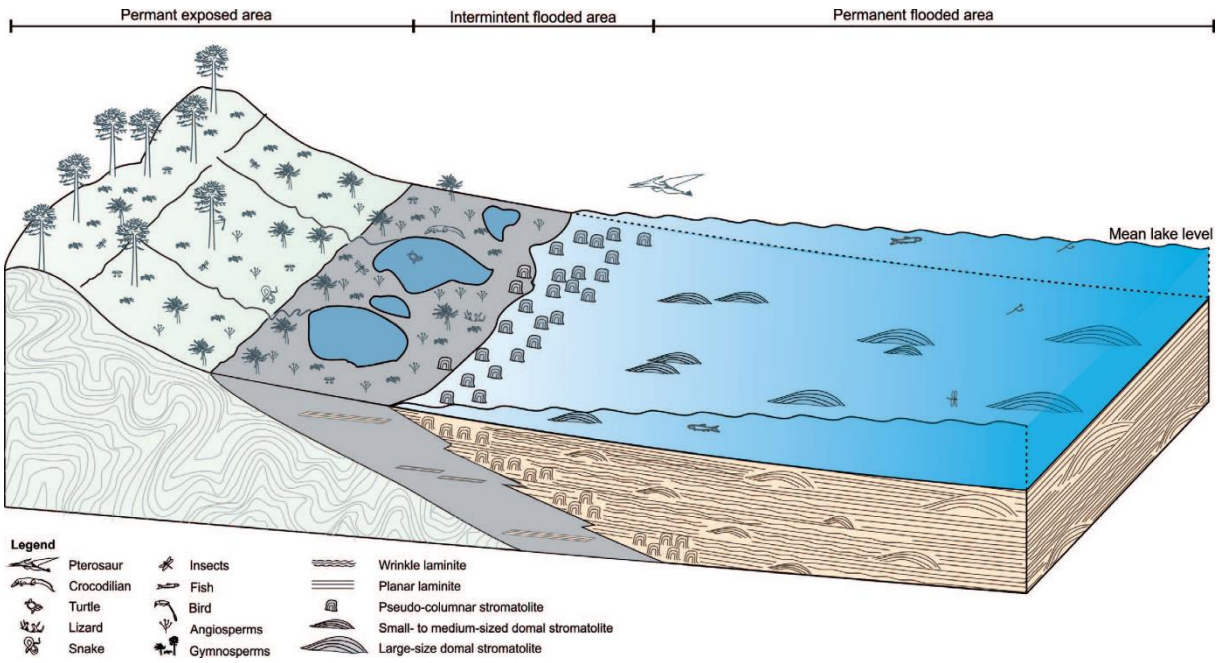

Figure 1.10. The model of the Crato Formation. The suggested palaeoenvironmental reconstruction of the Crato beds during the Aptian. This model is based on sedimentary and fossil evidences, as well as previous interpretations (cf. Martill, 1993). Image taken from Varejão et al. (2019).

Since the palaeolake bottom waters at the proximal regions were colonized by microbial mats (Catto et al., 2016), and carcasses could be trapped in these components. Once there, similarly to other deposits of exceptional preservation (Wilby et al., 1996), the fossilization could take place with a great contribution of microorganism activity (Varejão et al., 2019). As organism remains were isolated from the oxygenated environment, this may have favoured the activity sulphate and methanogenic reducing bacteria (SRB and MRB) (Osés et al., 2017). Thus, when in sulphate-reducing layer, the animal carcasses would become the source of nutrients for SRB (Osés et al., 2017). The activity of these microorganisms would lead to the precipitation of iron sulphides, replicating tissues in fine detail (Fig. 1.11). When introduced to the methanogenic layer, the decaying organic matter would be converted into kerogen and carbon-rich compounds by the activity of MRB (Osés et al., 2017). Therefore, it is clear that, the presence of microorganisms were responsible for the mineralization of tissues early in diagenesis as well as the decrease in decay rates, in a 'sarcophagus preservation' as proposed by Iniesto et al. (2016), but firstly suggested by Schultze-Lam et al. (1996). Consequently, many distinct fossildiagenetic models have been proposed for the preservation of the Crato exquisite fossils (see Bezerra et al., 2021). Nevertheless, all these concepts share some common ground, the presence of microbes in microbial mats that promoted general pyritization or kerogenization.

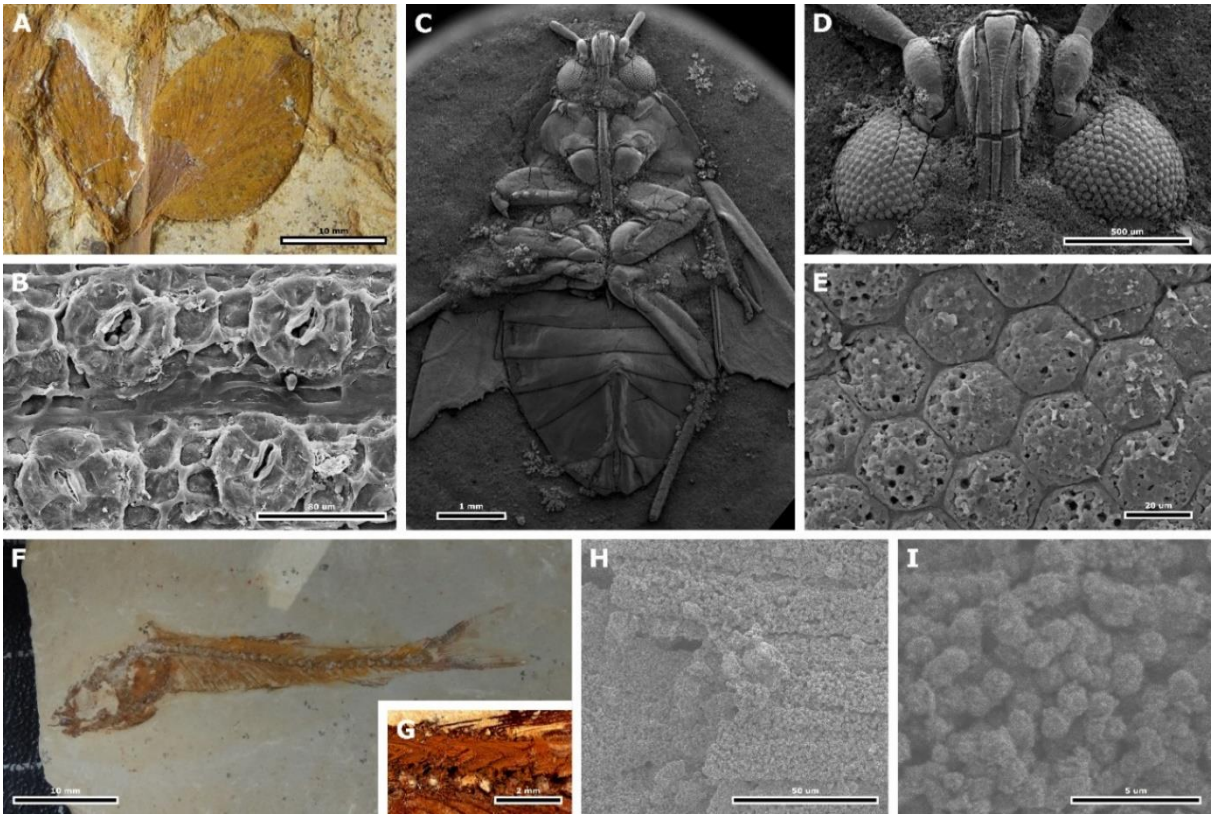

Figure 1.11 The exceptional preservation of the Crato Formation fossils. (**A**) A Gnetales plant with (**B**) fossilized stomata preserved. (**C**) An undescribed Hemiptera exhibiting a three-dimensional preservation with (**D**) eyes preserved in fine details, such as (**E**) the hexagonal ommatidia. (**F**) A specimen of *Dastilbe crandalli* exhibiting (**G**) the V-shaped myomeres, whose (**H**) muscle fibres consists of (**I**) small framboids of iron oxyhydroxides. Images extracted and modified from: (A and B) Rendon (2013); (C-E) Barling et al. (2015); (F-I) Osés et al. (2017).

Therefore, based on the current literature (see Delgado et al., 2014; Barling et al., 2015; Osés et al., 2016, 2017; Warren et al., 2017; Bezerra et al., 2018; Gomes et al., 2019; Varejão et al. 2019; Mendes et al., 2019; Barling et al., 2020; Bezerra et al., 2020; Dias & Carvalho, 2020; Bezerra et al., 2021; Iniesto et al., 2021; Prado et al., 2021; Storari et al., 2021; Dias & Carvalho, 2022) it is possible to suggest some of the factors that may have contributed to the high-quality preservation of fossils: (1) The absence of scavenging organisms that favoured carcasses to maintain their physical integrity; (2) The abrupt burial in MMs under euxinic/dysoxic waters that led to decrease in decay rates, and contributed with the conversion of organic matter into kerogen (by MRB), or pyrite (in SRB); (3) The preponderance of fine-grained carbonate surrounding fine body details, or the microbial mat 'sealing' that isolated the carcasses from the environment, which also promoted further mineral nucleation; (4) The relatively mild diagenesis, where details of fossils and their chemistry could be maintained without significant physicochemical alterations.

1.4. BIOCHROMES: AN OVERVIEW

One conspicuous aspect of the natural world is the variety of hues and patterns expressed by many organisms (Fig. 1.12). Coloration vary according to environment, diet, and genetic mutations. Hence, they are involved in different roles, such as protection, communication, sexual selection, among others (Cuthill et al., 2017; Shawkey & D'Alba, 2017).

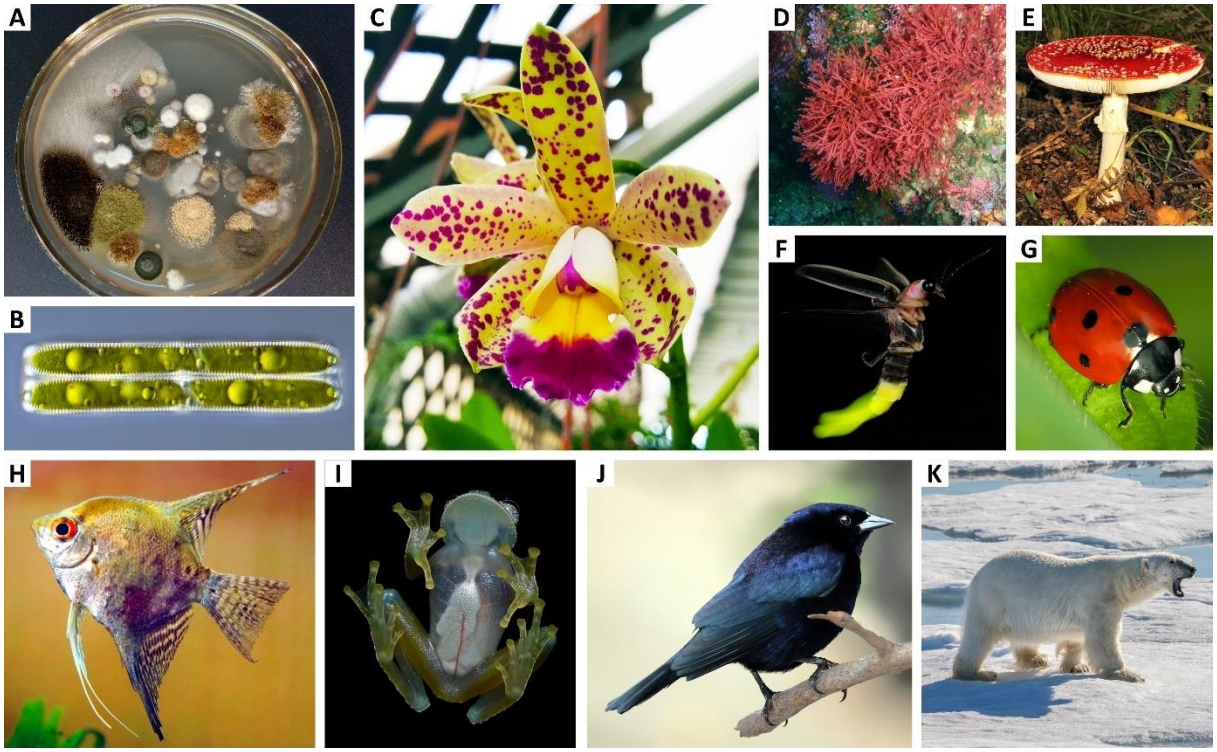

Figure 1.12. The diversity of colours in nature. (**A**) A multicoloured colonies of soil bacteria. (**B**) Green diatom *Pinnularia*. (**C**) Yellow and purple spotted cattley orchid (*Cattleya guttata*). (**D**) Red seaweed algae. (**E**) Red and white fly agaric mushroom (*Amanita muscaria*). (**F**) Luminescent firefly beetle (*Photinus pyralis*). (**G**) 7-spotted ladybug (*Coccinella septempunctata*). (**H**) Structural colouration of the fish. (**I**) Translucent ventral skin of the glass frog (*Cochranella pulverata*). (**J**) Purple-black iridescent plumage of bird. (**K**) White pelage of polar bear (*Ursus maritimus*). All images published under the CCBY 2.0, 3.0, and 4.0. Image credit: (A) Oksana Lastochkina, (B) Alexander Klepnev, (C) Don Ramey Logan, (D) Peter Southwood, (E) Tim Bekaert, (F) Terry Priest, (G) Dominik Stodulski, (H) Keven Law, (I) Geoff Gallice, (J) Charles J. Sharp, (K) Andreas Weith.

In nature, colour is an optical phenomenon caused by the interaction of light of the electromagnetic spectrum with matter (Fig. 2.13, A and B), and are perceived by eye receptors (Sliney, 2016). This diverse palette also reflects the two main mechanisms of colour-producing of matter, the structural coloration and biochromes[2] (Fig. 2.13, D and E).

[2] *Although in many cases 'biochromes' and 'pigments' are considered synonyms, and used interchangeably, the former term is more specific to colour producing biomolecules, whereas the latter also refers to the artificial compounds, such as dyes, paints, and colourants (Lindgren, 2016).*

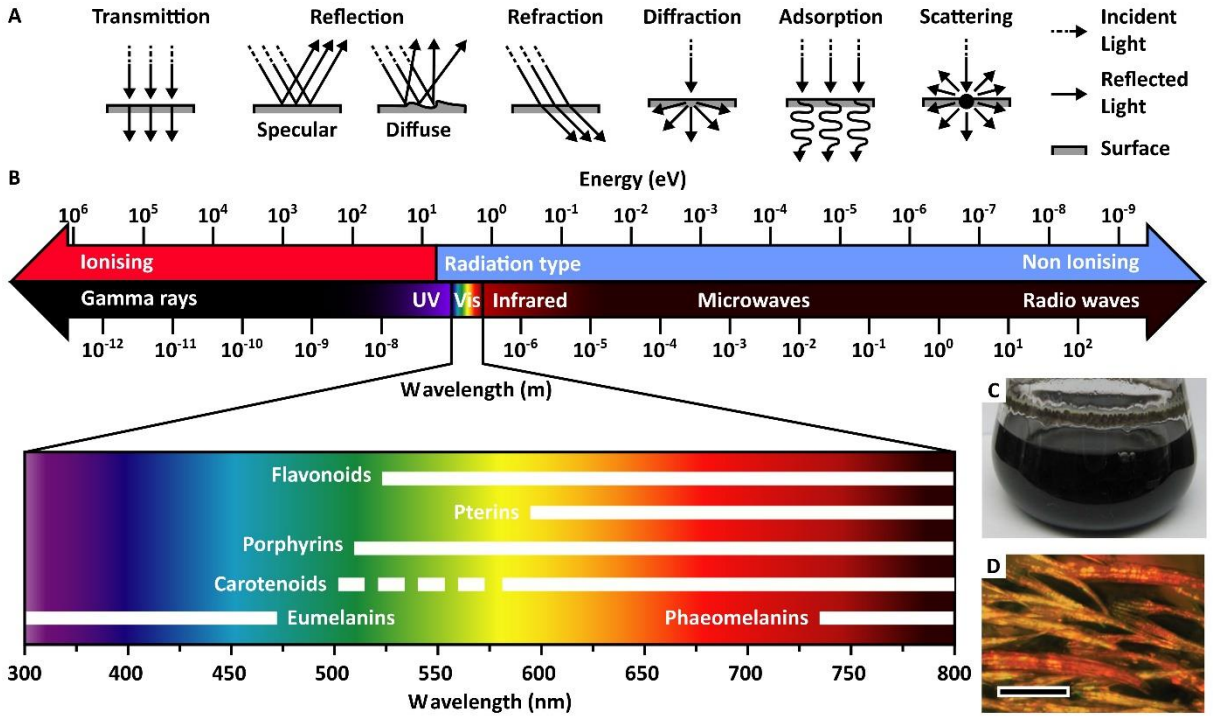

Figure 1.13. Physics aspects of the colours and mechanisms. (**A**) Examples of light interaction with material surface. (**B**) The electromagnetic radiation and its physical properties. When colour is provided by biochromes, hues are generally limited to the visible (Vis) spectrum that is constrained between ca 300 to 800 nm. (**C**) Broth of black melanin produced by the microorganism *Streptomyces glaucescens*. (**D**) Light microscopy of the scale of a modern beetle exhibiting the iridescent generated by the internal arrangement of structures. Figure (A) is based on Parker (1998a); images modified from (B) NASA, (C) El-Naggar & El-Ewasy (2017), (D) McNamara et al. (2014). Images (B-D) are licensed under CC BY 3.0 and 4.0. Scale bar of (D) 25 µm.

In structural colouration, the colour patterns are produced by the arrangement of microstructures in layers (e.g., stacking of guanine platelets or presence of air bubbles), layer spacing, and presence/absence of molecules (Parker, 1998a, 2004). This optical phenomenon occur when light interacts with multiple layers of integument, absorbing, scattering, and refracting at different forms, producing bright and multicoloured metallic hues (Parker, 1998a). For instance, the shimmery green and blue cuticles of wasps and beetles is due to the diffuse reflection of light, a feature also retained in fossils (McNamara, 2013).

The mechanism of colouration by biochromes, in turn, is more diverse, as these molecules has different chemical skeleton, molecular weight, biosynthesis, and distribution (Roy et al., 2019). Nevertheless, by their overall characteristics (e.g., basic skeleton), pigments can be grouped into broader classes (Fig. 2.14; Tab. 1). For instance, pteridines – here considered an "umbrella group" – is a type of biochrome group consisted of several pigments, such as biopterin, flavin, riboflavin, among others (Ikawa et al., 1995).

Table 1. Classes of natural pigments. Due to the existence of diverse types, these biochromes can be grouped into broader classes according to their shared basic molecular skeleton.

CLASS	TYPE OF BIOCHROMES
Carotenes	Carotene, Canthaxanthin, Lutein, Psittacofulvins, Xanthopylls
Flavonoids	Anthocyanins, Anthoxanthins, Flavans, Flavones, Flavonols
Melanins	Allomelanins, DHN, Eumelanin, Neuromelanin, Phaeomelanin
Porphyrins	Biliverdin, Chlorophylls, Heme, Turacins
Pteridines	Biopterin, Cyanopterin, Flavins, Monapterin, Pterine, Pteridine
Purines	Adenine, Guanine, Hypoxanthine
Others	Luciferin, Rhodopsin, Hemocyanins, Anthraquinone, Borolithochrome, Ommochromes

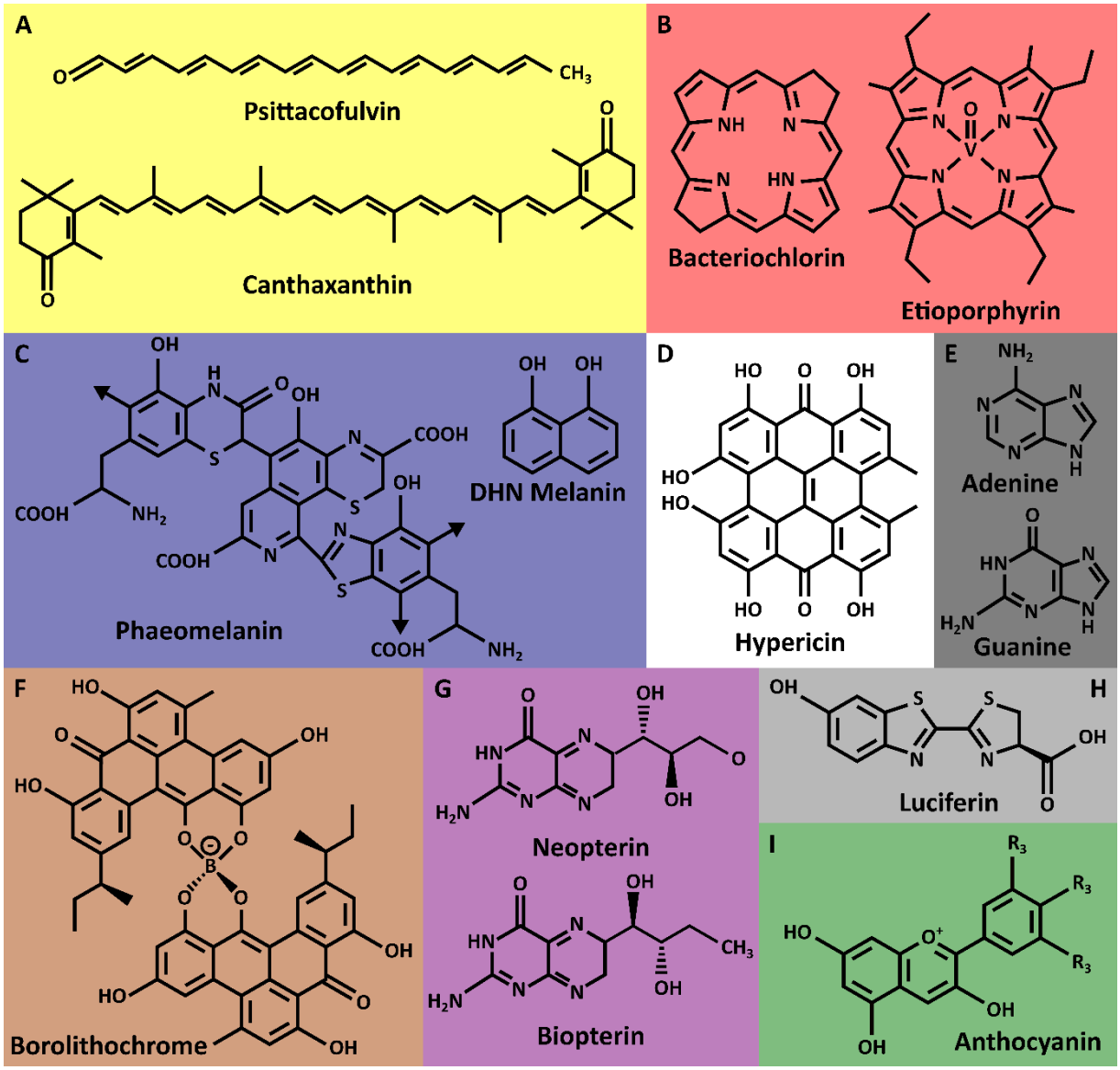

Figure 1.14. Example of the molecular diversity of biochromes. Groups represented by (**A**) Carotenes (yellow), (**B**) Porphyrins (red), (**C**) Melanins (blue); (**D**) Hypericins (white), (**E**) Purines (black); (**F**) Borolithochrome (brown); (**G**) Pterins (purple); (**H**) Luciferin (grey); (**I**) Flavonoids (green).

Despite these two colour-producing mechanisms, some animals, such as birds and insects, also have the ability of perceiving hues at ultraviolet and infrared bands. In places where dim light settings and alternate visual acuity prevails, such as in the floor of dense canopy forests, deep sea, or during twilight hours, it is not rare to found animals communicating via fluorescence or bioluminescence, which is produced by the interaction of biomolecules, oxygen, and electrons (White et al., 1963; Salih et al., 2000; Arnold et al., 2002; Marek et al., 2011; Wucherer & Michiels et al., 2014). Due to their varied distribution among animals, it is suggested that this strategy has evolved independently in several unrelated groups (Fig. 1.15), such as beetles (Bechara & Stevani, 2018), millipedes (Marek et al., 2011), and arachnids (Andrews et al., 2007).

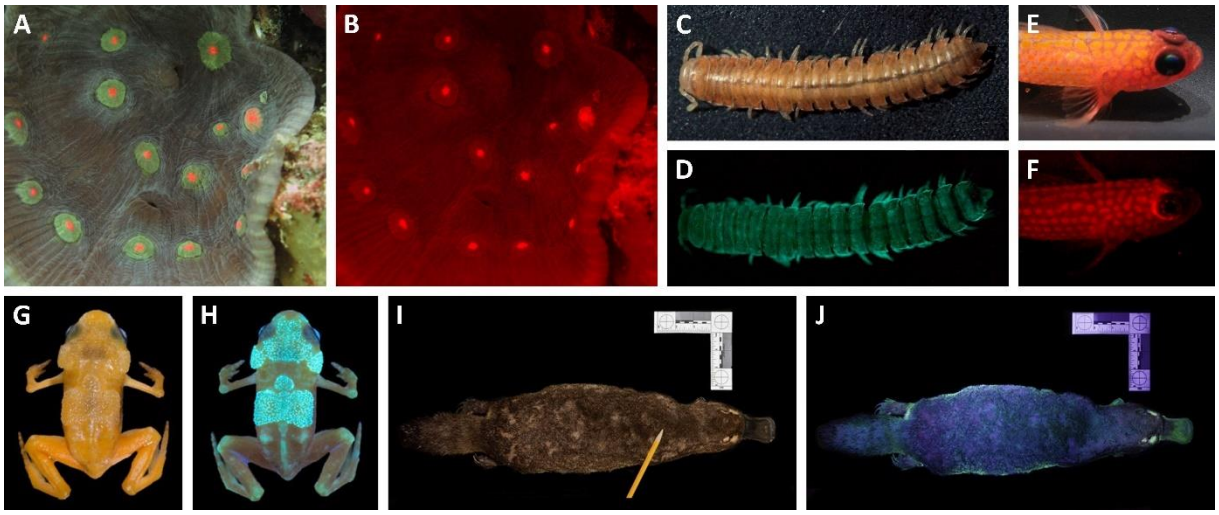

Figure 1.15. Examples of bioluminescence and fluorescence in animal groups. (**A** and **B**) The fluorescent coral reef Mycedium under visible and UV light. (**C** and **D**) The luminescent millipede *Motyxia sequoiae* under normal illumination and, with light emitted from the cuticle. (**E**) The fluorescent reef fish *Trimma avidori* with orange colour of the skin under normal light, and under UV light, which reveals a spotted pattern. (**G**) The fluorescent tropical frog (*Ischnocnema parva*) showing its yellowish pattern under visible light, and a bluish colour pattern under UV light. (**I** and **J**) The fluorescent platypus (*Ornithorhynchus anatinus*) showing their colouration under visible and UV light. All images published under CC BY License, and modified from (A, B, E, F) Michiels et al. (2008); (C and D) Marek & Moore (2015); (G, H) Goutte et al. (2019), (I,J) Anich et al. (2020).

Due to the difference in the distribution in the tree of life and main object of this thesis, only melanin was picked to be briefly introduced. This decision is based on the fact that all other pigments are frail to molecular alteration and are rarely preserved in fossils (Falk & Wolkenstein, 2017; Roy et al., 2019). Although melanins are the focus of this thesis, a more detailed approach can be seen in the reviews of Ito (2003), d'Ischia et al. (2013); Dubey & Roulin (2014); Solano et al. (2014); and D'Alba & Shawkey (2019); or books of Borovanský & Riley (2011) and Ma & Sun (2012).

1.4.1. Melanins and melanosomes

Melanins are dark biological substances that usually are found in cellular bodies of many archaeas, procaryotes, and eukaryotes (Fig. 1.16). In animals, melanins are present basically in two classes, eumelanin and phaeomelanin. While the former are insoluble in most solvents, the latter are more unstable and soluble in alkali solutions (d'Ischia et al., 2013; Solano, 2014).

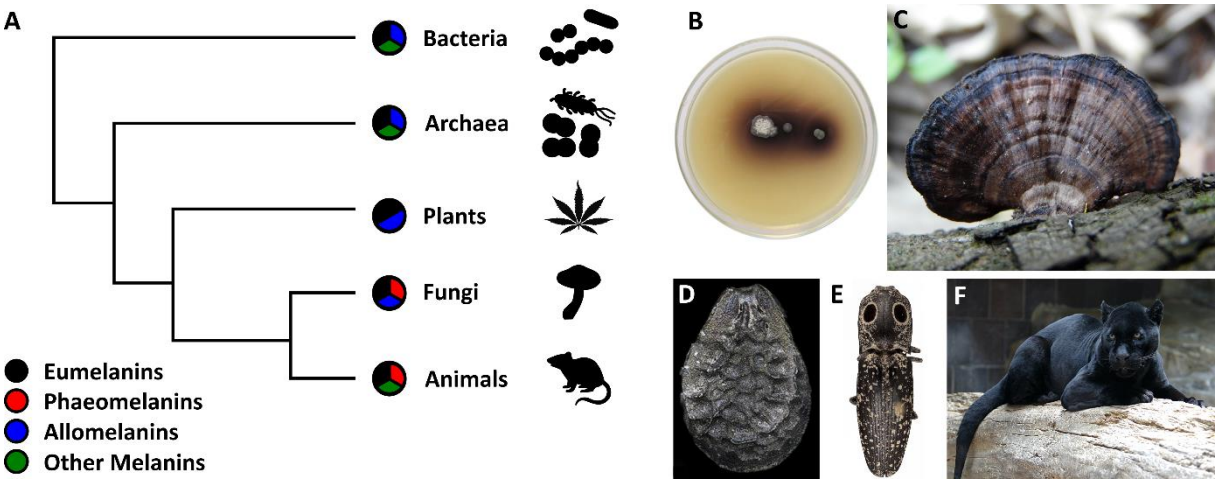

Figure 1.16. The distribution of melanins and the precursor molecules. (**A**) Cladistic scheme of the melanin-type in the Tree of Life. (**B**) Colony of melanising bacteria *Streptomyces glaucescens* cultured in petri dish. (**C**) Melanising fungi *Hexagonia tenuis*. (**D**) melanising sesame seed (*Sesamum indicum*), (**E**) The eyed elater click beetle (*Alaus oculatus*) with two melanised spots ("eyes") on the pronotum. (**F**) The melanistic morph jaguar (*Panthera onca*). With the exception of A, all images were published under Creative Commons Public Domain 3.0 and 4.0. Images credit: (B) El-Naggar & El-Ewasy (2017); (C) Liz Popich (2016), (D) Glagoleva et al. (2020); (E) Wong & Marek (2020); (F) Colin Burnett (2006).

In animals, melanin occur inside the melanosomes, an organelle produced in specialized cells called melanophores, or melanocytes in endothermic animals (Hsin-Su, 1999; Delevoye et al., 2019). These subcellular structures have an estimated size that ranges from 0.1 to 2.0 µm and are responsible for the synthesis and storage of melanin (Wasmeier et al., 2008). In terrestrial animals, melanosomes occur immersed in the dermis, epidermis, epidermal appendages (e.g., scales, feathers, and hair), randomly distributed in the melanocyte cytoplasm, in macrophage cells of hematopoietic tissues, or even as free granules in internal tissues and skin (Agius & Roberts, 2003; Haugarvoll et al., 2006; Wasmeier et al., 2008; Oliveira & Franco-Belussi, 2012). Due to the advantageous chemical properties, melanins have been of great interest for many different purposes. For example, in cosmetics, where it is studied as part of hair repair, strength, or bleach (Commo et al., 2012;

Gorniak et al., 2014a, 2014b; Itou, 2018; Itou et al., 2019); in food packaging, once the antioxidant activity may be effective in food storage for longer periods (Shankar et al., 2019); in radiation absorption, which might be used for better energy storage (Xu et al., 2019); in electricity, as its electron conductivity may be advantageous as photoconductor for electronic devices (Vahidzadeh et al., 2018).

In general terms, melanins are consisted of tyrosine and phenolic compounds that have undergone the oxidation and polymerization processes (d'Ischia et al., 2013). Because of their darkened colouration, they can be informally divided into black to dark brown eumelanins ("*εν*"= "good"), and chestnut phaeomelanins ("*φαεος*"= "dusky") (Ito et al., 2011). In fact, melanins are consisted of several chemically different compounds such as the neuromelanins, allomelanins, catechol melanins, DHN-melanin, pyomelanins, as well as true eumelanins and phaeomelanins (Solano, 2014; D'Alba & Shawkey, 2019). Despite this diversity, most of these pigments are distributed into Archaea, Bacteria, Fungi, and Plants. In one way or another, eumelanin, phaeomelanin, and neuromelanin are present in most animals, especially vertebrates; suggesting that these structures may be a synapomorphic trait of all eumetazoans (d'Ischia et al., 2013; Solano, 2014; D'Alba & Shawkey, 2019).

Due to the wide distribution throughout the tree of life, the highly heterogeneous nature, and different biosynthesis, the chemical structure of many melanins are still contentious subject (Powell et al., 2004; Tran et al., 2006; Prampolini et al., 2015). However, the precursors of these molecules are known (Fig. 1.17), where eumelanin is consisted of quinone 5,6-dihidroxiindole (DHI) and 5,6-dihidroxiindole-2-carboxilic acid (DHICA), and phaeomelanin by benzothiazole and benzothiazine. In turn, these precursors are products of the oxidation and hydroxylation of other derivatives, the indole-5,6-quinone (IQ) and indole-2-carboxylic acid-quinone (IQCA), quinone methide (QM), quinone imine (QI), and hydroquinone (HQ) (Meredith et al., 2006; Meng & Kaxiras, 2008; Davy & Birch, 2018). The dark black colours of eumelanins derives largely from the presence of carbonyls and carboxyls groups (Riley, 1997), while the brownish hues of phaeomelanins are due to the presence of sulphur from cysteine (d'Ischia et al., 2013). In addition, varying functional groups and organometals, such as hydroxyl (O=H) and carboxyl (C=O), as well as Ca, Co, Cu, Fe, Mn and S, occur bonded to melanin monomers (Horčičko et al., 1973; Liu & Simon, 2005; Watt et al., 2009; Bellono & Oancea, 2014; Riley & Stratford, 2015).

In particular the eumelanin, the ubiquitous type of all melanins, many theoretical studies suggest the possible skeleton (Fig. 1.17), as for example: (a) the polydopamine consisted of both DHI and DHICA units; (b) indolequinone monomer bonded with a hydroquinone at the first carbon site, with a carboxyl bridge bonded to a pyrrole-2,5-dicarboxylic acid (PDCA); (c) a chain of several monomers in a conjugated-bonded stacking, in which molecules are bonded at first and eight carbons; and (d) the porphyrin-like structure arranged into π-π stacking, where molecules are bonded at the first and seven carbon sites and composed of three to five oligomers, with four being considered the most stable variety (Stark et al., 2005; Kaxiras et al., 2006; Tran et al., 2006; Meng & Kaxiras, 2008; Feo et al., 2015; Kim et al., 2016; Supakar et al., 2019; Solano, 2020).

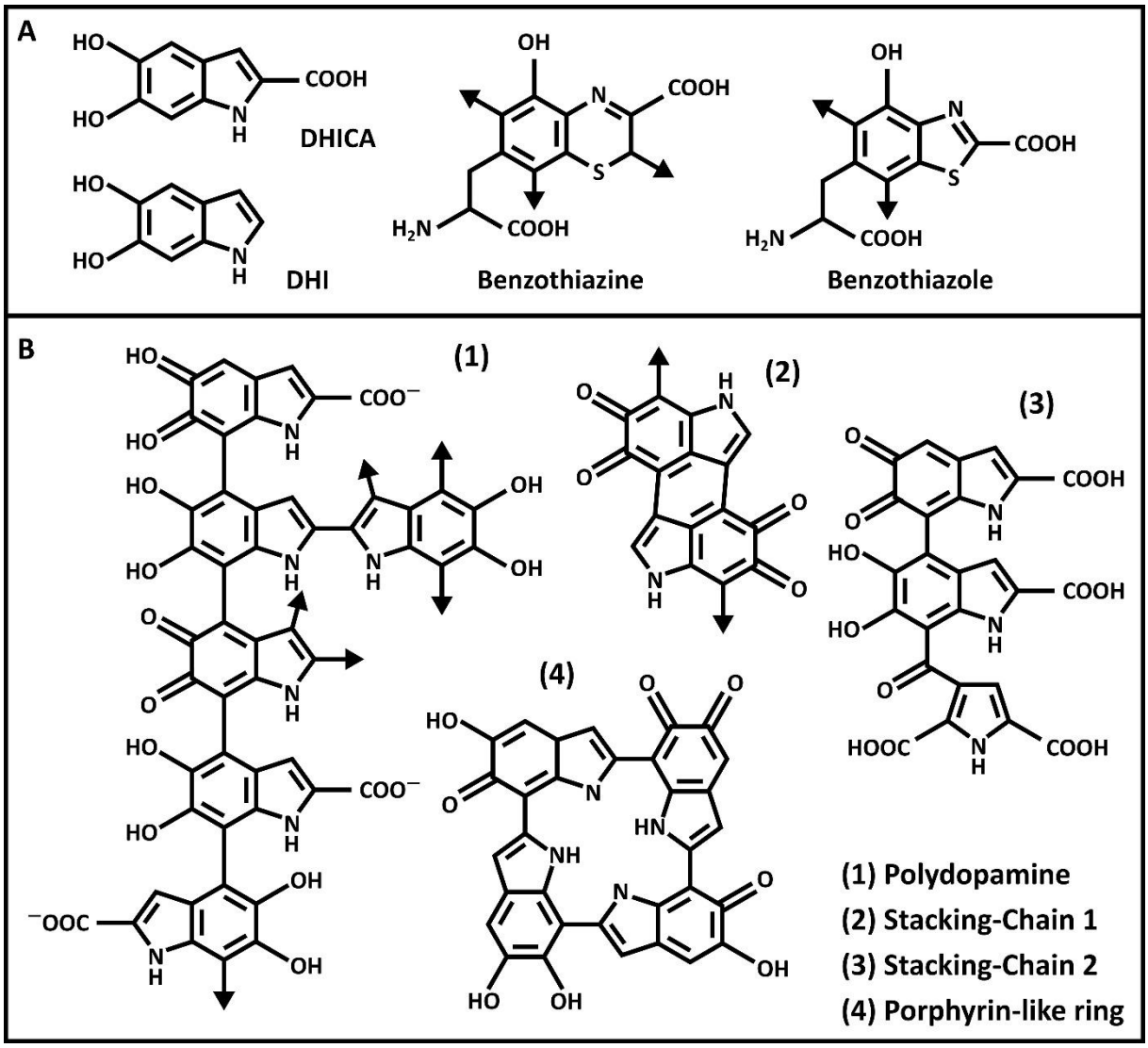

Figure 1.17. Eumelanin precursors and structures. (**A**) They are consisted of DHI and DHICA, and phaeomelanin by benzothiazine and benzothiazole units. (**B**) Examples of the eumelanin polymers, being consisted by the stacking-chain models, porphyrin-like ring, polydopamine and mix of DHI+DHICA.

Even though the chemical structures are estimates, it have been demonstrated experimentally that neuromelanins are distinct from eumelanins and phaeomelanins (Smythies, 1996). Its distribution is also limited to primates, where they constitute part of the *substantia nigra* of their brains and are related to Parkinson's disease (Bush et al., 2006). The formation of this pigment seem to be related to the mix of both polymers during the melanogenesis (Ito & Wakamatsu, 2008). Therefore, neuromelanins are composed of a phaeomelanin core with eumelanin sheath, where the former acts in photoprotection and the latter plays the antioxidant role (Ito & Wakamatsu, 2008).

1.4.2. The melanogenesis

The biosynthesis of melanins is complex and occur in parallel with the development of melanosomes. All these processes occur inside the melanophore or melanocytes. Although differences in melanogenesis exist, virtually all studies agree with the Raper-Mason pathway model, where it begins with the oxidation of the amino acid tyrosine (Fig. 1.18). Nevertheless, it is important to note that this biochemical route is not universal since in some animals, not all similar amino acids and enzymatic-catalysed mechanisms are required.

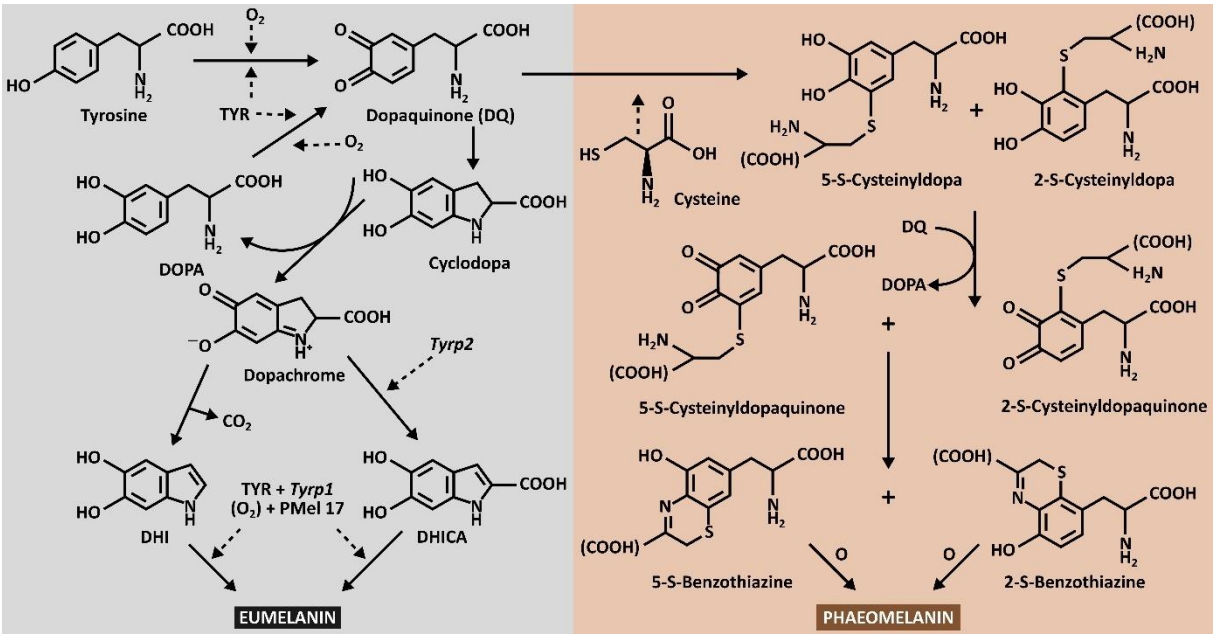

Figure 1.18. The synthesis of melanins. Simplified pathway of the Raper-Mason mode of melanogenesis of eumelanin and phaeomelanin, showing the amino acids involved in the biochemical reactions. From the oxidation of dopaquinone, two routes can be taken (not in this order), one will produce the eumelanin while the second will result in the cysteine-rich phaeomelanin. This image are based on several works, in particular of Ito (2003), Ito & Wakamatsu (2008), Ito et al. (2011), d'Ischia et al. (2013), and Solano (2014).

Despite this complexity, based on several works especially those of Ito (2003), Ito & Wakamatsu (2008), Wakamatsu et al. (2017), Ito et al. (2011), d'Ischia et al. (2013), Solano (2014), and Ito et al. (2018), the synthesis of eumelanins and phaeomelanins can be summarized. The melanogenesis begins with the incidence of the light radiation that stimulates the production of both autocrine and paracrine signals that induce the pro-opiomelanocortin hormone (POMC) in melanocytes/melanophores. The enzyme tyrosine hydroxylase (or simply tyrosinase, TYR) converts tyrosine into dihydroxyphenylalanine (DOPA). The repeated action of TYR oxides DOPA into dopaquinone (DQ). From there, the DQ can take two distinct routes where the dismutation of DQ will produce dopacysteine (CD) or dopachrome (DC) that eventually result in phaeomelanin and eumelanin, respectively. If weakly acidic media prevail, phaeomelanin will be favoured over eumelanin, which in turn, is dominated in neutral pH. In the first pathway, the DQ reacts with cysteine or thiol-containing compounds, which are mostly available at melanosome cell walls, giving rise to dopacysteine (CD) moieties. Further reactions with DQ and DOPA produces the dopacysteine-quinone, and the mixture of these derivatives result in the formation of benzothiazine and benzothiazole units, which upon oxidation and polymerization produce phaeomelanin. In the second path, the oxidation of DQ gives rise to cyclodopa, and further oxidizing effect transforms cyclodopa into dopachrome. This compound undergoes enzymatic reactions with dopachrome-tautomerase (DCT) that isomerize and oxidize, converting into DHI and DHICA. Subsequent reaction with TYR, tyrosine-related protein 1 (Tyr-1 or DHICA-oxidase), and premelanosome protein (Pmel-17) catalyse DHI and DHICA transforming it into many indole units that eventually polymerize into eumelanin.

The formation of small melanin grains (<120 nm) result in the creation of mature melanosomes. Perhaps, the first report of these nanometric particles was made by Girod (1882) who described the ink sacs of several cephalopod species; a process that was later demonstrated experimentally (Nofsinger et al., 2000; Palumbo, 2003; among others). Other authors were also able to report the earliest stages of melanosome development in other animals, such as in humans (Birbeck, 1963). For the sake of the rationale, here, the development of melanin grains are informally divided into five "phases" (Fig. 1.19). In the *phase I*, the indole monomers of melanin begin to bind each other at the unbranched carbon sites of the benzene ring. This assemblage end up in the *phase II* where groups of three to

five tetramers units set apart from each other at around 3.4 Å to 4.0 Å (Watt et al., 2009; Kim et al., 2016). During the *phase III*, these tetramers start to coalesce into small spherical nanometric vesicles (<60 nm) (Meng & Kaxiras, 2008). This assembling phenomenon continue to occur in the *phase IV*, where grains begin to aggregate into larger spheres (>100 nm) inside small and hollowed pre-melanosomal granules (Xiao et al., 2018). Finally, the *phase V* is characterized by the high number of these grains and their distribution inside the melanosomes, which can assume an organized form, in the case of rod-shaped and oblate eumelanosomes or organized/disorganized in spherical phaeomelanins (Xiao et al., 2018).

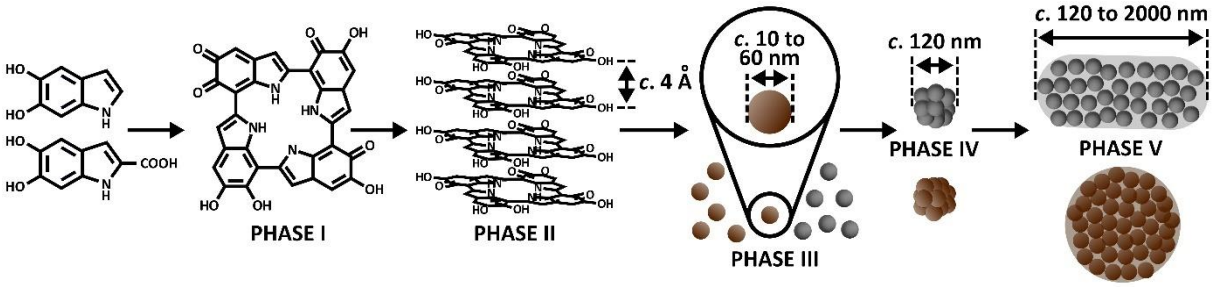

Figure 1.19. The synthesis of melanin grain. After the creation of small vesicles (ca. 10 to 60 nm), melanin start to be deposited inside and begin to coalescence into larger particles. When they reach an estimated size around 120 to 200 nm, grains cease to aggregate and the final format of melanosome begin to be formed, resulting in the elongated or oblate shape (eumelanosome) and spherical (phaeomelanin). This image are based on several works, in particular those of Birbeck (1963), Nofsinger et al. (2000); Palumbo (2003), and Xiao et al. (2018).

The melanosome granules began to take their typical shape when melanin grains are deposited into these unpigmented vesicles (pre-melanosomes). According to their size and morphology, melanosomes can be divided into spherical, rod-shaped, and oblate granules (Fig. 1.20, A and B). Other morphologies seem to derive from these shapes, such as the case of hollowed melanosomes (Fig. 1.20, C) that forms when the phaeomelanin core degrades during the late stages of melanosome development (Shawkey et al., 2015).

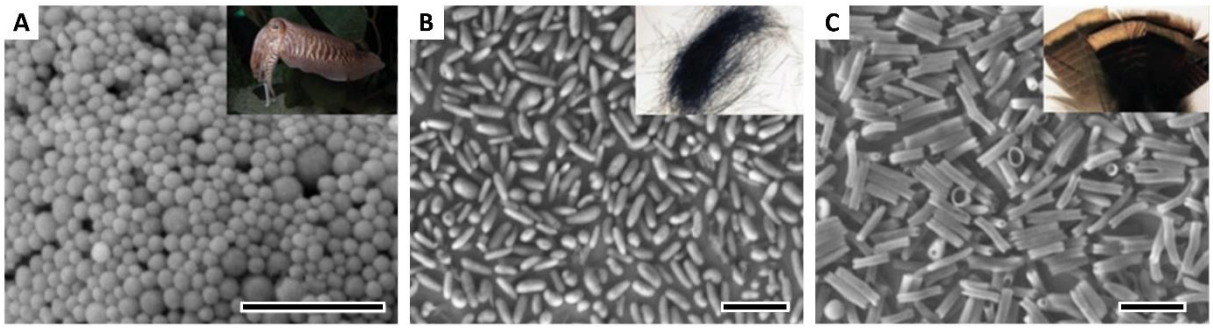

Figure 1.20. Shape diversity of melanosomes. (**A**) Spherical melanosomes from *Sepia officinalis*. (**B**) Rod-shaped and oblate shape of eumelanin from human hair. (**C**) Hollowed melanosomes from iridescent feathers of a wild turkey (*Melleagris gallopavo*). Images are modified from Xiao et al. (2018) with permission of the Royal Society (#1125707-2). Scalebars: (A) 1 µm, (B and C) 2 µm.

The development of melanosomes is marked by the increase in melanogenic activity, and hence, to internal pigmentation (Fig. 1.21, A and B), and the melanosome formation is also complex. However, it is summarized into four stages based on several studies (e.g., Raposo & Marks, 2002; Dell'Angelica, 2003; Raposo & Marks, 2007; Hurbain et al., 2008; Wasmeier et al., 2008; Delevoye et al., 2011; d'Ischia et al., 2013; Marks et al., 2013; D'Alba & Shawkey, 2019; Delevoye et al., 2019).

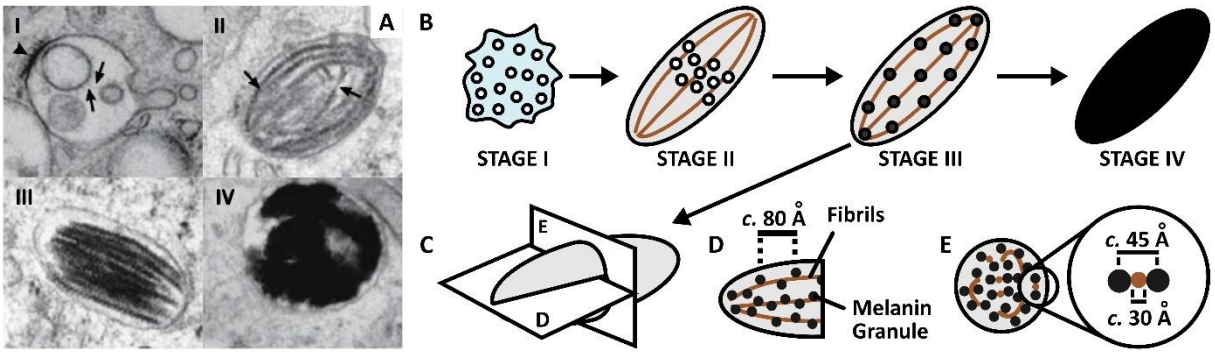

Figure 1.21. The synthesis of melanosome microbody. (**A**) Electron micrograph showing the four stages of melanosome development (each stage is outlined at top left) that is marked by the increase of melanisation; and (**B**) the interpretative drawing of the image in (A). (**C**) Axial plane of a melanosome (both Stage II and III), (**D**) transverse plane showing the fibrils and melanin granules, which usually are interspaced c. 80 Å. (**E**) Frontal plane exhibiting the arrangement of melanin granules and fibrils, as well as their dimensions (c. 45 Å and 30 Å, respectively). Image (A) extracted and modified from Raposo & Marks (2007) and used with permission of Springer Nature (#5083800485830), while all others are based on several works as explained in the text.

The *Stage I* begins with the formation and releasing of early endosomes from the endoplasmic reticulum (ER). Once in the melanocyte environment, these organelles can take two routes according to the prevail biochemistry; they can become lysosomes or pre-melanosomes. In the latter, the ER sends several biochemical signalling (e.g., TYR, Tyrp1, and Pmel-17) to the Golgi apparatus that deposits the melanogenic enzymes into these unpigmented vesicles. During the *Stage II*, the presence of Pmel-17 proteins result in the formation of the intraluminal protein fibrils (stretch marks), which are three-dimensional sheet-shape structures. Coeval to this process, and preceding melanin deposition, small spherical vesicles devoid of pigment ("*phase III*" of the formation of melanin grains) are also formed inside the pre-melanosome, where they end up attaching to fibrils. There, grains are apart to each other at around 45 Å to 80 Å, where they remain separated by the stretch marks that have an estimated dimension of ca. 30 Å (Fig. 1.21, C). In *Stage III*, the tyrosinase enzyme originated in the Golgi complex, is deposited in the melanosomes together with the TRP1 protein and the DCT. As the development unfolds and tyrosinase activity start to act, melanin is synthesized and deposited inside these microbodies or directly in the intralumenal

fibrils. This process results on browning and thickening of the organelle membranes. Sequentially, the increase of number or size of melanin grains spurs the development of an elongated or spherical morphology until the organelle becomes fully melanized. When the structure is completely darkened, the melanosome is finally matured, thus characterizing *Stage IV*.

1.4.3. The role of melanosomes

The primary role of melanins and melanosomes seem to protect organisms against environmental insults and pathogens. However, the remarkable characteristic of melanins is due to colour patterns that are widely used in many different ecological roles, especially in intra- and interspecific communication, camouflage, and display (Hill & McGraw, 2006). For instance, the plumage of sea-birds are generally darker in dorsal view while the ventral is predominantly light coloured. This pattern is important as it provides camouflage against predators (e.g., hawks) and preys (e.g., fish) by decreasing the contrast to the background environment colour (Cowan, 1972). Birds also use colouration as a form of communication between sexes, where bright strong colours of males are used as a honest signal of good health (McGraw et al., 2005; Hill & McGraw, 2006; Stavenga et al., 2011).

Melanin are also efficient in free radical scavenging, eliminating via reducing harmful species, such as singlet oxygen or superoxide anions, under varying pH and radical charge. In addition, due to its electronic properties, it is an efficient insulator converting light into heat. Therefore, this pigment is important for cellular protection, as it protects the cell nucleus and DNA from radiation and thermal damaging (Różanowska et al., 1999). Apart from colours, melanins and melanosomes also provides strengthen to deleterious physical effects, such as abrasion and softening of tissues. For example, experiments with melanized and unmelanized feathers demonstrated that pigmented feathers are 39% more resistant to than unpigmented counterparts, even when the keratin-matrix is thicker (Bonser, 1995).

Another role assumed by melanins is related to immune system of many organisms. In this scenario, melanisation of tissues can be seen during pathogens, acute diseases, inflammations, and tissue damaging both in invertebrates and vertebrates (Mackintosh, 2001; Agius & Roberts, 2003; Nappi & Christensen, 2005). For instance, matured melanosomes (Fig.

1.22, A) can be phagocyted by free moving macrophages, giving rise to melanomacrophages (Fig. 1.22, B). These cells are usually found in many hematopoietic tissues of vertebrates (e.g., spleen, kidney, and liver) and skin (Roberts, 1975; Wolke, 1992; Meseguer et al., 1994). When melanomacrophages aggregate in clusters, these cells forms larger bodies called melanomacrophages centres (Fig. 1.22, C). Their occurrence in tissues vary according to the age of the individual, tissue affected, number of pigment grains phagocyted, and overall size, which can reach up several micrometres (Agius & Roberts, 2003; Sayed & Younes, 2017). By its antibody-antigen and antimicrobial properties, the MMCs are involved in the removal of exogenous substances, in free radical scavenging, bacterial membrane breakdown, and recycling of wasted cellular residues (Agius & Roberts, 2003; Diaz-Satizabal & Magor, 2015).

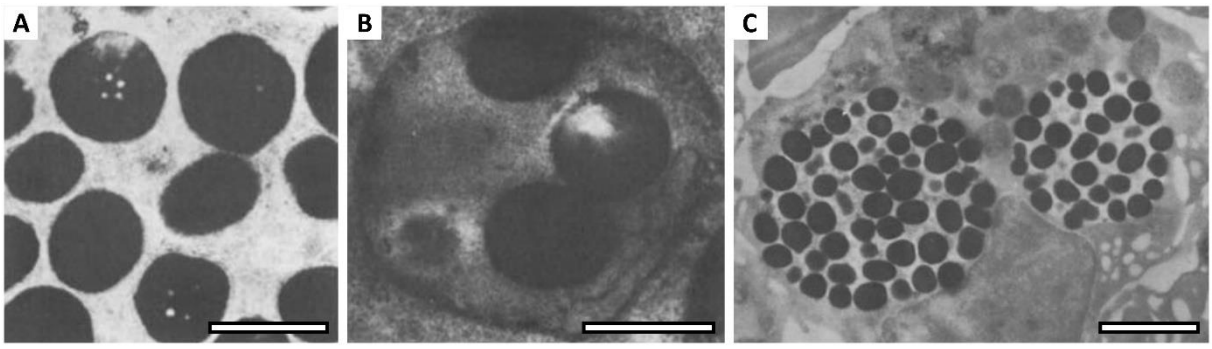

Figure 1.22. Melanosomes from melanomacrophage cells. (**A**) Electron micrograph of mature melanosomes from a melanomacrophage, where they exhibit a highly melanized internal content. (B) Melanomacrophage cell with three granules of melanosomes inside. (C) The melanomacrophage centre showing two melanomacrophages with multiple melanosomes inside. Images extracted from Agius & Agbede (1984) and are used with permission of John Wiley & Sons (#1125707-1). Scalebars: (A and B) 1 µm, (C) 3 µm.

1.4.4. Identification of melanins and melanosomes in extant samples and fossils

- ***Microscopic techniques.*** Because these organelles are nanometric (ca. 0.1 to 2.0 µm) in size, their identification in tissues (both fossil and extant) can only be accessed through the use of higher magnifications, such as optical microscopy (OM), confocal microscopy (COM), and scanning electron microscopy (SEM) (Fig. 1.23). In theory, both OM and COM are able to provide a maximum magnification of 1.000x, a feature that would make possible to inspect small areas (ca. 20 X 20 µm) of samples using normal light. Although COM is an easy and fast approach, the SEM is considered the most important as it allows the visualization of samples with even higher magnifications (up to 1×10^6), revealing topographical details. As such, SEM is a paramount technique to identify melanosomes in both extant samples and fossils, and hence, being used in virtually all studies in palaeocolour.

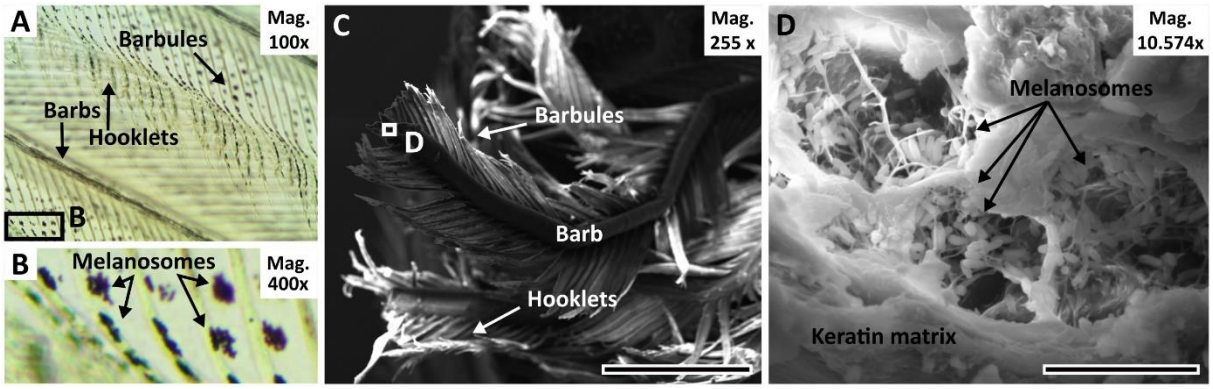

Figure 1.23. Melanosome identification in both optical and SEM. (**A**) OM image from a chicken wing feather and the (**B**) higher magnification of the black square in (A) showing melanosomes arranged in groups inside barbules. (**C**) SEM micrograph the hyacinth macaw (*Anodorhynchus hyacinthinus*) feather, and (D) higher magnification of the white square in (C). Scalebars: (C) 400 µm, (D) 10 µm.

- ***Elemental techniques.*** Although the morphologic identification of microbodies is sufficient for the recognition of melanosomes, the chemical analysis provides further evidence for these organelles. In this perspective, the Energy Dispersive Spectroscopy (EDS) is able to provide information about the presence and distribution of light elements above Be, in minute regions up to several nanometres (Fig. 1.24, A). Although semi-quantitative, through point-and-shoot and mapping analysis, it can also give information about relative intensity and concentrations (Schweitzer et al., 2008).

Another important technique is the Synchrotron Radiation micro-X-Ray Fluorescence (SR-µXRF), which is able to provide many elemental information in both, living and fossil specimens, such as the presence of heavy species, rare earth elements (RRE), major and trace elements, (Prado et al., 2021). In this perspective, the SR-µXRF allows the examination of elements that have affinity with melanin and melanosomes, such as Cu, Fe, Mn, Mg, and Zn (Wogelius et al., 2011; Gorniak et al., 2014a). Therefore, the SR-µXRF is important because: (1) it has a higher detecting resolution (of few microns); (2) high energy (between 5 to 20 kV), being able to detect minor elements; (3) it does not require vacuum conditions; (4) the interference between the electron beam and the sample surface is negligible or non-existent; (5) both point-and-shoot and mapping analysis can be performed in larger and thicker samples in much faster rate; (6) it also allows the quantitative analysis by using NIST standards (Prado et al., 2021).

Thus, the elemental analysis of both fossil and extant feathers can inform similarities in element concentrations or their diagenetic incorporation, giving clues about the taphonomic history of fossilized melanosomes/melanins (Fig. 1.24, A).

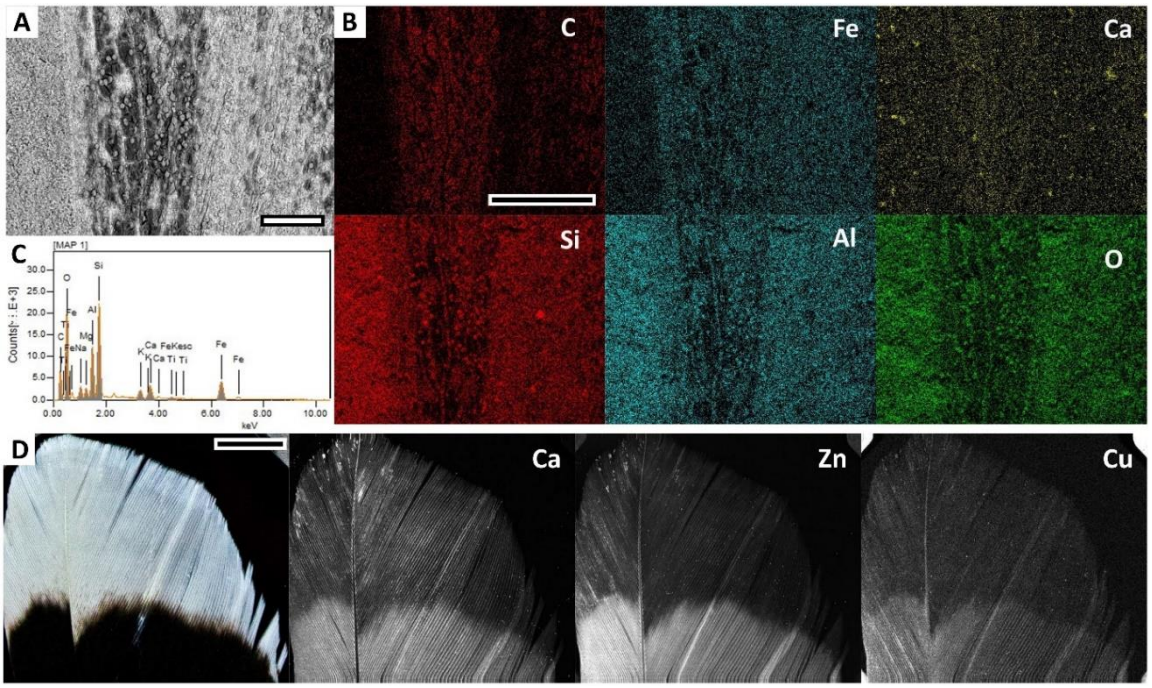

Figure 1.24. Elemental analysis of fossils with putative melanin. (**A-C**) EDS analysis of a fossil feather from the Eocene Green River Formation of USA showing the region analysed in the (A) backscattered image and the (B) elemental mapping and (C) spectroscopy. (**D**) Rapid Synchrotron Radiation X-Ray Fluorescence of extant feather tips showing different element distribution between melanized and unmelanized portions. Images are under CCBY 4.0 license and were taken and modified from (A-C) Moyer et al. (2014) and (D) Edwards et al. (2016). Scalebars: (A) 100 µm, (B) 200 µm, (D) 10 mm.

For instance, the presence of Cu and Zn in fossilized feathers and arthropods have been intensively studied as both elements are related to melanins and hemocyanin, respectively, but they can also be immobilized by diagenetic processes. In this scenario the recognition of their provenance and diagenetic behaviour (e.g., if they are native or if they migrated) is key to test whether these elements are either inorganic or remnants of the original pigment (Bergmann et al., 2010; Wogelius et al., 2011; Manning et al., 2013; Pushie et al., 2014; Barden et al., 2015; Egerton et al., 2015; Edwards et al., 2016). Therefore, SR-µXRF can reveal elements that may be chelated with organic molecules and recognize the molecular history of these fossils (Pushie et al., 2014). For instance, Edwards et al. (2016) performed the SR-µXRF analysis of several feathers to detect elements melanin (Fig. 1.24, B).

- ***Molecular techniques.*** The most common molecular techniques used to detect melanin (and other biochromes) are the vibrational spectroscopy (VS) and mass spectrometry (MS), such as: (a) Infrared (IR); (b) Raman Spectroscopy (RS); (c) High Performance Liquid Chromatography coupled with Mass Spectrometry (HPLC-MS); (d) Gas Chromatography Mass Spectrometry (GC-MS); (e) Time of Flight Secondary Ion Mass Spectrometry (TOF-SIMS).

Among the aforementioned techniques, the RS is an non-destructive, fast technique, relative costless, easier data processing, and most equipments and softwares are user friendly. This method is based on the photonic interaction with molecules on the sample surface, providing molecular information via the vibration modes between atoms (Fig. 1.25, A). For instance, bands of melanins are seen with peak shift varying around 8 to 41 cm^{-1} (Fig. 1.25, B), but centred in 1380 cm^{-1} where they are indicative of the vibration of N-H bonds of the pyrrole ring, while at 1580 cm^{-1} they indicate modes of C-C of phenyl rings or C-OH bonds of catechol (Fig. 1.25, A-C). Varied information can also be obtained through the analysis of spectral decomposition, where additional bands (i.e., functions) are revealed indicating further molecular bonds (Fig. 1.25, D)

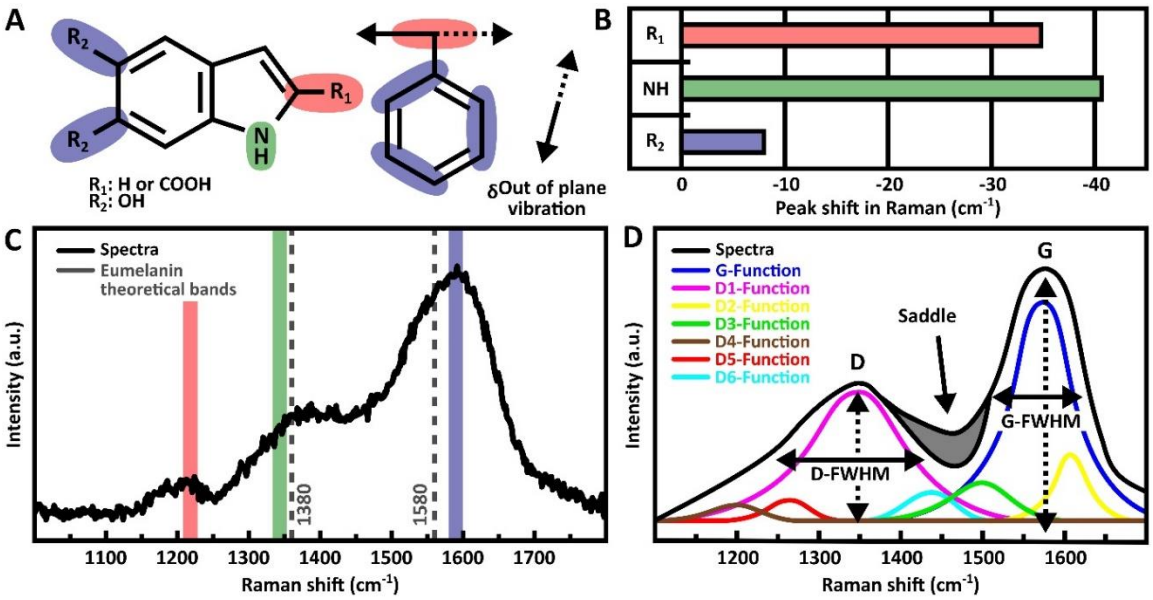

Figure 1.25. Characterization of the melanins through analytical techniques. (**A**) The generic 5,6-dihidroxiindole monomer and aryl showing the atomic bonds and sites that are excited by the laser beam. (**B**) Calculated peak shift from the standard melanin positions. (**C**) Spectra of Sepia melanin (Sigma-Aldrich M2649) exhibiting the sites of molecular interactions with laser excitation. (**D**) Decomposed spectra showing the components used to identify molecular bonds and spectral analysis. Image (A-C) is based on Kim et al. (2013) and (D) Henry et al. (2019).

Although RS and IR are suitable for chemical analysis of biochromes, for ancient materials the MS are quintessential since most are able to retrieve detailed molecular data (Schweitzer et al., 2008). Therefore, for the palaeocolour, they are able to provide information about the extent of alteration and preservation of biochromes in fossils. Inasmuch, the detection of melanin moieties via HPLC-MS is made through the degradation of the biochrome by an acidic/alkaline media followed by the identification of its subproducts (Fig. 1.26). For instance, the melanin breakdown is required to identify the molecules PDCA, PTCA, isoPTCA, and PTeCA from eumelanins (Fig. 1.26, A and B), and the aminohydroxyphenylalanine (AHP), 3-amino-4-hydroxyphenylalanine (3-AHP); 4-amino-3-hydroxyphenylalanine (4-AHP); 2-S-cysteinyldopa (2-S-CD) and 5-S-cysteinyldopa (5-S-CD), from phaeomelanins (Ito & Wakamatsu, 1998). Through the spectrogram analysis, it is possible to determine the precursor moiety based on the ratios of these monomers (Fig. 1.26, C), where DHI/DHICA indicate eumelanins and benzothiazole/benzothiazine for phaeomelanins. When PDCA/PTCA or PDCA/PTeCA values are high, it indicates DHI-rich melanin, whereas the opposite would indicate DHICA origin, and PTCA/PTeCA for geomelanins (Ito & Wakamatsu, 1998, 2003; Wakamatsu & Ito, 2002; Ito et al., 2004, 2011; Jarenmark et al., 2021).

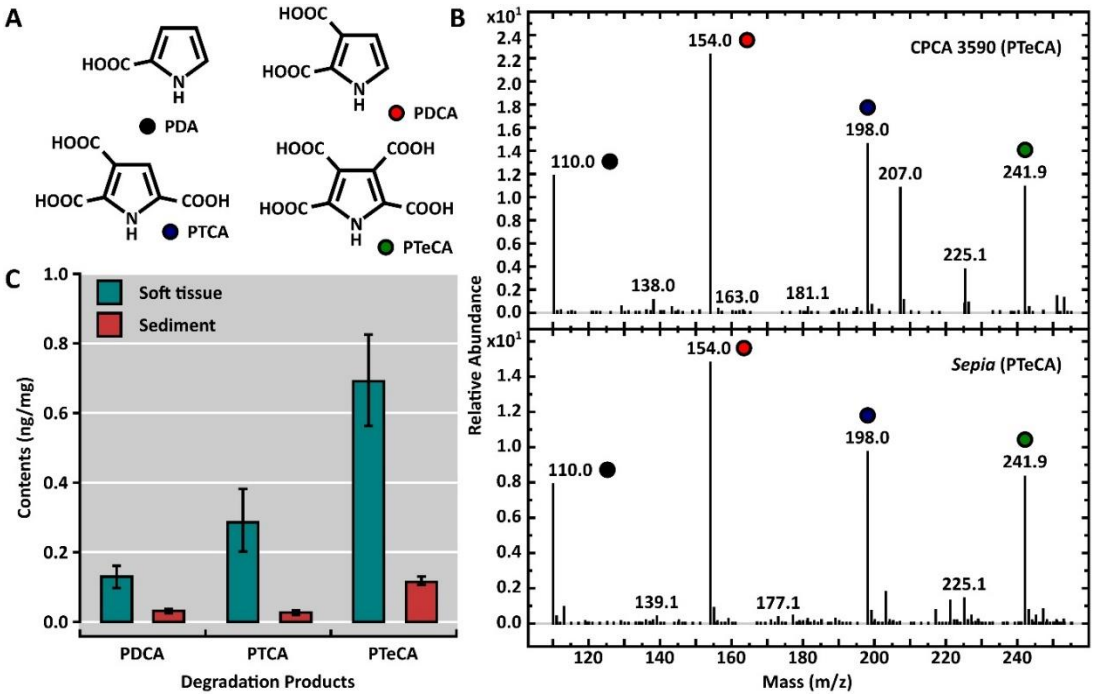

Figure 1.26. Characterization of the melanins through analytical techniques. (**A**) Mass spectrum of the aged eumelanin from a Cretaceous Crato Formation pterosaur *Tupandactylus imperator* (CPCA 3590), showing peaks of PDCA (red circle), PTCA (blue circle), and PTeCA (green circle). (**B**) The eumelanin yielding from the alkaline oxidation. Images (A and B) are a modified version of Pinheiro et al (2019) and used with CCBY 4.0 license.

1.5. REFERENCES

Agius, C., Agbede, S.A.(1984). An electron microscopical study on the genesis of lipofuscin, melanin and haemosiderin in the haemopoietic tissues of fish. *Journal of Fish Biology*, **24**, 471-488. DOI: 10.1111/j.1095-8649.1984.tb04818.x

Agius, C., Roberts, R.J. (2003). Melano-macrophage centres and their role in fish pathology. *Journal of Fish Diseases*, **26**, 499–509. DOI: 10.1046/j.1365-2761.2003.00485.x

Allison, P.A., Briggs, D.E.G. (1993). Exceptional fossil record: Distribution of soft-tissue preservation through the Phanerozoic. *Geology*, **21**, 527-530. DOI: 10.1130/0091-7613(1993)021<0527:EFRDOS>2.3.CO;2

Andrews, K., Reed, S.M., Masta, S.E. (2007). Spiders fluoresce variably across many taxa. *Biology Letters*, **3**, 265-267. DOI: 10.1098/rsbl.2007.0016

Anich, P.S., Anthony, S., Carlson, M., Gunnelson, A., Kohler, A.M., Martin, J.G., Olson, E.R. (2020). Biofluorescence in the platypus (*Ornithorhynchus anatinus*). *Mammalia*, **85**, 1-3. DOI: 10.1515/mammalia-2020-0027

Arnold, K.E., Owens, I.P.F., Marshall, N.J. (2002). Fluorescent signalling in parrots. *Science*, **295**, 92. DOI: 10.1126/science.295.5552.92

Assine, M.L. (1992). Análise estratigráfica da Bacia do Araripe, nordeste do Brasil. *Revista Brasileira de Geociências*, **22**, 289–300, DOI: 10.25249/0375-7536.1992289300

Assine, M.L. (2007). Bacia do Araripe. *Boletim de Geociências da Petrobrás*, **15**, 371–389.

Assine, M.L., Perinotto, J.A. de J., Custódio, M.A., Neumann, V.H., Varejão, F.G., Mescolotti, P.C. (2014). Sequências deposicionais do Andar Alagoas da Bacia do Araripe, nordeste do Brasil. *Boletim de Geociências da Petrobrás*, **22**, 3–28.

Barden, H.E., Behnsen, J., Bergmann, U., Leng, M.J., Manning, P.L., Withers, P.J., Wogelius, R.A., van Dongen, B.E. (2015). Geochemical evidence of the seasonality, affinity and pigmentation of *Solenopora jurassica*. *PLOS ONE*, **10**, e0138305. DOI: 10.1371/journal.pone.0138305

Barling, N., Martill, D.M., Heads, S.W. (2020). A geochemical model for the preservation of insects in the Crato Formation (Lower Cretaceous) of Brazil. *Cretaceous Research*, **116**, 104608. DOI: 10.1016/j.cretres.2020.104608

Barling, N., Martill, D.M., Heads, S.W., Gallien, F. (2015). High fidelity preservation of fossil insects from the Crato Formation (Lower Cretaceous) of Brazil. *Cretaceous Research*, **52**, 605–622, DOI: 10.1016/j.cretres.2014.05.007

Bechara, E.J.H., Stevani, C.V. (2018). Brazilian bioluminescent beetle: Reflections on catching glimpses of light in the Atlantic Forest and Cerrado. *Anais da Academia Brasileira de Ciências*, **90**, 663-679. DOI: 10.1590/0001-3765201820170504

Bellono, N.W., Oancea, E.V. (2014). Ion transport in pigmentation. *Archives of Biochemistry and Biophysics*, **563**, 35–41. DOI: 10.1016/j.abb.2014.06.020

Benton, M. (2017). Fossilization of soft tissues. *National Science Review*, **4**, 512–513. DOI: 10.1093/nsr/nwx095.

Bergmann, U., Morton, R.W., Manning, P.L., Sellers, W.I., Farrar, S., Huntley, K.G., Wogelius, R.A., Larson, P. (2010). *Archaeopteryx* feathers and bone chemistry fully revealed via synchrotron imaging. *Proceedings of the National Academy of Sciences of USA*, **107**, 9060-9065. DOI: 10.1073/pnas.1001569107

Bezerra, F.I., da Silva, J.H., Miguel, E. de C., Paschoal, A.R., Nascimento, D.R., Freire, P.T.C., Viana, B.C., Mendes, M. (2020). Chemical and mineral comparison of fossil insect cuticles from Crato *Konservat Lagerstätte*, Lower Cretaceous of Brazil. *Journal of Iberian Geology*, **46**, 61-76. DOI: 10.1007/s41513-020-00119-y

Bezerra, F.I., Silva, J.H., Paula, A.J., Oliveira, N.C., Paschoal, A.R., Freire, P.T.C., Neto, B.C.V., Mendes, M. (2018). Throwing light on an uncommon preservation of Blattodea from the Crato Formation (Araripe Basin, Cretaceous), Brazil. *Revista Brasileira de Paleontologia*, **21**, 245–254. DOI: 10.4072/rbp.2018.3.05

Bezerra, F.I., Solórzano-Kraemer, M.M., Mendes, M. (2021). Distinct preservational pathways of insects from the Crato Formation, lower Cretaceous of the Araripe Basin, Brazil. *Cretaceous Research*, **118**, 104631. DOI: 10.1016/j.cretres.2020.104631

Birbeck, M.S. (1963). Electron microscopy of melanocytes: The fine structure of hair-bulb premelanosomes. *Annals of the New York Academy of Sciences*, **100**, 540-547. DOI: 10.1111/j.1749-6632.1963.tb42871.x

Bonser, R.H.C. (1995). Melanin and the abrasion resistance of feathers. *The Condor*, **97**, 590–591. DOI: 10.2307/1369048

Borovanský, J., Riley, P.A. (2011). Melanin and Melanosomes: Biosynthesis, biogenesis, physiological, and pathological functions. *Wiley-Blackwell*, **429** p. DOI: 10.1002/9783527636150

Borovanský, J., Riley, P.A. (2011). Melanins and Melanosomes: Weinheim, Germany, Wiley-*VCH Verlag GmbH & Co. KGaA*, 430 p. DOI: 10.1002/9783527636150

Briggs, D.E.G. (2003). The role of biofilms in the fossilization of non-biomineralized tissues. In: Krumbein, W.E., Paternson, D.M., Zavarzin, G.A. (Eds.). Fossil and Recent Biofilm: A natural history of life on Earth. Amsterdam, Netherland: *Springer*, pp. 281-290. DOI: 10.1007/978-94-017-0193-8_18

Briggs, D.E.G., Moore, R.A., Shultz, J.W., Schweigert, G. (2005). Mineralization of soft-part anatomy and invading microbes in the horshoe crab *Mesolimulus* from the Upper Jurassic Lagerstätte of Nuspligen, Germany. *Proceedings of the Royal Society B*, **272**, 627-632. DOI: 10.1098/rspb.2004.3006

Briggs, D.E.G., McMahon, S. (2016). The role of experiments in investigating the taphonomy of exceptional preservation. *Palaeontology*, **59**, 1-11. DOI: 10.1111/pala.12219

Briggs, D.E.G., Summons, R.E. (2014). Ancient biomolecules: Their origins, fossilization, and role in revealing the history of life. *BioEssays*, **36**, 482–490. DOI: 10.1002/bies.201400010

Bush, W.D., Garguilo, J., Zucca, F.A., Albertini, A., Zecca, l., Edwards, G.S., Nemanich, R.J., Simon, J.D. (2006). The surface oxidation potential of human neuromelanin reveals a spherical architecture with a pheomelanin core and an eumelanin surface. *Proceedings of the National Academy of Sciences of USA*, **103**, 14785-14789. DOI: 10.1073/pnas.0604010103

Cabral, F.A.A., Silveira, A.C., Ramos, G.M.S., Miranda, T.S., Barbosa, J.A., Neumann, V.H.M.L. (2019). Microfacies and diagenetic evolution of the limestones of the upper part of the Crato Formation, Araripe Basin, northeastern Brazil. *Brazilian Journal of Geology*, **49**, e20180097. DOI: 10.1590/2317-4889201920180097

Campos, A.P.C., Carvalho, R.T. de, Straker, L.C., Salgado, L.T., Kellner, A., Fatina, M. (2019). Combined microscopy and spectroscopy techniques to characterize a fossilized feather with minimal damage to the specimen. *Micron*, **120**, 17–24, DOI: 10.1016/j.micron.2019.01.016.

Carvalho, M.S.S., Santos, M.E.C.M. (2005). Histórico das pesquisas paleontológicas na bacia do Araripe, nordeste do Brasil. *Anuário do Instituto de Geociências*, **28**, 15–34, http://www.ppegeo.igc.usp.br/index.php/anigeo/article/view/4845.

Castro, J.C., Valença, L.M.M., Neumann, V.H. (2006). Ciclos e Sequências Deposicionais das Formações Rio da Batateira e Santana (Andar Alagoas), Bacia do Araripe, Brasil. *Geociências*, **25**, 289–296.

Catto, B., Jahnert, R.J., Warren, L.V., Varejão, F.G., Assine, M.L. (2016). The microbial nature of laminated limestones: Lessons from the Upper Aptian, Araripe Basin, Brazil. *Sedimentary Geology*, **341**, 304–315, DOI: 10.1016/j.sedgeo.2016.05.007

Celestino, M.A.L., Miranda, T.S., Mariano, G., Alencar, M.L., Buckman, J., Roberts, N.M.W., Barbosa, J.A., Neumann, V.H.M.L., Souza, J.A.B., Roemers-Oliveira, E. (2021). Structural control and geochronology of Cretaceous carbonate breccia pipes, Crato Formation, Araripe Basin, NE Brazil. *Marine and Petroleum Geology*, **132**, 105190. DOI: 10.1016/j.marpetgeo.2021.105190

Cincotta, A., Nicolai, M., Nascimento-Campos, H.B., McNamara, M. D'Alba, L., Shawkey, M.D., Kischlat, E.-E., Yans, J., Carleer, R., Escuillié, F., Godefroit, P. (2022). Pterosaur melanosomes support signaling functiong for early feathers. *Nature*, **604**, 684-688. DOI: 10.1038/s41586-022-04622-3

Clements, T., Dolocan, A., Martin, P., Purnell, M.A., Vinther, J., Gabbott, S.E. (2016). The eyes of *Tullimonstrum* reveal a vertebrate affinity. *Nature*, **532**, 500–503, DOI: 10.1038/nature17647

Coimbra, J.C., Arai, M., Carreño, A.L. (2002). Biostratigraphy of Lower Cretaceous microfossils from the Araripe basin, northeastern Brazil. *Geobios*, **35**, 687–698, DOI: 10.1016/S0016-6995(02)00082-7

Colleary, C., Dolocan, A., Gardner, J., Singh, S., Wuttke, M., Rabenstein, R., Habersetzer, J., Schaal, S., Feseha, M., Clemens, M., Jacobs, B.F., Currano, E.D., Jacobs, L.L., Sylvestersen, R.L., Gabbott, S.E., Vinther, J. (2015). Chemical, experimental, and morphological evidence for diagenetically altered melanin in exceptionally preserved fossils. *Proceedings of the National Academy of Sciences of USA*, **112**, 12592–12597. DOI: 10.1073/pnas.1509831112

Commo, S., Wakamatsu, K., Lozano, I., Panhard, S., Loussouarn, G., Bernard, B.A., Ito, S. (2012) Age-dependent changes in eumelanin composition in hairs of various ethnic origins.

International Journal of Cosmetic Science, **34**, 102-107. DOI: 10.1111/j.1468-2494.2011.00691.x

Cowan, P.J. (1972). The contrast and coloration of sea-birds: An experimental approach. *Ibis*, **114**, 390-393. DOI: 10.1111/j.1474-919X.1972.tb00837.x

Cuthill, I.C., Allen, W.L., Arbuckle, K., Caspers, B., Chaplin, G., Hauber, M.E., Hill, G.E., Jablonski, N.G., Jiggins, C.D., Kelber, A., Mappes, J., Marshall, J., Merril, R., Osorio, D., Prum, R., Roberts, N.W., Roulin, A., Rowland, H.M., Sherrat, T.N., Skelhorn, J., Speed, M.P., Stevens, M., Stoddard, M.C., Stuart-Fox, D., Talas, L., Tibbets, E., Caro, T. (2017). The biology of color. *Science*, **357**, eaan0221. DOI: 10.1126/science.aan0221

D'Alba, L., Shawkey, M.D. (2019). Melanosomes: Biogenesis, properties, and evolution of an ancient organelle. *Physiological Reviews*, **99**, 1–19, DOI: 10.1152/physrev.00059.2017

Davy, A.D., Birch, D.J.S., 2018, Evidence for pheomelanin sheet structure. *Applied Physics Letters*, **113**, 263701. DOI: 10.1063/1.5066081

Delevoye, C., Giordano, F., Marks, M.S., Raposo, G. (2011). Biogenesis of melanosomes: In Borovanský, J., Riley, P.A. (eds). Melanins and melanosomes: Biosynthesis, biogenesis, physiological, and pathological functions. *Wiley-Blackwell*, 247-284. ISBN: 978-3-527-32892-5

Delevoye, C., Marks, M.S., Raposo, G. (2019). Lysosome-related organelles as functional adaptations of the endolysosomal system. *Current Opinion in Cell Biology*, **59**, 147-158. DOI: 10.1016/j.ceb.2019.05.003

Delgado, A.D.O., Buck, P.V., Osés, G.L., Ghilardi, R.P., Rangel, E.C., Pacheco, M.L.A.F. (2014). Paleometry: A brand new area in Brazilian science. *Materials Research*, **17**, 1434-1441. DOI: 10.1590/1516-1439.288514

Dell'angelica, E.C. (2003). Melanosome biogenesis: shedding light on the origin of an obscure organelle. *Trends in Cell Biology*, **13**, 503-506. DOI: 10.1016/j.tcb.2003.08.001

Dias, J.J., Carvalho, I.S. (2020). Remarkable fossil crickets preservation from Crato Formation (Aptian, Araripe Basin), a *Lagerstätten* from Brazil. *Journal of South American Earth Sciences*, **98**, 102443. DOI: 10.1016/j.jsames.2019.102443

Dias, J.J., Carvalho, I.S. (2022). The role of microbial mats in the exquisite preservation of Aptian insect fossils from the Crato Lagerstätte, Brazil. *Cretaceous Research*, **130**, 105068. DOI: 10.1016/j.cretres.2021.105068

Diaz-Satizabal, l., Magor, B.G. (2015). Isolation and cytochemical characterization of melanomacrophages and melanomacrophage clusters from goldfish (*Carassius auratus*, L.). *Developmental & Comparative Immunology*, **48**, 221-228. DOI: 10.1016/j.dci.2014.10.003

d'Ischia, M., Wakamatsu, K., Napolitano, A., Briganti, S., Garcia-Borron, J.-C., Kovacs, D., Meredith, P., Pezzella, A., Ricardo, M., Sarna, T., Simon, J.D., Ito, S. (2013). Melanins and melanogenesis: methods, standards, protocols. *Pigment Cell & Melanoma Research*, **26**, 616-633. DOI: 10.1111/pcmr.12121

Dubey, S., Roulin, A. (2014). Evolutionary and biomedical consequences of internal melanins. *Pigment Cell & Melanoma Research*, **27**, 327-338. DOI: 10.1111/pcmr.12231

Edwards, N.P., Manning, P.L., Wogelius, R.A. (2014). Pigments through time. *Pigment Cell & Melanoma Research*, **27**, 684–685, DOI: 10.1111/pcmr.12271

Edwards, N.P., van Veelen, A., Anné, J., Manning, P.l., Bergmann, U., Sellers, W.I., Egerton, V.M., Sokaras, D., Alonso-Mori, R., Wakamatsu, K., Ito, S., Wogelius, R.A. (2016). Elemental characterisation of melanin in feathers via synchrotron X-ray imaging and absorption spectroscopy. *Scientific Reports*, **6**, 34002. DOI: 10.1038/srep34002

Egerton, V.M., Wogelius, R.A., Norell, M.A., Edwards, N.P., Sellers, W.I., Bergmann, U., Sokaras, D., Alonso-Mori, R., Ignatyev, K., van Veelen, A., Anné, j., van Dongen, B., Knoll, F., Manning, P.L. (2015). The mapping and differentiation of biological and environmental elemental signatures in the fossil remains of a 50 million year old bird. *Journal of Analytical Atomic Spectrometry*, **30**, 627-634. DOI: 10.139/c4a00395k

Eliason, C.M., Hudson, L., Watts, T., Garza, H., Clarke, J.A. (2017). Exceptional preservation and the fossil record of tetrapod integument. *Proceedings of the Royal Society B: Biological Sciences*, **284**, 20170556, DOI: 10.1098/rspb.2017.0556

Eliason, C.M., Shawkey, M.D., Clarke, J.A. (2016). Evolutionary shifts in the melanin-based color system of birds. *Evolution*, **70**, 445–455. DOI: 10.1111/evo.12855

El-Naggar, N., El-Ewasy, S.M. (2017). Bioproduction, characterization, anticancer and antioxidant activities of extracelullar melanin pigment produced by newly isolated microbial cell factories Streptomyces glaucescens NEAE-H. *Scientific Reports*, **7**, 42129. DOI: 10.1038/srep42129

Falk, H., Wolkenstein, K. (2017). Natural product molecular fossils. In: A.D. Kinghorn, A.D., Falk, H., Gibbons, S., Kobayashi, J. (Eds). Progress in the chemistry of organic natural products. *Springer International Publishing AG*, **104**, 1-109. DOI: 10.1007/978-3-319-45618-8_1

Fambrini, G.L., Menezes-Filho, J.A.B., Jesuíno, P.C.L., Araújo, J.T., Durval, L.G.L., Neumann, V.H.M.L. (2015). Sucessão Faciológica da Formação Barbalha, Bacia do Araripe, Nordeste do Brasil. *Estudos Geológicos*, **25**, 137–164. DOI: 10.18190/1980-8208/estudosgeologicos.v25n1p137-164

Feo, T.J., Field, D.J., Prum, R.O. (2015). Barb geometry of asymmetrical feathers reveals a transitional morphology in the evolution of avian flight. *Proceedings of the Royal Society B*, **282**, 20142864. DOI: 10.1098/rspb.2014.2864

Gabbott, S.E., Donoghue, P.C.J., Sansom, R.S., Vinther, J., Dolocan, A., Purnell, M.A. (2016). Pigmented anatomy in carboniferous cyclostomes and the evolution of the vertebrate eye. *Proceedings of the Royal Society B*, **283**, 20161151. DOI: 10.1098/rspb.2016.1151

Girod, P. (1882). Recherches sur la poche du noir des Céphalopodes des côtes de France. *Archives de Zoologie Expérimentale et Générale*, **10**, 1-100. ISSN: 00039667

Glagoleva, A.Y., Shoeva, O.Y., Khlestkina, E.K. (2020). Melanin pigment in plants: Current knowledge and future perspective. *Frontiers in Plant Science*, **11**, 770. DOI: 10.3389/fpls.2020.00770

Glass, K., Ito, S., Wilby, P.R., Sota, T., Nakamura, A., Bowers, C.R., Miller, K.E., Dutta, S., Summons, R.E., Briggs, D.E.G., Wakamatsu, K., Simon, J.D. (2013). Impact of diagenesis and maturation on the survival of eumelanin in the fossil record. *Organic Geochemistry*, **64**, 29-37. DOI: 10.1016/j.orggeochem.2013.09.002

Glass, K., Ito, S., Wilby, P.R., Sota, T., Nakamura, A., Bowers, C.R., Vinther, J., Dutta, S., Summons, R., Briggs, D.E.G., Wakamatsu, K., Simon, J.D. (2012). Direct chemical evidence for eumelanin pigment from the Jurassic period. *Proceedings of the National Academy of Sciences of USA*, **109**, 10218-10223. DOI: 10.1073/pnas.1118448109

Gomes, A.L.S., Becker-Kerber, B., Osés, G.L., Prado, G., Becker Kerber, P., de Barros, G.E.B., Galante, D., Rangel, E., Bidola, P., Herzen, J., Pfeiffer, F., Rizzutto, M.A., Pacheco, M.L.A.F. (2019). Paleometry as a key tool to deal with paleobiological and astrobiological issues:

some contributions and reflections on the Brazilian fossil record. International Journal of *Astrobiology*, **18**, 1–15. DOI: 10.1017/S1473550418000538

Gorniak T, Haraszti T, Garamus VM, Buck AR, Senkbeil T, Priebe, M., Hedberg-Buenz, A., Koehn, D., Salditt, T., Grunze, M., Anderson, M.G., Rosenhahn, A. (2014a). Nano-Scale morphology of melanosomes revealed by small-angle X-ray scattering. *PLOS ONE*, **9**, e90884. DOI: 10.1371/journal.pone.0090884

Gorniak, T., Haraszti, T., Suhonen, H., Yang, Y., Hedberg-Buenz, A., Koehn, D., Heine, R., Grunze, M., Rosenhahn, A., Anderson, M. G. (2014b). Support and challenges to the melanosomal casing model based on nanoscale distribution of metals within iris melanosomes detected by X-ray fluorescence analysis. *Pigment Cell & Melanoma Research*, **27**, 831-834. DOI: 10.1111/pcmr.12278

Goutte, S., Mason, M.J., Antoniazzi, M.M., Jared, C., Merle, D., Cazes, L., Toledo, L.F., el-Hafci, H., Pallu, S., Portier, H., Schramm, S., Gueriau, P., Thoury, M. (2019). Intense bone fluorescence reveals hidden patterns in pumpkin toadlets. *Scientific Reports*, **9**, 5388. DOI: 10.1038/s41598-019-41959-8

Gren, J.A., Sjövall, P., Eriksson, M.E., Sylvestersen, R.L., Marone, F., Sigfridsson Clauss, K.G. V., Taylor, G.J., Carlson, S., Uvdal, P., Lindgren, J. (2017). Molecular and microstructural inventory of an isolated fossil bird feather from the Eocene Fur Formation of Denmark. *Palaeontology*, **60**, 73–90. DOI: 10.1111/pala.12271

Gueneli, N., McKenna, A.M., Ohkouchi, N., Boreham, C.J., Beghin, J., Javaux, E.J., Brocks, J.J. (2018). 1.1-billion-year-old porphyrins establish a marine ecosystem dominated by bacterial primary producers. *Proceedings of the National Academy of Sciences of USA*, **115**, E6978–E6986. DOI: 10.1073/pnas.1803866115

Gupta, N.S. (2014). Biopolymers. Dordrecht, Springer Netherlands, *Topics in Geobiology*, **38**, 174 p. DOI: 10.1007/978-94-007-7936-5

Haugarvoll, E., Thorsen, J., Laane, M., Huang, Q., Koppang, E.O. (2006). Melanogenesis and evidence for melanosome transport to the plasma membrane in a CD83+ teleost leukocyte cell line. *Pigment Cell Research*, **19**, 214–225. DOI: 10.1111/j.1600-0749.2006.00297.x

Heimhofer, U., Ariztegui, D., Lenniger, M., Hesselbo, S.P., Martill, D.M., Rios-Netto, A.M. (2010). Deciphering the depositional environment of the laminated Crato fossil beds (Early

Cretaceous, Araripe Basin, North-eastern Brazil). *Sedimentology*, **57**, 677–694. DOI: 10.1111/j.1365-3091.2009.01114.x

Heimhofer, U., Martill, D.M. (2007). The sedimentology and depositional environment of the Crato Formation. In: Martill, D.M., Bechly, G., Loveridge, R.F. (eds). The Crato Fossil Beds of Brazil: Window into an Ancient World. Oxford, UK, *Cambridge University Press*, 44–62. DOI: 10.1017/CBO9780511535512.005

Henry, D.G., Jarvis, I., Gillmore, G., Stephenson, M. (2019). Raman spectroscopy as a tool to determine the thermal maturity of organic matter: Application to sedimentary, metamorphic and structural geology. *Earth-Science Reviews*, **198**, 102936. DOI: 10.1016/j.earscirev.2019.102936

Hill, G.E., McGraw, K.J. (2006). Bird coloration Volume II: Function and evolution. Cambridge, Massachusetts, *Harvard University Press*, 477 p. ISBN: 97806740211761

Horčičko, J., Borovanský, J., Duchoň, J., Procházková, B. (1973). Distribution of zinc and copper in pigmented tissues. *Hoppe-Seyler's Zeitschrift fur Physiologische*, **354**, 203-204. DOI: 10.1515/bchm2.1973.354.1.203

Hsin-Su, Y. (1999). The Pigmentary System. *Physiology and Pathophysiology*, **135**, 478–478. DOI: 10.1001/archderm.135.4.478

Hurbain, I., Geerts, W.J.C., Boudier, T., Marco, S., Verkleij, A.J., Marks, M.S., Raposo, G. (2008). Electron tomography of early melanosomes: Implications for melanogenesis and the generation of fibrillar amyloid sheets. *Proceedings of the National Academy of Sciences of USA*, **105**, 19726-19731. DOI: 10.1073/pnas.0803488105

Ikawa, M., Sasner, J.J., Haney, J.F., Foxall, T.L. (1995). Pterins of the cyanobacterium *Aphanizomenon flos-aquae*. *Phytochemistry*, **38**, 1229-1232. DOI: 10.1016/0031-9422(94)00775-O

Iniesto, M., Blanco-Moreno, C., Villalba, A., Buscalioni, A.D., Guerrero, M.C., López-Archilla, A.I. (2018). Plant tissue decay in long-term experiments with microbial mats. *Geosciences*, **8**, 387. DOI: 10.3390/geosciences8110387

Iniesto, M., Gutiérrez-Silva, P., Dias, J.J., Carvalho, I.S., Buscalioni, A.D., López-Achilla, A.I. (2021). Soft tissue histology of insect larvae decayed in laboratory experiments using microbial mats: Taphonomic comparison with Cretaceous fossil insects from the

exceptionally preserved biota of Araripe, Brazil. *Palaeogeography, Palaeoclimatology, Palaeoecology*, **564**, 110156. DOI: 10.1016/j.cretres.2021.105068

Ito, S. (2003). A chemist's view of melanogenesis. *Pigment Cell Research*, **16**, 230-236. DOI: 10.1034/j.1600-0749.2003.00037.x

Ito, S., Nakanishi, Y., Valenzuela, R.K., Brilliant, M.H., Kolbe, L., Wakamatsu, K. (2011). Usefulness of alkaline hydrogen peroxide oxidation to analyze eumelanin and pheomelanin in various tissue samples: application to chemical analysis of human hair melanins. *Pigment Cell & Melanoma Research*, **24**, 605-613, DOI: 10.1111/j.1755-148X.2011.00864.x

Ito, S., Wakamatsu, K. (1998). Chemical degradation of melanins: Application to identification of dopamine-melanin. *Pigment Cell Research*, **11**, 120–126, DOI: 10.1111/j.1600-0749.1998.tb00721.x

Ito, S., Wakamatsu, K. (2003). Quantitative analysis of eumelanin and pheomelanin in humans, mice, and other animals: A comparative review. *Pigment Cell Research*, **16**, 523–531. DOI: 10.1034/j.1600-0749.2003.00072.x

Ito, S., Wakamatsu, K., Glass, K.E., Simon, J.D. (2013). High-performance liquid chromatography estimation of cross-linking of dihydroxyindole moiety in eumelanin. *Analytical Biochemistry*, **434**, 221–225, DOI: 10.1016/j.ab.2012.12.005

Ito, S., Wakamatsu, K., Ozeki, H. (2004). Chemical analysis of melanins and its application to the study of the regulation of melanogenesis. *Pigment Cell Research*, **13**, 103–109, DOI: 10.1034/j.1600-0749.13.s8.19.x

Itou, T. (2018). Morphological changes in hair melanosomes by aging. *Pigment Cell & Melanoma Research*, **31**, 630–635. DOI: 10.1111/pcmr.12697

Itou, T., Ito, S., Wakamatsu, K. (2019). Effects of aging on hair color, melanosome morphology, and melanin composition in japanese females. *International Journal of Molecular Science*, **20**, 3739. DOI: 10.3390/ijms20153739

Jarenmark, M., Sjövall, P., Ito, S., Wakamatsu, K., Lindgren, J. (2021). Chemical evaluation of eumelanin maturation by ToF-SIMS and Alkaline Peroxide Oxidation HPLC Analysis. *International Journal of Molecular Sciences*, **22**, 161. DOI: 10.3390/ijms22010161

Kaxiras, E., Tsolakidis, A., Zonios, G., Meng, S. (2006). Structural model of eumelanin. *Physical Review Letters*, **97**, 1-4. DOI: 10.1103/PhysRevLett.97.218102

Kim, Y.J., Khetan, A., Wu, W., Chun, S.-E., Viswanathan, V., Whitacre, J.F., Bettinger, C.J. (2016). Evidence of porphyrin-like structures in natural melanin pigments using electrochemical fingerprinting. *Advanced Materials*, **28**, 3173-3180. DOI: 10.1002/adma.201504650

Kim, Y.J., Wu, W., Chun, S.-E., Whitacre, J.F., Bettinger, C.J. (2013). Biologically derived melanin electrodes in aqueous sodium-ion energy storage devices. *Proceedings of the National Academy of Sciences of USA*, **110**, 20912-20917. DOI: 10.1073/pnas.1314345110

Košták, M., Jagt, J.W.M. (2018). A new species of *Sepia* (Cephalopoda, Coleoidea) from the Miocene of northwest Germany: a contribution to sepiid palaeobiogeography. *Neues Jahrbuch für Geologie und Paläontologie - Abhandlungen*, **288**, 273-281. DOI: 10.1127/njgpa/2018/0741

Košťák, M., Schlögl, J., Culka, A., Tomašových, A., Mazuch, M., Hudáčková, N. (2018). The unique preservation of *Sepia* soft tissues in the Miocene deposits (Serravalian, Vienna Basin): Implications for the origin of microbodies in the fossil record. *Palaeogeography, Palaeoclimatology, Palaeoecology*, **493**, 111-118. DOI: 10.1016/j.palaeo.2018.01.005

Leite, K.J.G. (2013). Novo anuro do Membro Crato (Aptiano) da Formação Santana, Bacia do Araripe. Dissertação (Mestrado em Geologia). *Universidade Federal do Ceará*, 76 f.

Li, Q., Clarke, J.A., Gao, K.-Q., Zhou, C.-F., Meng, Q., Li, D., D'Alba, L., Shawkey, M.D. (2014). Melanosome evolution indicates a key physiological shift within feathered dinosaurs. *Nature*, **507**, 350–353. DOI: 10.1038/nature12973

Li, Q., Gao, K.-Q., Meng, Q., Clarke, J.A., Shawkey, M.D., D'Alba, L., Pei, R., Ellison, M., Norell, M.A., Vinther, J. (2012). Reconstruction of *Microraptor* and the Evolution of Iridescent Plumage. *Science*, **335**, 1215–1219. DOI: 10.1126/science.1213780

Liebig, K., Westall, F., Schmitz, M. (1996). A study of fossil microstructures from the Eocene Messel Formation using Transmission Electron Microscopy. *Neues Jahrbuch fur Geologie und Palaontologie-Monatshefte*, **1996**, 218-231. DOI: 10.1127/njgpm/1996/1996/218

Limaverde, S., Pêgas, R.V., Damasceno, R., Villa, C., Oliveira, G., Bonde, N., Leal, M.E.C. (2018). Interpreting character variation in turtles: *Araripemys barretoi* (Pleurodira: Pelomedusoides) from the Araripe Basin, Early Cretaceous of Northeastern Brazil. *PeerJ Preprints*, **6**, e27262v1. DOI: 10.7287/peerj.preprints.27262v1

Lindgren, J., Uvdal, P., Sjövall, P., Nilsson, D.E., Engdahl, A., Schultz, B.P., Thiel, V. (2012). Molecular preservation of the pigment melanin in fossil melanosomes. *Nature Communications*, **3**, 824. DOI: 10.1038/ncomms1819

Lindgren, J., Sjövall, P., Carney, R.M., Uvdal, P., Gren, J.A., Dyke, G., Schultz, B.P., Shawkey, M.D., Barnes, K.R., Polcyn, M.J. (2014). Skin pigmentation provides evidence of convergent melanism in extinct marine reptiles. *Nature*, **506**, 484–488. DOI: 10.1038/nature12899

Lindgren, J., Kuriyama, T., Madsen, H., Sjövall, P., Zheng, W., Uvdal, P., Engdahl, Moyer, A.E., Gren, J.A., Kamezaki, N., Ueno, S., Schweitzer, M.H. (2017). Biochemistry and adaptive colouration of an exceptionally preserved juvenile fossil sea turtle. *Scientific Reports*, **7**, 13324. DOI: 10.1038/s41598-017-13187-5

Lindgren, J., Sjövall, P., Thiel, V., Zheng, W., Ito, S., Wakamatsu, K., HAuff, R., Kear, B.P., Engdahl, A., Alwmark, C., Eriksson, M.E., Jarenmark, M., Sachs, S., Ahlberg, P.E., Marone, F., Kuriyama, T., Gustafsson, O., Malmberg, P., Thomen, A., Rodríguez-Meizoso, I., Uvdal, P., Ojika, M., Schweitzer, M.H. (2018). Soft-tissue evidence for homeothermy and crypsis in a Jurassic ichthyosaur: *Nature*, **564**, 359–365. DOI: 10.1038/s41586-018-0775-x

Lindgren, J., Moyer, A., Schweitzer, M.H., Sjövall, P., Uvdal, P., Nilsson, D.E.; Heimdal, J.; Engdahl, A.; Gren, J.A.; Schultz, B.P.; Kear, B.P. (2015a). Interpreting melanin-based coloration through deep time: a critical review. Proceedings of the Royal Society B, **282**, 20150614. DOI: 10.1098/rspb.2015.0614

Lindgren, J., Sjövall P., Carney, R.M., Cincotta, A., Uvdal, P., Hutcheson, S.W., Gustafsson, O., Lefèvre, U., Escuillié, F., Heimdal, J., Engdahl, A., Gren, J.A., Kear, B.P., Wakamatsu, K., Yans, J., Godefroit, P. (2015b). Molecular composition and ultrastructure of Jurassic paravian feathers. *Scientific Reports*, **5**, 13520. DOI: 10.1038/srep13520

Liu, Y., Simon, J.D. (2005). Metal-ion interaction and the structural organization of *Sepia* eumelanin. *Pigment Cell Research*, **18**, 42-48. DOI: 10.1111/j.1600-0749.2004.00197.x

Ma, X.-P., Sun, X.-X. (2012). Melanin: Biosynthesis, functions and health effects. New York, NY: *Nova Science Publishers Inc.*, 267 p. ISBN: 9781621009917

Mabesoone, J.M. (1986). Petrografia de alguns sedimentos calcários e microclásticos do Grupo Araripe (Nordeste do Brasil). In: Anais do XXXIV Congresso Brasileiro de Geologia, Goiânia, GO, *Sociedade Brasileira de Geologia*, **1**, 262–270.

Mackintosh, J.A. (2001). The antimicrobial properties of melanocytes, melanosomes and melanin and the evolution of black skin. *Journal of Theoretical Biology*, **211**, 101-113. DOI: 10.1006/jtbi.2001.2331

Maisey, J.G. (1991). Santana Fossils: An Illustrated Atlas. Neptune, New Jersey, USA, *T. H. F. Publications Inc.*, 459 p.

Manning, P.L., Edwards, N.P., Wogelius, R.A., Bergmann, U., Barden, H.E., Larson, P.L., Schwarz-Wings, D., Egerton, V.M., Sokaras, D., Mori, R.A., Sellers, W.I. (2013). Synchrotron-based chemical imaging reveals plumage patterns in a 150 million year old early bird. *Journal of Analytical Atomic Spectrometry*, **28**, 1024-1030. DOI: 10.1039/C3JA50077B

Marek, P., Papaj, D., Yeager, J., Molina, S., Moore, W. (2011). Bioluminescent aposematism in millipedes. *Current Biology*, **21**, R680–R681. DOI: 10.1016/j.cub.2011.08.012

Marek, P.E., Moore, W. (2015). Discovery of a glowing millipede in California and the gradual evolution of bioluminescence in Diplopoda. *Proceedings of the National Academy of Sciences of USA*, **112**, 6419-6424. DOI: 10.1073/pnas.1500014112

Marks, M.S., Heijen, H.F.G., Raposo, G. (2013). Lysosome-related organelles: unusual compartments become mainstream. *Current Opinion in Cell Biology*, **25**, 495-505. DOI: 10.1016/j.ceb.2013.04.008

Marshall, C.P., Carter, E.A., Leuko, S., Javaux, E.J. (2006). Vibrational spectroscopy of extant and fossil microbes: Relevance for the astrobiological exploration of Mars. *Vibrational Spectroscopy*, **41**, 182-189. DOI: 10.1016/j.vibspec.2006.01.008

Martill, D.M. (1987). Prokaryote mats replacing soft tissues in Mesozoic marine reptiles. *Modern Geology*, **11**, 265-269.

Martill, D.M. (1993). Fossils of the Santana and Crato Formations, Brazil. London, UK, *The Palaeontological Association*, 160 p.

Martill, D.M., Wilby, P.R. (1994). Lithified prokaryotes associated with fossil soft tissues from the Santana Formation (Cretaceous) of Brazil. *Kaupia*, **2**, 71-77.

Martill, D.M. (2007). The age of the Cretaceous Santana Formation fossil *Konservat Lagerstätte* of north-east Brazil: a historical review and an appraisal of the biochronostratigraphic utility of its palaeobiota. *Cretaceous Research*, **28**, 895–920. DOI: 10.1016/j.cretres.2007.01.002.

Martill, D.M., Bechly, G., Loveridge, R.F. (2007a). The Crato fossil beds of Brazil. Oxford, UK, *Cambridge University Press*, 674 p. DOI: 10.1017/CBO9780511535512

Martill, D.M., Heimhofer, U. (2007). Stratigraphy of the Crato Formation: In: The Crato Fossil Beds of Brazil: Window into an Ancient World. Oxford, UK, *Cambridge University Press*, p. 25–43. DOI: 10.1017/CBO9780511535512.004

Martill, D.M., Loveridge, R., Heimhofer, U. (2007b). Halite pseudomorphs in the Crato Formation (Early Cretaceous, Late Aptian–Early Albian), Araripe Basin, northeast Brazil. further evidence for hypersalinity. *Cretaceous Research*, **28**, 613–620. DOI: 10.1016/j.cretres.2006.10.003

Martill, D.M., Loveridge, R.F., Heimhofer, U. (2008). Dolomite pipes in the Crato Formation fossil *Lagerstätte* (Lower Cretaceous, Aptian), of northeastern Brazil. *Cretaceous Research*, **29**, 78–86. DOI: 10.1016/j.cretres.2007.04.007

McGraw, K.J., Safran, R.J., Wakamatsu, K. (2005). How feather colour reflects its melanin content. *Functional Ecology*, **19**, 816-821. DOI: 10.1111/j.1365-2435.2005.01032.x

McNamara, M.E. (2013). The taphonomy of colour in fossil insects and feathers. *Palaeontology*, **56**, 557–575. DOI: 10.1111/pala.12044

McNamara, M.E., Saranathan, V., Locatelli, E.R., Noh, H., Briggs, D.E.G., Orr, P.J., Cao, H. (2014). Cryptic iridescence in a fossil weevil generated by single diamond photonic crystals. *Journal of Royal Society Interface*, **11**, 20140736. DOI: 10.1098/rsif.2014.0736

McNamara, M.E., Zhang, F., Kearns, S.L., Orr, P.J., Toulouse, A., Foley, T., Hone, D.W.E., Rogers, C.S., Benton, M.J., Johnson, D., Xu, X., Zhou, Z. (2018a). Fossilized skin reveals coevolution with feathers and metabolism in feathered dinosaurs and early birds. *Nature Communications*, **9**, 2072. DOI: 10.1038/s41467-018-04443-x

McNamara, M.E., Kaye, J.S., Benton, M.J., Orr, P.J., Rossi, V., Ito, S., Wakamatsu, K. (2018b). Non-integumentary melanosomes can bias reconstructions of the colours of fossil vertebrates. *Nature Communications*, **9**, 2878. DOI: 10.1038/s41467-018-05148-x

Mendes, M., Vasconcelos, S.M.O.L., Oliveira, F.I.B. (2019). A New Fossil Stick Grasshopper (Proscopioidea: Proscopiidae) from the Crato Formation of Brazil. *Anuário do Instituto de Geociências*, **42**, 437–443. DOI: 10.11137/2019_2_437_443

Mendes, M., Bezerra, F.I., Adami, K. (2021). Ecosystem structure and trophic network in the late Early Cretaceous Crato Biome. In: Iannuzzi, R., Rößler, R., Kunzmann, L. (eds). Brazilian Paleofloras. *Springer Cham*, 1-19. DOI: 10.1007/978-3-319-90913-4_33-1

Meng, S., Kaxiras, E. (2008) Theoretical models of eumelanin protomolecules and their optical properties. *Biophysical Journal*, **94**, 2095–2105. DOI: 10.1529/biophysj.107.121087

Meredith, P., Powell, B.J., Riesz, J., Nighswander-Rempel, S.P., Pederson, M.R., Moore, E.G. (2006). Towards structure-property-function relationships for eumelanin. *Soft Matter*, **2**, 37–44. DOI: 10.1039/b511922g

Meseguer, J., López-Ruiz, A., Esteban, M.A. (1994). Melano-macrophages of the seawater teleosts, sea bass (*Dicentrarchus labrax*) and gilthead seabeam (*Sparus aurata*): morphology, formation and possible function. *Cell & Tissue Research*, **277**, 1-10. DOI: 10.1007/BF00303074

Miranda, T.S., Barbosa, J.A., Gomes, I.F., Neumann, V.H.M.L., Santos, R.F.V.C., Matos, G.C. de, Guimarães, L.J. do N., Florêncio, R.Q., Alencar, M. de L. (2011). Aplicação da técnica de scanline à modelagem geológica-geomecânica de sistemas de fraturamentos. *Boletim de Geociências da Petrobrás*, **20**, 305–3026.

Miranda, T.S., Barbosa, A., Gomes, I., Soares, A., Santos, R., Matos, G., McKinnon, E., Neumann, V., Marrett, R. (2017). Petrophysics and Petrography of Aptian Tight Carbonate Reservoir, Araripe Basin, NE Brazil. *78th EAGE Conference and Exhibition*, **2016**, 6. DOI: 10.3997/2214-4609.201600890

Miranda, T.S., Santos, R.F., Barbosa, J.A., Gomes, I.F., Alencar, M.L., Correia, O.J., Falcão, T.C., Gale, J.F.W., Neumann, V.H. (2018). Quantifying aperture, spacing and fracture intensity in a carbonate reservoir analogue: Crato Formation, NE Brazil. *Marine and Petroleum Geology*, **97**, 556–567. DOI: 10.1016/j.marpetgeo.2018.07.019

Moyer, A.E., Zheng, W., Johnson, E.A., Lamanna, M.C., Li, D., Lacovara, K.J., Schweitzer, M.H. (2014). Melanosomes or Microbes: Testing an alternative hypothesis for the origin of microbodies in fossil feathers. *Scientific Reports*, **4**, 4233. DOI: 10.1038/srep04233

Moyer, A.E., Zheng, W., Schweitzer, M.H. (2016a). Keratin durability has implications for the fossil record: Results from a 10 year feather degradation experiment. *PLOS ONE*, **11**, e0157699. DOI: 10.1371/journal.pone.0157699

Moyer, A.E., Zheng, W., Schweitzer, M.H. (2016b). Microscopic and immnohistochemical analyses of the claw of the nesting dinosaur, *Citipati osmolskae*. *Proceedings of the Royal Society B,* **283**, 20161997. DOI: 10.1098/rspb.2016.1997

Muscente, A.D., Czaja, A.D., Anne, L., Colleary, C. (2018). Organic Matter in Fossils. In: White, W.M. (eds). Encyclopedia of Geochemistry, Encyclopedia of Earth Sciences Series, Cham, *Springer International Publishing*, 1–5. DOI: 10.1007/978-3-319-39193-9_185-1

Nappi, A.J., Christensen, B.M. (2005). Melanogenesis and associated cytotoxic reactions: applications to insect innate immunity. *Insect Biochemistry and Molecular Biology*, 35, 443-459. DOI: 10.1016/j.ibmb.2005.01.014

Neumann, V.H. (1999). Sistemas lacustres aptiense-albienses de la Cuenca de Araripe, NE, Brasil. Thesis (Doctorate in Geology) *Universidad de Barcelona*, 250 f.

Neumann, V.H., Borrego, A.G., Cabrera, L., Dino, R. (2003). Organic matter composition and distribution through the Aptian-Albian lacustrine sequences of the Araripe Basin, northeastern Brazil. *International Journal of Coal Geology*, **54**, 21–40. DOI: 10.1016/S0166-5162(03)00018-1

Neumann, V.H., Cabrera, L. (2000). Significance and genetic interpretation of the sequential organization of the Aptian-Albian. *Anais da Academia Brasileira de Ciências*, **72**, 607–608.

Neumann, V.H.M.L., Cabrera, L. (2002). Características Hidrogeológicas gerais, mudanças de salinidade e caráter endorréico do sistema lacustre Cretáceo do Araripe, NE Brasil. *Revista de Geologia*, **15**, 43–54.

Neumann, V.H., Cabrera, L., Mabesoone, J.M., Valença, L.M.M., Silva, A.L. (2002). Ambiente sedimentar e facies da sequência lacustre Aptiana-Albiana da Bacia do Araripe, NE do Brasil. In: Boletim do 6° Simpósio sobre o Cretácio do Brasil. São Pedro, SP: *Sociedade Brasileira de Geologia*, 37–41.

Neumann, V.H., Gale, J., Reed, R.M., Barbosa, J.A. (2008). Padrão de fraturamento nos calcários laminados aptianos da região de Nova Olinda-Santana do Cariri, Bacia do Araripe. Uma aplicação da técnica de escalas. *Estudos Geológicos*, **18**, 101–116.

Nofsinger, J.B., Forest, S.E., Eibest, L.M., Gold, K.A., Simon, J.D. (2000). Probing the building blocks of eumelanins using scanning electron microscopy. *Pigment Cell Research*, **13**, 179-184. DOI: 10.1034/j.1600-0749.2000.130310.x

Nordlund, J.J., Abdel-Malek, Z.A., Boissy, R.E., Rheins, L.A. (1989). Pigment Cell Biology: An Historical Review. *Journal of Investigative Dermatology*, **92**, S53-S60. DOI: 10.1038/jid.1989.33

Oliveira, C., Franco-Belussi, L. (2012). Melanic Pigmentation in Ectothermic Vertebrates: Occurrence and Function. In: Ma, X.-P., Sun, X.-X. eds., Melanin: Biosynthesis, functions and health effects. New York, NY: *Nova Science Publishers, Inc.*, p. 213–225. ISBN: 978-1621009917

Osés, G.L. (2016). Tafonomia de grupos fósseis do membro crato (Formação Santana, Bacia do Araripe, Eocretáceo, NE do Brasil): implicações geobiológicas, paleoecológicas e paleoambientais. Dissertation (master's in sciences) Institute of Geosciences, *Universidade de São Paulo*, 45 f. DOI: 10.11606/D.44.2017.tde-27032017-152718

Osés, G.L., Petri, S., Becker-Kerber, B., Romero, G.R., Rizzutto, M.A., Rodrigues, F., Galante, D., Silva, T.F., Curado, J.F., Rangel, E.C., Ribeiro, R.P., Pacheco, M.L.A.F. (2016). Deciphering the preservation of fossil insects: a case study from the Crato Member, Early Cretaceous of Brazil. *Peerj*, **4**, 2756. DOI: 10.7717/peerj.2756

Osés, G.L., Petri, S., Voltani, C.G., Prado, G.M.E.M., Galante, D., Rizzutto, M.A., Rudnitzki, I.D., Silva, E.P., Rodrigues, F., Rangel, E.C., Sucerquia, P.A., Pacheco, M. L.A.F. (2017). Deciphering pyritization-kerogenization gradient for fish soft-tissue preservation. *Scientific Reports*, **7**, 1468. DOI: 10.1038/s41598-017-01563-0

Palumbo, A. (2003). Melanogenesis in the ink gland of Sepia officinalis. *Pigment Cell Research*, **16**, 517-522. DOI: 10.1034/j.1600-0749.2003.00080.x

Pan, Y., Zheng, W., Moyer, A.E., O'Connor, J.K., Wang, M., Zheng, X., Wang, X., Schroeter, E.R., Zhou, Z., Schweitzer, M.H. (2016). Molecular evidence of keratin and melanosomes in feathers of the Early Cretaceous bird Eoconfuciusornis. *Proceedings of the National Academy of Sciences of USA*, **113**, E7900-E7009. DOI: 10.1073/pnas.1617168113

Pan, Y., Zheng, W., Sawyer, R.H., Pennington, M.W., Zheng, X., Wang, X., Wang, M., Hu, L., O'Connor, J., Zhao, T., Li, Z., Schroeter, E.R., Wu, F., Xu, X., Zhou, Z., Schweitzer, M.H. (2019). The molecular evolution of feathers with direct evidence from fossils. *Proceedings of the National Academy of Sciences of USA*, **116**, 3018-3023. DOI: 10.1073/pnas.1815703116

Pan, Y., Li, Z., Wang, M., Zhao, T., Wang, X., Zheng, X. (2022). Unambiguous evidence of brilliant iridescent feather color from hollow melanosomes in an Early Cretaceous bird. *National Science Review*, **9**, nwab225. DOI: 10.1093/nsr/nwab227

Parker, A.R. (1998). The diversity and implications of animal structural colours. *The Journal of Experimental Biology*, **201**, 2343-2347. DOI: 10.1242/jeb.201.16.2343

Parker, A.R. (2004). A vision for natural photonics. *Philosophical Transactions of the Royal Society of London A*, **362**, 2709-2720. DOI: 10.1098/rsta.2004.1458

Parry, L.A., Smithwick, F.M., Nordén, K.K., Saitta, E.T., Lozano-Fernandez, J., Tanner, A.R., Caron, J.B., Edgecombe, G.D., Briggs, D.E.G., Vinther, J. (2018). Soft-Bodied Fossils Are Not Simply Rotten Carcasses – Toward a Holistic Understanding of Exceptional Fossil Preservation: Exceptional Fossil Preservation Is Complex and Involves the Interplay of Numerous Biological and Geological Processes. *BioEssays*, **40**, 1–11. DOI: 10.1002/bies.201700167

Pereira, A. (2018). Guia fotográfico: Aves do litoral do Rio Grande do Sul. Imbé, RS, *Universidade Federal do Rio Grande do Sul*, 49 p.

Pinheiro, F.L., Prado, G., Ito, S., Simon, J.D., Wakamatsu, K., Anelli, L.E., Andrade, J.A.F.G., Glass, K.E. (2019). Chemical characterization of pterosaur melanin challenges color inferences in extinct animals. *Scientific Reports*, **9**, 15947. DOI: 10.1038/s41598-019-52318-y

Pires, E.F., Jasper, A., Lima, F.J., Saraiva, A.Á.F., Sayão, J.M., Uhl, D. (2019). Fire in the paradise: evidence of repeated palaeo-wildfires from the Araripe Fossil Lagerstätte (Araripe Basin, Aptian-Albian), Northeast Brazil. *Palaeobiodiversity and Palaeoenvironments*, **99**, 367-378. DOI: 10.1007/s12549-018-0359-7

Pough, F.H., Janis, C.M., Heiser, J.B. (2013). Vertebrate Life. Glenview, Illinois, USA: *Pearson Education Inc.*, 730 p.

Powell, B.J., Baruah, T., Bernstein, N., Brake, K., McKenzie, R.H., Meredith, P., Pederson, M.R. (2004). A first-principles density-functional calculation of the electronic and vibrational structure of the key melanin monomers. *Journal of Chemical Physics*, **120**, 8608–8615. DOI: 10.1063/1.1690758

Prado, G., Arthuzzi, J.C.L., Osés, G.L., Callefo, F., Maldanis, L., Sucerquia, P., Becker-Kerber, B., Romero, G.R., Quiroz-Valle, F.R., Galante, D. (2021). Synchrotron radiation in

palaeontological investigations: Examples from Brazilian fossils and its potential to South American palaeontology. *Journal of South American Earth Sciences*, **108**, 102973. DOI: 10.1016/j.jsames.2020.102973

Prado, G.M.E.M. (2017). Pigmentação fóssil: Tafonomia física de penas fósseis das bacias do Araripe (Cretáceo) e Taubaté (Paleógeno), Brasil. Dissertation (Master in Geology) Institute of Geosciences, *University of São Paulo*, 118 f.

Prado, G.M.E.M., Anelli, L.E., Petri, S., Romero, G.R. (2016). New occurrences of fossilized feathers: systematics and taphonomy of the Santana Formation of the Araripe Basin (Cretaceous), NE, Brazil. *PeerJ*, **4**, e1916. DOI: 10.7717/peerj.1916

Prado, G.M.E.M., Becker-Kerber, B., Osés, G.L., Campo, V.B.D., Romero, G.R., Galente, D., and Rodrigues, F. (2015). The exquisite preservation of the biota from Tremembé Formation (Taubaté Basin). In: Riff, D., Lima, F.J., Oliveira, G.C., Oliveira, G.R., Sayão, J.M., Sucerquia, P.A., Andrade, R.C.L.P., Bantim, R.A.M. (eds.) Paleontologia em Destaque - Boletim de Resumos XXIV Congresso Brasileiro de Paleontologia, Crato, CE, Brasil, *Sociedade Brasileira de Paleontologia*, p. 225–226.

Prampolini, G., Cacelli, I., Ferretti, A. (2015). Intermolecular interactions in eumelanins: A computational bottom-up approach. I. small building blocks. *RSC Advances*, **5**, 38513–38526. DOI: 10.1039/c5ra03773e

Purnell, M.A., Donoghue, P.J.C., Gabbott, S.E., McNamara, M.E., Murdock, D.J.E., Sansom, R.S. (2018). Experimental analysis of soft-tissue fossilization: opening the black box. *Palaeontology*, **61**, 317–323. DOI: 10.1111/pala.12360

Pushie, M.J., Pratt, B.R., Macdonald, T.C., George, G.N., Pickering, I.J. (2014). Evidence for biogenic copper (Hemocyanin) in the Middle Cambrian arthropod *Marrella* from the Burgess Shale. *PALAIOS*, **29**, 512-524. DOI: 10.2120/palo.2014.073

Raff, E.C., Schollaert, K.L., Nelson, D.E., Donoghue, P.C.J., Thomas, C.-W., Turner, F.R., Stein, B.D., Dong, X., Bengtson, S., Huldtgren, T., Stampanoni, M., Chongyu, Y., Raff, R.A. (2008). Embryo fossilization is a biological process mediated by microbial mats. *Proceedings of the National Academy of Sciences of USA*, **105**, 19360-19365. DOI: 10.1073/pnas.0810106105

Raposo, G., Marks, M.S. (2002). The dark side of lysosome-related organelles: Specialization of the endocytic pathway for melanosome biogenesis. *Traffic*, **3**, 237-248. DOI: 10.1034/j.1600-0854.2002.030401.x

Raposo, G., Marks, M.S. (2007). Melanosomes — dark organelles enlighten endosomal membrane transport. *Nature Reviews Molecular Cell Biology*, **8**, 786-797. DOI: 10.1038/nrm2258

Regali, M.S.P. (1989). A idade dos evaporitos da plataforma continental do Ceará, Brasil, e sua relação com os outros evaporitos das bacias nordestinas. *Boletim IG-USP - Publicação Especial*, **7**, 139–143.

Rendón, P.A.S. (2013). Taxonomia, modos de preservação e fitogeografia de Coníferas aptianas da região Paleoequatorial da América do Sul. Dissertation (Master's in Sciences). Instituto de Geociências, *Universidade de São Paulo*, 86 f. DOI: 10.11606/T.44.2016.tde-31012014-142803

Ribeiro, A.C., Ribeiro, G.C., Varejão, F.G., Battirola, L.D., Pessoa, E.M., Simões, M.G., Warren, L.V., Riccomini, C., Poyato-Ariza, F. (2021). Towards an actualistic view of the Crato *Konservat-Lagerstätte* paleoenvironment: A new hypothesis as an Early Cretaceous (Aptian) equatorial and semi-arid wetland. *Earth-Science Reviews*, **216**, 103573. DOI: 10.1016/j.earscirev.2021.103573

Riley, P.A. (1997). Melanin. *International Journal of Biochemistry Cell Biology*, **29**, 1235-1239. DOI: 10.1016/s1357-2725(97)00013-7

Riley, P.A., Stratford, M.R.L. (2015). Oxidative calcium release from catechol. *Bioorganic & Medicinal Chemistry Letters*, **25**, 1453-1454. DOI: 10.1016/j.bmcl.2015.02.036

Rios-Netto, A. de M., Regali, M. da S.P., Carvalho, I. de S., Freitas, F.I. (2012). Palinoestratigrafia do intervalo Alagoas da Bacia do Araripe, Nordeste do Brasil. *Revista Brasileira de Geociências*, **42**, 331–342. DOI: 10.25249/0375-7536.2012422331342

Roberts, R.J. (1975). Melanin-containing cells of teleost fish and their relation to disease. In: Ribelin, W.E. (Org.). 1975. The pathology of fishes. *The University of Wisconsin Press*, 1st Ed., pp. 399-428. ISBN: 0299065200

Rojas, F.H.M. (2009). Estratigrafia de sequências do intervalo Aptiano ao Albiano na Bacia do Araripe, NE do Brasil. Dissertation (master's in science). *Universidade Federal do Rio Grande do Norte*, 120 p.

Roy, A., Rogers, C.S., Clements, T., Pittman, M., Habimana, O., Martin, P., Vinther, J. (2020a). Fossil microbodies are melanosomes: Evaluating and rejecting the "fossilized decay-associated microbes" hypothesis. In: Pittman, M., Xu, X. (eds). Pennaraptoran theropod

dinosaurs: past progress and new frontiers. *Bulletin of the American Museum of Natural History*, p. 251-276. ISSN: 00030090.

Roy, A., Pittman, M., Kaye, T., Saitta, E. (2020b). Sediment-encased pressure-temperature maturation experiments chemically simulate natural diagenesis of melanin. *Research Square PrePrints*, **1**, 1-15p. DOI: 10.21203/rs.3.rs-106894/v1

Roy, A., Pittman, M., Saitta, E.T., Kaye, T.G., Xu, X. (2019). Recent advances in amniote palaeocolour reconstruction and a framework for future research. *Biological Reviews*, **95**, 22-50. DOI: 10.1111/brv.12669

Różanowska, M., Sarna, T., Land, E.J., Truscott, T.G. (1999). Free radical scavenging properties of melanin. *Free Radical Biology and Medicine*, **26**, 518–525. DOI: 10.1016/S0891-5849(98)00234-2

Saitta, E.T., Rogers, C., Brooker, R.A., Abbott, G.D., Kumar, S., O'Reilly, S.S., Donohoe, P., Dutta, S., Summons, R.E., Vinther, J. (2017a). Low fossilization potential of keratin protein revealed by experimental taphonomy. *Palaeontology*, **60**, 547–556. DOI: 10.1111/pala.12299

Saitta, E.T., Rogers, C.S., Brooker, R.A., Vinther, J. (2017b). Experimental taphonomy of keratin: A structural analysis of early taphonomic changes. *PALAIOS*, **32**, 647–657. DOI: 10.2110/palo.2017.051

Saitta, E.T., Kaye, T.G., Vinther, J. (2018a). Sediment-encased maturation: a novel method for simulating diagenesis in organic fossil preservation. *Palaeontology*, **62**, 135–150. DOI: 10.1111/pala.12386

Saitta, E.T., Clapham, C., Vinther, J. (2018b). Experimental subaqueous burial of a bird carcass and compaction of plumage. *PalZ*, **92**. 727–732. DOI: 10.1007/s12542-018-0411-y

Salih, A., Larkum, A., Cox, G., Kühl, M., Hoegh-Guldberg, O. (2000). Fluorescent pigments in corals are photoprotective. *Nature*, **408**, 850-853. DOI: 10.1038/35048564

Santos, F.H., Azevedo, J.M., Nascimento, D.R., Souza, A.C.B., Mendes, M., Bezerra, I., Limaverde, S. (2017). Análise de fácies e petrografia de uma seção do Membro Crato em Nova Olinda (CE): contribuições à história deposicional e diagenética do neoaptiano na Bacia do Araripe. *Geologia USP - Série Científica*, **17**, 3–18. DOI: 10.11606/issn.2316-9095.v17-319

Sayed, A.H., Younes, H.A.M. (2017). Melanomacrophage centers in *Clarias gariepinus* as an immunological biomarker for toxicity of silver nanoparticles. *Journal of Microscopy and Ultrastructure*, **5**, 97-104. DOI: 10.1016/j.jmau.2016.07.003

Schultze-Lam, S., Fortin, D., Davis, B.S., Beveridge, T.J. (1996). Mineralization of bacterial surfaces. *Chemical Geology*, **132**, 171–181. DOI: 10.1016/s0009-2541(96)00053-8

Schweitzer, M.H., Avci, R., Collier, T., Goodwin, M.B. (2008). Microscopic, chemical and molecular methods for examining fossil preservation. *Comptes Rendus Palevol*, **7**, 159-184. DOI: 10.1016/j.crpv.2008.02.005

Schweitzer, M.H., Lindgren, J., Moyer, A.E. (2015). Melanosomes and ancient coloration re-examined: A response to - Vinther 2015 (DOI 10.1002/bies.201500018). *BioEssays*, **37**, 1174-1183. DOI: 10.1002/bies.201500061

Schweitzer, M.H., Zheng, W., Moyer, A.E., Sjövall, P., Lindgren, J. (2018). Preservation potential of keratin in deep time. *PLOS ONE*, **13**, e0206569. DOI: 10.1371/journal.pone.0206569

Shankar, S., Wang, L.-F., Rhim, J.-W., 2019, Effect of melanin nanoparticles on the mechanical, water vapor barrier, and antioxidant properties of gelatin-based films for food packaging application. *Food Packaging and Shelf Life*, **21**, 100363. DOI: 10.1016/j.fpsl.2019.100363

Shawkey, M.D., D'Alba, L. (2017). Interactions between colour-producing mechanisms and their effects on the integumentary colour palette. *Philosophical Transactions of the Royal Society B*, **372**, 20160536. DOI: 10.1098/rstb.2016.0536

Shawkey, M.D., D'Alba, L., Xiao, M., Schutte, M., Buchholz, R. (2015). Ontogeny of an iridescent nanostructure composed of hollow melanosomes. *Journal of Morphology*, **276**, 378–384. DOI: 10.1002/jmor.20347

Silva, A.L., Neumann, V.H., Cabrera, L. (2002). Fácies carbonáticas laminadas da Formação Crato (Aptiano), Bacia do Araripe: Litofácies, microfácies e microestruturas. In: Boletim do 6° Simpósio sobre o Cretácio do Brasil, São Pedro, SP: *Sociedade Brasileira de Geologia*, p. 31–36.

Silva, V.R., Varejão, F.G., Matos, S.A., Fürsich, F.T., Skawina, A., Schneider, S., Warren, L.V., Assine, M.L., Simões, M.G. (2020a). Cratonaia novaolindensis gen. et sp. nov. (Unionida, Silesunionoidea) from the Aptian of Brazil (Araripe Basin), and its implications for the early

evolution of freshwater mussels. *Cretaceous Research*, **107**, 104275. DOI: 10.1016/j.cretres.2019.104275

Silva, V.R., Varejão, F.G., Matos, S.A., Rodrigues, M.G., Fürsich, F.T., Skawina, A., Schneider, S., Warren, L.V., Assine, M.L., Simões, M.G. (2020b). New freshwater mussels (Bivalvia, Unionida) with potential trigonioidid and hyriid affinities from the Early Cretaceous of Brazil. *Geobios*, **61**, 41-54. DOI: 1016/j.geobios.2020.06.001

Simpson, M.J., Glass, K.E., Wilson, J.W., Wilby, P.R., Simon, J.D., Warren, W.S. (2013). Pump–Probe Microscopic Imaging of Jurassic-Aged Eumelanin. *The Journal of Physical Chemistry Letters*, **4**, 1924–1927. DOI: 10.1021/jz4008036

Slater, T.S., McNamara, M.E., Orr, P.J., Foley, T.B., Ito, S., Wakamatsu, K. (2020). Taphonomic experiments resolve controls on the preservation of melanosomes and keratinous tissues in feathers. *Palaeontology*, **63**, 103–115. DOI: 10.1111/pala.12445

Sliney, D. (2016). What is light? The visible spectrum and beyond. *Eye*, **30**, 222–229. DOI: 10.1038/eye.2015.252

Smithwick, F., Vinther, J. (2020). Palaeocolour: A history and state of the art. In: Foth, C., Rauhut, O.W.M. (eds.). The Evolution of Feathers. Cham, Switzerland: *Springer Nature*, pp. 185-211. DOI: 10.1007/978-3-030-27223-4_11

Smythies, J. (1996). On the function of neuromelanin. *Proceedings of the Royal Society B*, **263**, 487-489. DOI: 10.1098/rspb.1996.0073

Solano, F. (2014). Melanins: skin pigments and much more-types, structural models, biological functions, and formation routes. *New Journal of Science*, **2014**, 498276. DOI: 10.1155/2014/498276

Solano, F. (2020). Photoprotection and skin pigmentation: Melanin-related molecules and some other new agents obtained from natural sources. *Molecules*, **25**, 1537. DOI: 10.3390/molecules25071537

Srivastava, N.K. (1996). Estromatólitos cretácicos continentais na Bacia do Araripe. *Anais da Academia Brasileira de Ciências*, **68**, 267–268.

Stark, K.B., Gallas, J.M., Zajac, G.W., Golab, J.T., Gidanian, S., McIntire, T., Farmer, P.J. (2005). Effect of Stacking and Redox State on Optical Absorption Spectra of Melanins−Comparison of Theoretical and Experimental Results. *The Journal of Physical Chemistry B*, **109**, 1970–1977. DOI: 10.1021/jp046710z

Stavenga, D.G., Leertouwer, H.L., Marshall, N.J., Osorio, D. (2011). Dramatic colour changes in a bird of paradise caused by uniquely structured breast feather barbules. *Proceedings of the Royal Society B*, **278**, 2098-2104. DOI: 10.1098/rspb.2010.2293

Storari, A.P., Rodrigues, T., Bantim, R.A.M., Lima, F.J., Saraiva, A.A.F. (2021). Mass mortality events of autochthonous faunas in a Lower Cretaceous Gondwanan *Lagerstätte*. *Scientific Reports*, **11**, 6976. DOI: 10.1038/s41598-021-85953-5

Supakar, S., Banerjee, A., Jha, T. (2019). Intermolecular association of some selected melanin monomers and their optical absorption. *Computational and Theoretical Chemistry*, **1151**, 43–49. DOI: 10.1016/j.comptc.2019.02.001

Tanaka, G., Parker, A.R., Hasegawa, Y., Siveter, D.J., Yamamoto, R., Miyashita, K., Takahashi, Y., Ito , S., Wakamatsu, K., Mukuda, T., Matsuura, M., Tomikawa, K., Furutani, M., Suzukim K., Maeda, H. (2014) Mineralized rods and cones suggest colour vision in a 300 Myr old fossil fish. *Nature Communications*, **5**, 5920. DOI: 10.1038/ncomms6920

Tran, M.L., Powell, B.J., Meredith, P. (2006). Chemical and structural disorder in eumelanins: A possible explanation for broadband absorbance. *Biophysical Journal*, **90**, 743-752. DOI: 10.1529/biophysj.105.069096

Vahidzadeh, E., Kalra, A.P., Shankar, K. (2018). Melanin-based electronics: From proton conductors to photovoltaics and beyond. *Biosensors and Bioelectronics*, **122**, 127-139. DOI: 10.1016/j.bios.2018.09.026

Varejão, F.G., Warren, L. V., Simões, M.G., Fürsich, F.T., Matos, S.A., Assine, M.L. (2019). Exceptional preservation of soft tissues by microbial entombment: Insights into the taphonomy of the Crato *Konservat-Lagerstätte*. *PALAIOS*, **34**, 331–348. DOI: 10.2110/palo.2019.041

Varejão F.G., Warren, L.V., Simões, M.G., Buatois L.A., Mángano M.G., Rumbelsperger, A.M.B., Assine, M.L. (2020). Mixed siliciclastic–carbonate sedimentation in an evolving epicontinental sea: Aptian record of marginal marine settings in the interior basins of north-eastern Brazil. *Sedimentology*, **68**, 2125-2164. DOI: 10.1111/sed.12846

Varejão, F.G., Silva, V.R., Assine, M.L., Warren, L.V., Matos, S.A., Rodrigues, M.G., Fürsich, F.T., Simões, M.G. (2021). Marine or freshwater? Accessing the paleonenvironmental parameters of the Caldas Bed, a key marker bed in the Crato Formation (Araripe Basin, NE

Brazil). *Brazilian Journal of Geology*, **51**, e2020009. DOI: 10.1590/2317-4889202120200009

Vinther, J. (2015). A guide to the field of palaeo colour: Melanin and other pigments can fossilise: Reconstructing colour patterns from ancient organisms can give new insights to ecology and behaviour. *BioEssays*, **37**, 643–656. DOI: 10.1002/bies.201500018

Vinther, J. (2017). The true colors of dinosaurs. *Scientific American*, **316**, 50–57. DOI: 10.1038/scientificamerican0317-50

Vinther, J. (2020). Reconstructing vertebrate paleocolor. *Annual Review of Earth and Planetary Sciences*, **48**, 345-375. DOI: 10.1146/annurev-earth-073019-045641

Vinther, J., Briggs, D.E.G., Prum, R.O., Saranathan, V. (2008). The colour of fossil feathers. *Biology Letters*, **4**, 522–525. DOI: 10.1098/rsbl.2008.0302

Vinther, J., Nicholls, R., Lautenschlager, S., Pittman, M., Kaye, T.G., Rayfield, E., Mayr, G., Cuthill, I.C. (2016). 3D Camouflage in an ornithischian dinosaur. *Current Biology*, **26**, 2456–2462. DOI: 10.1016/j.cub.2016.06.065

Wakamatsu, K., Ito, S. (2002). Advanced chemical methods in melanin determination. *Pigment Cell Research*, **15**, 174–183. DOI: 10.1034/j.1600-0749.2002.02017.x

Wakamatsu, K., Nagao, A., Watanabe, M., Nakao, K., Ito, S. (2017). Pheomelanogenesis is promoted at a weakly acidic pH. *Pigment Cell & Melanoma Research*, **30**, 353-367. DOI: 10.1111/pcmr.12587

Warren, L.V., Varejão, F.G., Quaglio, F., Simões, M.G., Fürsich, F.T., Poiré, D.G., Catto, B., Assine, M.L. (2017). Stromatolites from the Aptian Crato Formation, a hypersaline lake system in the Araripe Basin, northeastern Brazil. *Facies*, **63**, 1–19. DOI: 10.1007/s10347-016-0484-6

Wasmeier, C., Hume, A.N., Bolasco, G., Seabra, M.C. (2008). Melanosomes at a glance. *Journal of Cell Science*, **121**, 3995–3999. DOI: 10.1242/jcs.040667

Watt, A.A.R., Bothma, J.P., Meredith, P. (2009). The supramolecular structure of melanin. *Soft Matter*, **5**, 3754. DOI: 10.1039/b902507c

White, E.H., McCapra, F., Field, G.F. (1963). The structure and synthesis of firefly luciferin. *Journal of the American Chemical Society*, **85**, 337–343. DOI: 10.1021/ja00886a019

Wiemann, J., Fabbri, M., Yang, T., Stein, K., Sander, P.M., Norell, M.A., Briggs, D.E.G. (2018). Fossilization transforms vertebrate hard tissue proteins into N-heterocyclic polymers. *Nature Communications*, **9**, 4741. DOI: 10.1038/s41467-018-07013-3

Wilby, P.R., Briggs, D.E.G., Bernier, P., Gaillard, C. (1996). Role of microbial mats in the fossilization of soft tissues. *Geology*, **24**, 787–790. DOI: 10.1130/0091-7613(1996)024<0787:ROMMIT>2.3.CO;2

Wogelius, R.A., Manning, P.L., Barden, H.E., Edwards, N.P., Webb, S.M., Sellers, W.I., Taylor, K.G., Larson, P.L., Dodson, P., You, H., Da-Quing, L., Bergmann, U. (2011). Trace metals as biomarkers for eumelanin pigment in the fossil record. *Science*, **333**, 1622-1626. DOI: 10.1126/science.1205748

Wolke, R.E. (1992). Piscine macrophage aggregates: A review. *Annual Review of Fish Diseases*, **2**, 91-108. DOI: 10.1016/0959-8030(92)90058-6

Wong, V.L., Marek, P.E. (2020). Structure and pigment make the eyed elater's eyespot black. *PeerJ*, **8**, e8161. DOI: 10.7717/peerj.8161

Wucherer, M.F., Michiels, N.K. (2014). Regulation of red fluorescent light emission cryptic marine fish. *Frontier in Zoology*, **11**, 1-8. DOI: 10.1186/1742-9994-11-1

Wuttke, M. (1983). Weichteil-Erhaltung'durch lithifizierte Mikroorganismen bei mitteleoz änen Vertebraten aus den Ölschiefern der 'Grube Messel'bei Darmstadt. *Senckenbergiana Lethaea*, **64**, 509-527.

Xiao, M., Chen, W., Li, W., Zhao, J., Hong, Y., Nishiyama, Y., Miyoshi, T., Shawkey, M.D., Dhinojwala, A. (2018). Elucidation of the hierarchical structure of natural eumelanins. *Journal of The Royal Society Interface*, **15**, 20180045. DOI: 10.1098/rsif.2018.0045

Xu, R., Gouda, A., Caso, M.F., Soavi, F., Santato, C. (2019). Melanin: A greener route to enhance energy storage under solar light. *ACS Omega*, **4**, 12244−12251. DOI: 10.1021/acsomega.9b01039

Yang, Z., Jiang, B., McNamara, M.E., Kearns, S.L., Pittman, M., Kaye, T.G., Orr, P.J., Xu, X., Benton, M.J. (2019). Pterosaur integumentary structures with complex feather-like branching. *Nature Ecology & Evolution*, **3**, 24–30. DOI: 10.1038/s41559-018-0728-7

Zhao, T., Hu, J., Hu, L., Pan, Y. (2020). Experimental maturation of feathers: Implications for interpretations of fossil feathers. *PALAIOS*, **35**, 67-76. DOI: 10.2110/palo.2019.064

Zhao, T., Hu, L., Pan, Y. (2022). Silicification of feathers in a modern hot spring in New Zealand. *Earth and Environmental Science Transactions of The Royal Society of Edinburgh*, **113**, 119-125. DOI: 10.1017/S1755691022000068

CHAPTER 2 - MATERIAL AND METHODS

2.1. MATERIAL

The fossils (Table 2.1) come from the Crato Formation (Cretaceous, Araripe Basin, NE Brazil) and are contained in two facies; (1) the greyish, or (2) buff-coloured limestones (Osés et al., 2017). Albeit both rocks are composed of sparry and micrite calcite grains, the former is richer in clay minerals and amorphous organic matter; whereas the latter is richer in evaporitic minerals (e.g., halite) and iron oxides (Neumann et al., 2003). Although the general information (e.g., animal taxonomy, integument type, etc.) and images can be seen in each appropriated chapter, all samples are fossil specimens are housed at the public repositories with different numbers/acronyms, such as: GP/2E, Vertebrate Collection of the Palaeontological Collection of the Institute of Geosciences of University of São Paulo; UFPE-CTG, Palaeontological Collection of Centre of Technology and Geosciences of the Federal University of Pernambuco; and, CPCA, Centre of Palaeontological Research of the National Mining Agency in Crato-CE (ANM). Apart from fossils, for comparison purposes, various samples of modern materials were analysed using varied techniques, especially Raman spectroscopy, which was applied in all specimens.

Table 2.1. Samples analysed in this thesis. Abbreviations: GL – Grey Limestone; BL – Beige Limestone; ML – Morphological; CH – Chemical; N – Number of samples; NA – Not Applied.

SAMPLE ID	SCIENTIFIC NAME	LIMESTONE FACIES	INSTITUTIONAL NUMBER	TYPE OF ANALYSIS
Fossil Fish	?*Dastilbe crandalli*	GL	GP/2E-9378b	ML and CH
Fossil Fish	?*Dastilbe crandalli*	GL	UFPE-CTG-8746	ML and CH
Fossil Frog	*Primaevorana cratensis*	GL	GP/2E-9497	ML and CH
Fossil Feathers	Dinosauria	GL/BL	Various*	ML and CH
Pterosaur	*Tupandactylus imperator*	GL	CPCA-3590	ML and CH
Pterosaur	*Tupandactylus navigans*	BL	GP/2E-9266	ML and CH
Synthetic Melanin	Tyr-oxidized Melanin	NA	M8631	CH
Natural Melanin	*Sepia officinalis* Melanin	NA	M2649	CH
Extant Feather	*Helmeted Guineafowl*	NA	NA	ML and CH
Extant Feather	*Celeus flavescens*	NA	NA	CH

* Numbers (82 specimens in total): GP/2E-7853, GP/2E-7854, GP/2E-8771, GP/2E-9378 to GP/2E-9443 (66 samples), GP/2E-9467, GP/2E-9476 to GP/2E-9486 (11 samples), and GP/2E-9494.

2.2. METHODS

To obtain information about the pigmentation of fossil and extant vertebrates, samples of the soft tissues (e.g., skin, eyes, and feathers) were collected and analysed both morphologically (using microscopes), chemically, and statistically, as follows:

- ***Optical Stereomicroscope (OM)*** – Because OM is able to show hand samples at higher magnifications (up to x100), this approach was used to observe and register the overall characteristics of samples and their structural details, such as feather barbs and barbules of feathers.
- ***Confocal Optical Microscopy (COM)*** - Due to the fact that the COM is attached to the Raman spectrometer, this method was used mainly to aid Raman spectroscopy experiments. However, this device was also used to explore small portions (ca. 10 µm) of the samples. Furthermore, once this apparatus proved to be useful to detect melanosomes *in situ*, COM was also used as a screening method of the most suitable samples for SEM investigations. In any case, in all aforementioned approaches, images were taken from the whole specimen or regions of interest (ROI).
- ***Petrographic Microscopy (PTM)*** - Reusing the thin sections (ca. 30 µm) of two feather matrices made by Prado (2017), samples were re-analysed under petrographic microscopy and Raman spectroscopy aiming at the identification of textures, cementation, mineralogy, among others, not detected previously.
- ***Scanning Electron Microscopy (SEM)*** – Since this technique reveal the topographic (i.e., surface) images of minute regions of the sample (Echlin, 2009), in this thesis, SEM was used aiming at the identification of ultrastructures, such as crystals and melanosomes.
- ***Energy Dispersive Spectroscopy (EDS)*** – Used in conjunction with SEM, this technique was used to help the identification of microbodies through the detection of the light element, both in spectral and/or spatial distribution modes (Echlin, 2009).
- ***Synchrotron Radiation micro-X-ray Fluorescence (SR-µXRF)*** **–** This technique was used to determine the presence and distribution of heavy elements (Pérez et al., 2016), especially those related to eumelanin (Horčičko et al., 1973; Liu & Simon, 2005; Hong & Simon, 2007), such as Cu^{2+}, Fe^{2+}, Mn^{2+}, S^{2+}, Zn^{2+}. Spectra were

processed (fitted) and elemental maps saved in SVG using PyMCA software (Solé et al., 2007), and images were processed using Inkscape 0.92.3 (2405546, 2018-03-11). All analyses were performed at the LNLS D09BXRF-XRF beamline (Pérez et al., 1999) of the UV and Soft X-Ray Light Source of the Brazilian Synchrotron Light Laboratory (UVX/LNLS), under the proposals XRF-20150110, XRF-20160161, XRF-20190140.

- ***Synchrotron-Radiation X-Ray Absorption Near Edge Spectroscopy (SR-XANES)*** – Since this technique allows the identification of elemental species as well as the chemical environment of an atom (for details see Callefo et al., 2019; Prado et al., 2021), this method was used to identify the elemental species of Fe that may be related to the melanin in fossil feathers. Data were processed at ATHENA software from the IFEFFIT package (Ravel & Newville, 2005), and for aesthetically purposes, they were manipulated in Inkscape. The experiments were conducted at the LNLS D09BXRF-XRF beamline (Pérez et al., 1999) of the UVX/LNLS under the proposal XRF-20180327.
- ***Raman Spectroscopy (RS)*** – This technique was used virtually in all samples to obtain information about the molecular nature of organic and inorganic compounds (Lafuente et al., 2016), especially eumelanin (Galván et al., 2018a, 2018b). Since this method allows the identification of molecular fingerprints in ROI as well as the spatial distribution of molecules, the analyses were performed as point-and-shoot and mapping modes. For multivariate analysis of spectra, which was also performed (Gautam et al., 2015). Furthermore, To obtain the temperature of structural (i.e., diagenetic) alteration of melanin, we followed the rationale used for carbonaceous maturation. We also calculated the temperature of melanin alteration using the first equation (1) of Kouketsu et al. (2014).

$$T\ (°C) = -2.15 \times (FWHMD1) + 478\ (\pm 30°\ C) \quad (1)$$

The spectrometers used are housed at the Laboratory of Molecular Spectroscopy (LEM/IQ-USP) and LC/IQ-USP (Equipment process number: FAPESP 12/18936-0), both from the Institute of Chemistry of University of São Paulo.

- ***Alkaline Hydrogen Peroxide Oxidation High-Performance Liquid Chromatography-Mass Spectrometry (AHPO-HPLC-MS)*** – Due to its very high resolution, this analysis is deemed as essential in the identification of melanin molecules and determination of the real nature of the ultrastructures (Ito & Wakamatsu, 1998; Wakamatsu & Ito, 2002; Ito & Wakamatsu, 2003; Ito et al., 2011, 2013). This technique was applied only in one sample, to confirm the identification of the melanin moiety following the protocols of Ito et al. (2011) and Glass et al. (2012). All procedures were carried out by co-authors of the Pinheiro et al. (2019) paper, and the detailed procedure can be found therein.
- ***Statistics*** - Using SEM micrographs and chemical analysis, the ultrastructures were analysed aiming to recognize the following aspects: (i) morphology; (ii) dimension; (iii) occurrence; (iv) distribution; (v) density (n/µm^2); (vi) possible chemistry (mineralogy of fossilization); and (vii) diagenetic history. Aiming the best-represented microbodies, at the field of view, axes (length - L and width - W) were measured using ImageJ 1.52a (Schneider et al., 2012). Each particle measured was labelled, and the images and measurement tables were saved in TIFF and XLS, respectively. The descriptive statistics, such as the microbody aspect ratio (length/width) were calculated using Microsoft Excel and Minitab (SAS Institute Inc.). To verify the correlation between axes, which can also indicate the level of sphericity, scatterplots and linear regression of the length and width were plotted. To dimensional distributions, boxplots of the axes ratio and length were prepared, in addition to histograms of the width. All the latter approaches were done using Origin 2022 (OriginLab Co., Northampton, MA, USA). Multivariate analysis, such as principal coordinate analysis (PCA), linear discriminant analysis (LDA), and canonical quadratic discriminant analysis (CQDA) were carried out using JMP 16.2.0 (SAS Institute Inc., Cary, NC, USA) and PAST 4.08 (Hammer et al., 2001). To compare these results and to perform colour predictions, it was used the database of Li et al. (2012), refined by later studies (Eliason et al., 2016; Babarović et al., 2019).

2.3. REFERENCES

Babarović, F., Puttick, M.N., Zaher, M., Learmonth, E., Gallimore, E.-J., Smithwick, F.M., Mayr, G., Vinther, J. (2019). Characterization of melanosomes involved in the production of non-iridescent structural feather colours and their detection in the fossil record. *Journal of the Royal Society Interface*, **16**, 20180921. DOI: 10.1098/rsif.2018.0921

Callefo, F., Maldanis, L., Teixeira, V.C., Abans, R.A.O., Monfredini, T., Rodrigues, F., Galante, D. (2019). Evaluating biogenicity on the geological record with synchrotron-based techniques. *Frontiers in Microbiology*, **10**, 1–12. DOI: 10.3389/fmicb.2019.02358

Echlin, P. (2009). Handbook of Sample Preparation for Scanning Electron Microscopy and X-Ray Microanalysis. Boston, MA, USA: *Springer*, 330 p. DOI: 10.1007/b100727

Eliason, C.M., Shawkey, M.D., Clarke, J.A. (2016). Evolutionary shifts in the melanin-based color system of birds. *Evolution*, **70**, 445–455. DOI: 10.1111/evo.12855

Galván, I., Araújo-Andrade, C., Marro, M., Loza-Alvarez, P., Wakamatsu, K. (2018a). Raman spectroscopy quantification of eumelanin subunits in natural unaltered pigments. *Pigment Cell Melanoma Research*, **31**, 673-682. DOI: 10.1111/pcmr.12707

Galván, I., Cerezo, J., Jorge, A., Wakamatsu, K. (2018b). Molecular vibration as a novel explanatory mechanism for the expression of animal colouration. *Integrative Biology*, **10**, 464-473. DOI: 10.1039/c8ib00100f

Gautam, R., Vanga, S., Ariese, F., Umapathy, S. (2015). Review of multidimensional data processing approaches for Raman and Infrared spectroscopy. *EPJ Techniques and Instrumentation*, **2**, 1-38. DOI: 10.1140/epjti/s40485-015-0018-6

Glass, K.E., Ito, S., Wilby, P.R., Sota, T., Nakamura, A., Bowers, C.R., Vinther, J., Dutta, S., Summons, R., Briggs, D.E.G., Wakamatsu, K., Simon, J.D. (2012). Direct chemical evidence for eumelanin pigment from the Jurassic period. *Proceedings of the National Academy of Sciences of USA*, **109**, 10218–10223. DOI: 10.1073/pnas.1118448109

Hammer, Ø., Harper, D.A.T., Ryan, P.D. (2001). PAST: Paleontological statistics software package. *Palaeontologica Electronica*, **4**, 1–9. Available at: https://tinyurl.com/f3de96ku (10/07/21)

Hong, L., Simon, J.D. (2007). Current understanding of the binding sites, capacity, affinity, and biological significance of metals in melanin. *Journal of Physical Chemistry*, **111**, 7938-7947.

DOI: 10.1021/jp071439h

Horčičko, J.; Borovanský, J.; Duchoň, J.; Procházková, B. (1973). Distribution of zinc and copper in pigmented tissues. *Hoppe-Seylers Zeitschrift fur Physiologische Chemie*, **354**, 203-204. DOI: 10.1515/bchm2.1973.354.1.203

Ito, S., Wakamatsu, K. (1998). Chemical Degradation of Melanins: Application to Identification of Dopamine-melanin. *Pigment Cell Research*, **11**, 120–126. DOI: 10.1111/j.1600-0749.1998.tb00721.x

Ito, S., Wakamatsu, K. (2003). Quantitative analysis of eumelanin and pheomelanin in humans, mice, and other animals: A comparative review. *Pigment Cell Research*, **16**, 523–531. DOI: 10.1034/j.1600-0749.2003.00072.x

Ito, S., Nakanishi, Y., Valenzuela, R.K., Brilliant, M.H., Kolbe, L., Wakamatsu, K. (2011). Usefulness of alkaline hydrogen peroxide oxidation to analyze eumelanin and pheomelanin in various tissue samples: application to chemical analysis of human hair melanins. *Pigment Cell & Melanoma Research*, **24**, 605–613. DOI: 10.1111/j.1755-148X.2011.00864.x

Ito, S., Wakamatsu, K., Glass, K.E., Simon, J.D. (2013). High-performance liquid chromatography estimation of cross-linking of dihydroxyindole moiety in eumelanin. *Analytical Biochemistry*, **434**, 221–225. DOI: 10.1016/j.ab.2012.12.005

Kouketsu, Y., Mizukami, T., Mori, H., Endo, S., Aoya, M., Hara, H., Nakamura, D., Wallis, D. (2014). A new approach to develop the Raman carbonaceous material geothermometer for low-grade metamorphism using peak width. *Island Arc*, **23**, 33-50. DOI: 10.1111/iar.12057

Lafuente, B., Downs, R.T., Yang, H., Stone, N. (2016). The power of databases. The RRUFF project. In: Armbruster, T., Danisi, R.M. *Highlights in Mineralogical Crystallography. De Gruyter (O)*, 1–29 p. DOI: 10.1515/9783110417104-003

Li, Q., Gao, K.-Q., Meng, Q., Clarke, J.A., Shawkey, M.D., D'Alba, L., Pei, R., Ellison, M., Norrell, M.A., Vinther, J. (2012). Reconstruction of *Microraptor* and the evolution of iridescent plumage. *Science*, **335**, 1215–1219. DOI: 10.1126/science.1213780

Liu, Y., Simon, J.D. (2005). Metal-ion interactions and the structural organization of *Sepia* melanin. *Pigment and Cell Research*, **18**, 42-48. DOI: 10.1111/j.1600-0749.2004.00197.x

Neumann, V.H., Borrego, A.G., Cabrera, L., Dino, R. (2003). Organic matter composition and

distribution through the Aptian-Albian lacustrine sequences of the Araripe Basin, northeastern Brazil. *International Journal of Coal Geology*, **54**, 21–40. DOI: 10.1016/S0166-5162(03)00018-1

Osés, G.L., Petri, S., Voltani, C.G., Prado, G.M.E.M., Galante, D., Rizzutto, M.A., Rudnitzki, I.D., Silva, E.P., Rodrigues, F., Range, E.C., Sucerquia, P.A., Pacheco, M.L.A.F. (2017). Deciphering pyritization-kerogenization gradient for fish soft-tissue preservation. *Scientific Reports*, **7**, 1468. DOI: 10.1038/s41598-017-01563-0

Pérez, C.A., Radtke, M., Sánchez, H.J., Tolentino, H., Neuenshwander, R.T., Barg, W., Rubio, M., Bueno, M.I.S., Raimundo, I.M., Rohwedder, J.R. (1999). Synchrotron radiation X-ray fluorescence at the LNLS: Beamline instrumentation and experiments. *X-Ray Spectrometry*, **28**, 320-326. DOI: 10.1002/(SICI)1097-4539(199909/10)28:5<320::AID-XRS359>3.0.CO;2-1

Pérez, C.A., Murari, J.F.J., Moreno, G.B.Z.L., Silva, J.L., Piton, J.R. (2016). Development of fast scanning X-ray fluorescence microscopy at the LNLS D09BXRF beamline. *AIP Conference Proceedings*, **1764**, 030001-1-030001-3. DOI: 10.1063/1.4961135

Pinheiro, F.L., Prado, G., Ito, S., Simon, J.D., Wakamatsu, K., Anelli, L.E., Andrade, J.A.F.G., Glass, K.E. (2019). Chemical characterization of pterosaur melanin challenges color inferences in extinct animals. *Scientific Reports*, **9**, 15947. DOI: 10.1038/s41598-019-52318-y

Prado, G., Arthuzzi, J.C.L., Osés, G.L., Callefo, F., Maldanis, L., Sucerquia, P., Becker-Kerber, B., Romero, G., Quiroz-Valle, F.R., Galante, D. (2021). Synchrotron radiation in palaeontological investigations: Examples from Brazilian fossils and its potential to South American palaeontology. *Journal of South American Earth Sciences*, **108**, 102973. DOI: 10.1016/j.jsames.2020.102973

Prado, G.M.E.M. (2017). Pigmentação fóssil: Tafonomia física de penas fósseis das das bacias do Araripe (Cretáceo) e Taubaté (Paleógeno), Brasil. Dissertação (Mestrado em Ciências), *Instituto de Geociências*, Universidade de São Paulo, São Paulo. 118 p.

Ravel, B., Newville, M. (2005). ATHENA, ARTEMIS, HEPHAESTUS: data analysis for X-ray absorption spectroscopy using IFEFFIT. *Journal of Synchrotron Radiation*, **12**, 537–541. DOI: 10.1107/S0909049505012710

Schneider, C.A., Rasband, W.S., Eliceiri, K.W. (2012). NIH Image to ImageJ: 25 years of image

analysis. *Nature Methods*, **9**, 671–675. DOI: 10.1038/nmeth.2089

Schweitzer, M.H., Avci, R., Collier, T., Goodwin, M.B. (2008). Microscopic, chemical and molecular methods for examining fossil preservation. *Comptes Rendus Palevol*, **7**, 159-184. DOI: 10.1016/j.crpv.2008.02.005

Solé, V.A., Papillon, E., Cotte, M., Walter, P., Susini, J. (2007). A multiplatform code for the analysis of energy-dispersive X-ray fluorescence spectra. *Spectrochimica Acta Part B: Atomic Spectroscopy*, **62**, 63–68. DOI: 10.1016/j.sab.2006.12.002

Wakamatsu, K., Ito, S. (2002). Advanced Chemical Methods in Melanin Determination. *Pigment Cell Research*, **15**, 174–183. DOI: 10.1034/j.1600-0749.2002.02017.x

CHAPTER 05 - CHEMICAL CHARACTERIZATION OF PTEROSAUR MELANIN CHALLENGES COLOUR INFERENCES IN EXTINGT ANIMALS

www.nature.com/scientificreports

SCIENTIFIC REPORTS
nature research

OPEN

Chemical characterization of pterosaur melanin challenges color inferences in extinct animals

Felipe L. Pinheiro[1*], Gustavo Prado[2*], Shosuke Ito[3], John D. Simon[4], Kazumasa Wakamatsu[3], Luiz E. Anelli[2], José A. F. Andrade[5] & Keely Glass[6]

Melanosomes (melanin-bearing organelles) are common in the fossil record occurring as dense packs of globular microbodies. The organic component comprising the melanosome, melanin, is often preserved in fossils, allowing identification of the chemical nature of the constituent pigment. In present-day vertebrates, melanosome morphology correlates with their pigment content in selected melanin-containing structures, and this interdependency is employed in the color reconstruction of extinct animals. The lack of analyses integrating the morphology of fossil melanosomes with the chemical identification of pigments, however, makes these inferences tentative. Here, we chemically characterize the melanin content of the soft tissue headcrest of the pterosaur *Tupandactylus imperator* by alkaline hydrogen peroxide oxidation followed by high-performance liquid chromatography. Our results demonstrate the unequivocal presence of eumelanin in *T. imperator* headcrest. Scanning electron microscopy followed by statistical analyses, however, reveal that preserved melanosomes containing eumelanin are undistinguishable to pheomelanin-bearing organelles of extant vertebrates. Based on these new findings, straightforward color inferences based on melanosome morphology may not be valid for all fossil vertebrates, and color reconstructions based on ultrastructure alone should be regarded with caution.

Fossilization is a rapid process that degrades and converts the biomolecules that define the characteristics of living organisms into long, nearly indistinguishable chains of stable hydrocarbons[1,2]. Melanins, however, demonstrate surprising resilience in the geological record due to their polymeric, highly cross-linked structures[3–6]. Widely distributed within vertebrates as one of the main colour-producing biochromes, melanins constitute a class of heterogenous molecules derived from L-tyrosine[6,7]. In animals, melanins are found either as eumelanins, associated to dark brown/black hues, or phaeomelanins, which correspond to pale yellow to rufous brown tones[8]. In vertebrates, melanins are synthesized and stored in specialized organelles called melanosomes, which are usually found in integuments (and its appendages) as well as in internal organs[9]. Melanosomes are fairly common in exceptionally preserved fossils as 200–2000 nm long microbodies, and are generally associated with keratinized soft tissues, such as feathers and hairs[10–12]. Melanosome morphology is often used as a proxy for animal color, so the presence of these organelles in the fossil record has broad biological implications[11,12].

The morphological similarities between melanosomes and exogenous bacteria means that the observation of microbodies found in fossilized soft tissues does not guarantee the preservation of pigments[13–18]. On account of this, direct chemical protocols are necessary for the unequivocal identification of these microbodies as preserved melanosomes.

Pterosaurs were a diverse group of Mesozoic flying archosaurs, which usually borne conspicuous cranial ornamentation in the shape of the bone or soft tissue headcrests. Pterosaur headcrests display strong positive allometric growth[19] and are sexually dimorphic traits in some species[20], which support their function as display structures[21,22]. Here, portions of the Brazilian pterosaur *Tupandactylus imperator* headcrest (Fig. 1A–C) were degraded and analyzed using alkaline hydrogen peroxide oxidation and high-performance liquid

[1]Laboratório de Paleobiologia, Universidade Federal do Pampa, São Gabriel, 97300-162, Brazil. [2]Instituto de Geociências, Universidade de São Paulo, São Paulo, Brazil. [3]Department of Chemistry, Fujita Health University School of Medical Sciences, Toyoake, Aichi, 470-1192, Japan. [4]Lehigh University, Bethlehem, PA, 18015, USA. [5]Centro de Pesquisas Paleontológicas da Chapada do Araripe, Departamento Nacional de Produção Mineral, 63100-440, Crato, Brazil. [6]Department of Chemistry, Duke University, Durham, NC, 27708, USA. *email: felipepinheiro@unipampa.edu.br; gustavo.marcondes.prado@usp.br

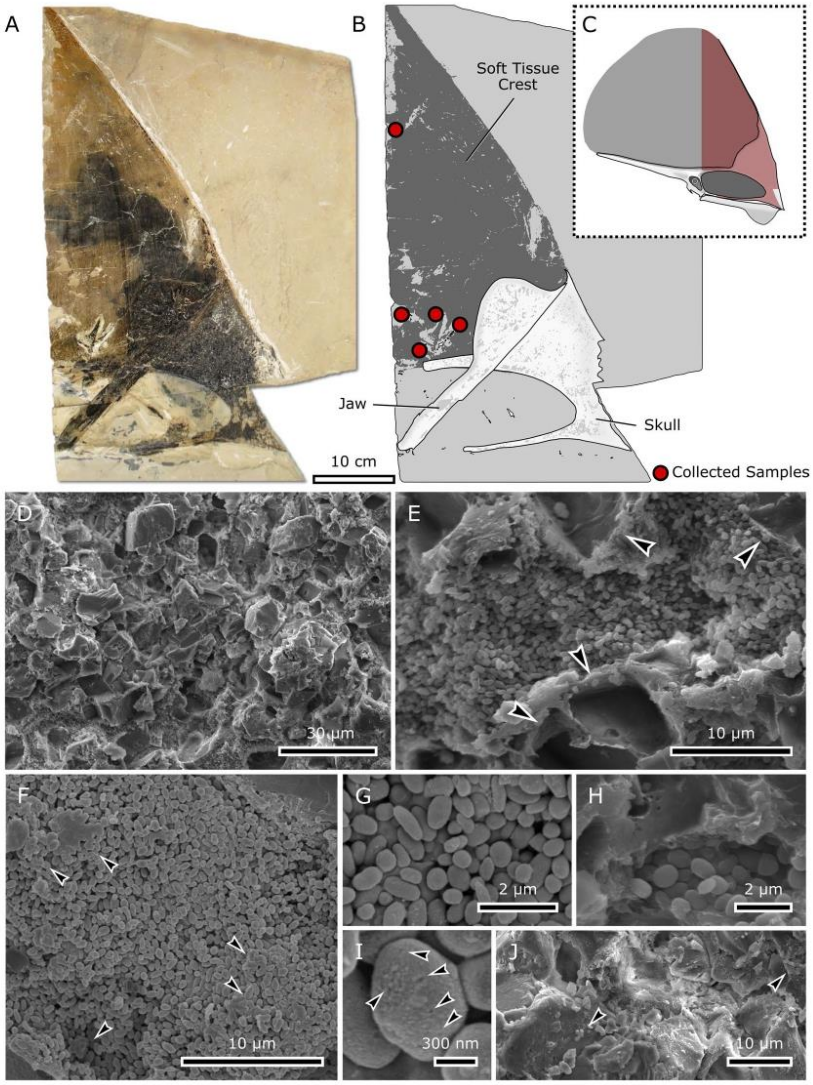

Figure 1. *Tupandactylus imperator* (specimen CPCA 3590) from the Crato Formation and headcrest microbodies. (**A**) Partial skull with its lower jaw overlying the headcrest. (**B**) Interpretative drawings of the figure (**A**,**C**) according to skull position. (**D**) Headcrest tissue exhibiting the blocky calcite crystals, and (**E**) melanosomes amidst external molds of neomorphic crystals (arrowheads). (**F**,**G**) Densely packed microbodies with subspherical morphology. (**H**) Keratin-like structure overlying or surrounding particles. (**I**) Scattered pits (arrowheads) on the microbody surface. (**E**) Calcite crystals blocks located amongst microbodies, with several pigmentary particles scattered on their surface (arrowheads).

chromatography. Samples of the crest tissue were also analyzed using Raman Spectroscopy and Synchrotron Radiation X-Ray Fluorescence (Supplementary Information). Our results are the first to demonstrate the presence of preserved melanin in an archosaur and challenge color inferences in extinct animals using melanosome morphology alone.

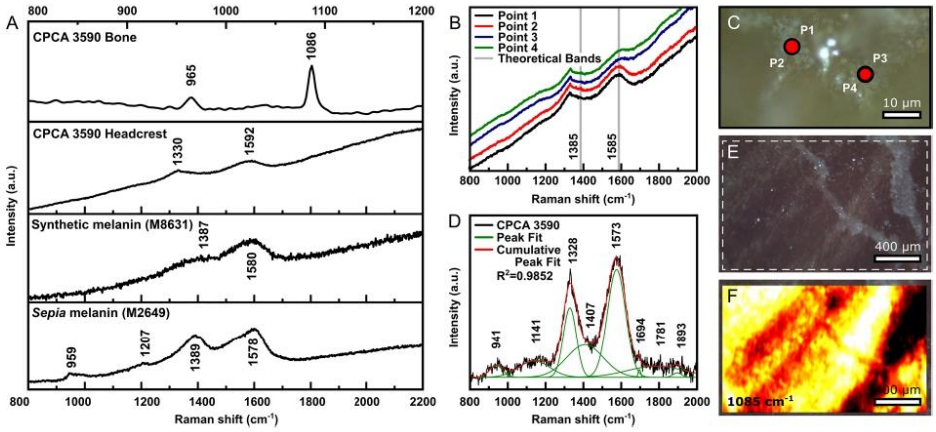

Figure 2. Raman spectra from *T. imperator* (CPCA 3590) headcrest and melanins. (**A**) The top spectrum is from the bony area of the headcrest showing peaks of CO_3^{2-} (at 1086 cm^{-1}) and PO_4^{3-} (at 965 cm^{-1}), which is consistent with a bioapatite variety. The second spectrum is that of the headcrest, and is similar to the two shown below, those of synthetic and *Sepia* melanins, respectively. (**B**) Raman spectra from dark bands of the headcrest exhibiting a signal variation between the two regions of measurement (red circles indicate the two points where four measurements were made) (**C**). Grey dashed lines in (B) represent the theoretical bands of eumelanin. (**D**) Fitted spectra using Gaussian function ($R^2 = 0.9852$) from the Point 1 seen in (**B**), showing that multiple bands are also observed as predicted in other studies. (**E**) Microscopic image from the headcrest surface, showing the region where the fluorescence mapping was performed (white dashed lines). (**F**) Map of the 1085 cm^{-1} region that is diagnostic of calcite, from the area seen in (**E**), indicating a faint signal of the soft tissues, suggesting that calcite from matrix predominates.

Results

Scanning electron microscopy (SEM). While limited to the headcrest, microbodies exhibit a wide distribution throughout the tissue, albeit forming local clusters (Fig. 1D). They occur amidst neomorphic crystals rather similar to "blocky calcite crystals"[23] (Fig. 1E). There is also evidence of lamellar minerals typical of clays, such as phyllosilicates.

The microbodies are densely packed (Fig. 1F,G), with an average size of 441 ± 96.5 nm in diameter and 653 ± 148 nm in length ($n = 331$), indicating that their morphology is predominantly prolate (Supplementary Information). The microbodies retained their integrity without being warped or broken throughout the imaged region, with the exception of a small portion of microbodies. The scattered pits on their rough surfaces, occurring in several parts and indiscriminately to morphology, are attributed to the 10 nm layer of Au/Pd coating applied to the surface to increase spatial resolution (Fig. 1I). In highly dense regions, microbodies are also attached to an amorphous structure (Fig. 1F), but these are much rarer than the free microbodies. Particles can also be found onto blocky crystals, where they occur in small bundles (Fig. 1J).

Raman spectroscopy (RS). The Raman spectra of *T. imperator* headcrest contain diagnostic peaks both of calcium phosphate and eumelanin (Fig. 2A; Fig. S4)[24–31]. Although the peaks for apatite and eumelanin are present throughout the tissue, the associated bands are more intense in the dark stripped regions of the headcrest (Fig. 2B,C; Fig. S4, A, B). Based on the presence of 318 cm^{-1} and 1077 cm^{-1} peaks (Figs 2E,F and S4C), comparative analysis with standard minerals indicates that CPCA 3590 bone and soft-tissues consists of hydroxyapatite ($Ca_5(PO_4)_3(OH)$). More important, the identified bands at *ca*. 1330 to 1592 cm^{-1} are in overall agreement with the diagnostic spectra of eumelanin[24–31].

The fitting of CPCA 3590 spectra (Fig. 2D) yielded several bands but the most diagnostic ones occur centered at about 1328 cm^{-1} and 1575 cm^{-1} (Table S2). Despite the former is slightly shifted to the left, both bands are similar to those of synthetic and *Sepia officinalis* melanins (Sigma-Aldrich M2649) from our experiments (Fig. 2A) and reported in the literature. For synthetic melanin (Sigma-Aldrich M8631), the two most intense peaks occur at 1387 cm^{-1} and 1580 cm^{-1}, whereas for the *Sepia*-derived melanin, they are centered at about 1389 cm^{-1} and 1578 cm^{-1}. Other compounds present in the sample, such as carbonates and phosphates, may be influencing the spectra and affecting the melanin peak intensities (Fig. 2E,F). Furthermore, the broad bandwidth is reflective of the heterogeneity/disorder of eumelanin structure[24], which may have incorporated metals, especially Ca and Mn, among its oligomer sheets[32]. Moreover, the slight shift in the Raman peaks may also indicate that *T. imperator* eumelanin went through a substantial change, possibly related to loss of functional groups, or may also be derived from the C–N stretching from the indole ring[33]. Regardless of these features, both bands can be confidently assigned to the stretching and plane vibrations of C–C, C–OH, C–N, C–O from pyrrole and indole rings[25,27–29,31,33]

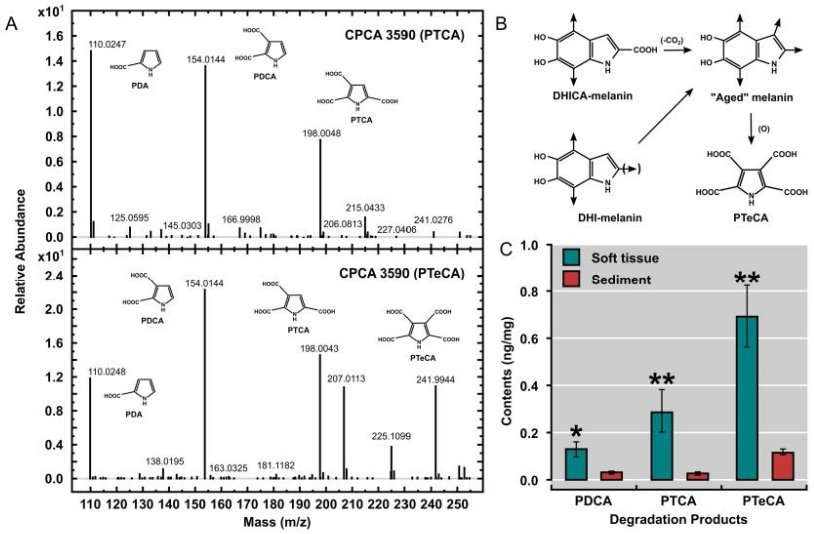

Figure 3. Mass spectrum of CPCA 3590 headcrest melanin. (**A**) Mass spectrum from the degradation products of alkaline peroxide oxidation. (**B**) Hypothetic structural modifications of eumelanin from *T. imperator* (based on Ito *et al.*[5]), according to the most abundant yielding recovered from the oxidation process (i.e. PTeCA). (**C**) Oxidation was performed on four separate occasions and the results were shown as mean ± SEM. Values for the sediment are close to the detection limits. Values are in ng/mg. Differences as evaluated by students' t-Test (two-tailed) are $P < 0.01$ except for PDCA ($P < 0.05$).

(Supplementary Information). The less intense peaks in CPCA 3590 may result from the trace amounts of melanin. In contrast to carbon-rich compounds that exhibit overtone scattering bands (second-order peaks) above 2400 cm^{-1} [34], these peaks are absent, supporting the argument that they are derived from eumelanin[28,29]. The previous interpretation of phosphatization of the headcrest and microbodies[35] is also supported by RS.

Identification of eumelanin by chemical degradation and high-performance liquid chromatography (HPLC). The first modern attempt to chemically characterize melanins in the fossil record used synchrotron X-ray to identify trace metals alleged to be unique markers of the presence of eumelanin[36]. Since then, several attempts have been made using this methodology to evaluate different types of fossils[37]. However, this method did not survive scrutiny, as several taphonomic processes are able to concentrate metals and originate similar patterns under synchrotron light sources[13,37]. More recently, chemical fingerprints identified by time-of-flight secondary ion mass spectrometry (ToF-SIMS) was successfully employed to characterize both pheo- and eumelanins in fossils[4,10,15,16,38–40]. Direct and conclusive chemical evidence, however, requires carrying out chemical degradation of the organic matter by alkaline hydrogen peroxide oxidation, which, if melanin is present, generates specific and unique chemical markers[3,41,42].

Specifically, pyrrole-2,3,5-tricarboxylic acid (PTCA) and pyrrole-2,3-dicarboxylic acid (PDCA) are the chemical degradation markers of 5,6-dihydroxyindole-2-carboxylic acid (DHICA) and 5,6-dihydroxyindole (DHI), respectively, and, hence, of eumelanin[41]. Similarly, pyrrole-2,3,4,5-tetracarboxylic acid (PTeCA) is considered an index of highly cross-linked, "aged" melanin[5]. As a consequence, it is suggested that PTeCA must be the most common moiety in ancient materials that underwent mild thermal maturation[42].

In this study, samples of *Tupandactylus imperator* headcrest (CPCA 3590) were oxidized by alkaline hydrogen peroxide after demineralization, in accordance to standard protocols[3,41,42] (Materials and Methods; Supplementary Information). HPLC analysis of the oxidation products yielded melanin markers PTCA, PDCA, and PTeCA (Figs 3, S4, Table S3). Although their levels were trace, they were significantly higher than those in the adjacent sediment, and their identification was also confirmed by liquid chromatography-mass spectrometry (LC-MS, See Fig. S5). It is noteworthy that the level of PTeCA is much higher than that of PTCA, with a PTeCA/PTCA ratio being 2.41 ± 0.16, which is characteristic of highly cross-linked eumelanin[3,5]. Ergo, the results of HPLC (Fig. 3A) indicate that most of the *T. imperator* eumelanin is derived from the crosslinking of DHICA and DHI fractions (Fig. 3B). Although the contribution of PDCA from DHI units cannot be excluded, because PTCA occur twice as much (Fig. 3C), it is suggested that this moiety is more involved in structural alterations[5,42].

Pheomelanin oxidation produces thiazole-2,4,5-tricarboxylic acid (TTCA) and thiazole-4,5-dicarboxylic acid (TDCA); both markers are derive from the pigment's benzothiazole moiety[5,41]. As neither marker were detected in this samples, the predominant pigment in the CPCA 3590 headcrest is eumelanin.

Discussion

Previous microstructural analyses of CPCA 3590 identified the subspherical microbodies as autolithified bacteria[35], an assumption mainly based on (i) their comparable size with modern microorganisms; (ii) the lack of the typical organization patterns often seen in melanosomes; (iii) the presence of supposed extracellular polymeric substances and (iv) the putative ongoing cellular division[35]. This interpretation was debated in subsequent publications – questioned by some[43] and favored by others[13–16]. As pointed out by the authors that favored the bacterial alternative, the physical aspects of these microbodies, such as morphology, distribution, and size, were insufficient to completely eliminate the hypothesis of both endogenous or exogenous bacteria[17,18,44–46]. However, it is widely accepted that chemical analysis can significantly aid in their identification[10,13–16,45,47,48].

Although microbes are rarely preserved, the fossilization of animal soft-tissues usually involves the presence of microorganisms that alter geochemical processes at the microscopic level, inducing the precipitation of several minerals[44,49,50]. Experiments simulating diagenesis in microbes indicate that although their molecular signatures can be slightly altered[51], their morphology often exhibits significant changes, mostly in the form of body deflation or partial degradation[52]. These features are absent in our sample, in which microbodies are predominantly solid particles. Furthermore, *T. imperator* microbodies also show several characteristics that are consistent with being melanosomes, such as absence of morphotype diversity, no evidence of binary fission and lack of bacterial by-products (such as honeycomb-like structures)[53], distinct chemistry differences in chemical composition between former soft tissue and matrix[54], and limited microbody distribution (Supplementary Information).

Energy dispersive spectroscopy (EDS) data show that *T. imperator* microbodies are Ca- and P-rich, suggesting that they are composed of calcium phosphate[35]. In addition, SR-μXRF indicates the presence of Ca, Cu, Fe, Mn and Zn (Fig. S3). Since phosphatization is the common type of bacterial preservation[50], these microbodies could indeed represent phosphatized microorganisms. However, the chemical signatures revealed in our study show that the CPCA 3590 headcrest contains eumelanin. Therefore, the combination of morphological and chemical analyses confirms an unequivocal identification of the microbodies as melanosomes.

Since the seminal work of Vinther *et al.*[55], inferences about the color patterns of fossil animals rely mainly on melanosome morphology[13], in spite of other studies that indicate the lack of correlation between melanosome shape and their melanin content[56,57]. While the connection between shape and color is unresolved[13–15,58], it is commonly invoked that high-aspect-ratio ("sausage-like") melanosomes contain eumelanins (black to dark brown in color), whereas globular, low-aspect-ratio melanosomes normally reflect the presence of pheomelanin (rufous red to pale yellow). Moreover, statistical analyses testing the correlation between melanosome morphology and color of extant birds demonstrated a high (up to 82% accuracy) predictive potential for animals in which hues are mainly determined by melanins[13,59,60].

A recent contribution[59], however, demonstrated that a similar predictive model cannot be extrapolated to lepidosaurs, turtles, and crocodiles, whereas it is reasonably accurate for bird feathers and mammalian hair. As such, these latter animals would present a high diversity of melanosome morphologies and usually a clear correlation between different morphotypes, the type of melanin they contain and, as a consequence, expressed color[59]. The transition between the primitive low melanosome diversity displayed by lizards, turtles and crocodiles and the pattern displayed by present-day mammals and birds would have been driven by a distinct physiological shift[59]. Alternatively, this change in pattern would be a consequence of the loss of the chromatophore complex, responsible for the color diversity of amniotes showing the primitive condition[13]. The chromatophore system might be superfluous for animals in which color patterns are expressed in well-developed integumentary structures, such as feathers and fur[13].

It would, however, be expected that pterosaurs did not depend on chromatophores to express color patterns, as these archosaurs were also covered by a dense layer of supposedly keratinous filamentous structures that were potentially homologous to feathers[61]. The analyses of Li *et al.*[59] included two pterosaur specimens, in which the microstructure of the hair-like coverage showed a low diversity of low-aspect-ratio melanosomes, more consistent with what is observed in lepidosaur, turtle and crocodile skin than to feathers or mammal fur. A similar pattern is also displayed in *Tupandactylus imperator* headcrest (based on CPCA 3590). Morphologically, the vast majority of the microbodies revealed by SEM images would be identified as pheomelanin-like melanosomes. In spite of that, the chemical degradation performed yielded the specific markers of eumelanin (i.e. PTCA, PDCA, and PTeCA) in concentrations compatible with highly cross-linked eumelanin[3,5,42], and the absence of the specific markers for pheomelanin. Thus, these results imply that a clear distinction between high-aspect-ratio eumelanosomes and spherical phaeomelanosomes is not valid for pterosaurs, and by extrapolation, for amniotes that share the primitive condition of low melanosome diversity. Indeed, CPCA 3590 organelles are remarkably similar to internal eumelanosomes[58] from basal-most vertebrates, such as the amphibians, cyclostomes[38,39] and cuttlefish[3]. Consequently, any color inference in animals presenting the plesiomorphic condition based on melanosome morphology would be equivocal, as ellipsoidal, low-aspect-ratio bodies can contain both pheo- and eumelanins. We should also stress that the circumstances surrounding the physiological shift proposed by Li *et al.*[59] are still obscure, and it would be precipitate to imply that animals such as non-avian dinosaurs shared with birds a straightforward correlation between melanosome morphology and their pigment content.

Most chemical surveys of fossil pigments have thus far identified eumelanosomes and eumelanin fingerprints. The reason for the low occurrence of pheomelanin or pheomelanosomes is still unknown; it remains possible that pheomelanin preservations may not be as robust as that of eumelanin[62]. Although other classes of biochromes (e.g. carotenoids and porphyrins) are relatively common in sedimentary deposits, these compounds are extremely frail and prone to chemical alterations[1,63,64]. For instance, following deposition, porphyrins, and carotenoids readily experience several chemical reactions such as oxidation and polymerization, transforming them into long chains of hydrocarbons[1,65,66]. Because melanin is a highly conserved polymer[5,10], and eumelanins are the most common class of melanins in nature, it is expected that this pigment is present in the majority of exceptionally preserved fossils[12,13].

Studies that identified pheomelanin have rarely found corresponding microbodies preserved in three dimensions. As a consequence, phaeomelanic colorations were often based on the recognition of melanosome external molds[67] or chemical fingerprints[40]. Despite the latter approach being a more reliable way to identify pheomelanin, the former possesses serious issues to color inferences. Our results support this claim, as spherical and subspherical microbodies can potentially bear one or both types of melanin pigments or be composed mainly by one type of moiety. This may be true to some dinosaurs, such as *Sinosauropteryx*[67], *Anchiornis*[68], *Yi qi*[69], and *Psittacosaurus*[70], whose color inferences were based solely on the morphology of molds, with no further chemical and/or statistical support.

The extremely selective nature of fossilization has the effect of building a virtually insurmountable barrier between post-diagenetic remains of organisms and living beings. The recent recognition of the persistence of melanins and melanin-containing organelles in the fossil record[3,42] allowed reconstructions of color patterns of extinct animals. However, many paleocolor studies relied basically on the microbody morphology, raising questions about the validity of their outcomes. Correspondingly, our results strongly support these disputes. Since melanins are directly involved in complex social and ecological behaviors, such as camouflage, intraspecific recognition, and sexual display, their correct characterization can sum to the understanding of the biology of extinct animals[13], and color reconstruction cannot rely solely on microstructural analysis[13,71].

Materials and Methods

Specimen CPCA 3590 is preserved in a grayish-color laminated limestone typical of Crato Formation beds[35] (Supplementary Information). This fossil is comprised of a fairly complete skull with headcrest's soft tissues, which allows it to be assigned to the tapejarid species *Tupandactylus imperator* (for taxonomic details, see Pinheiro *et al.*[70]). This specimen is permanently housed in the Paleontological collection of the *Centro de Pesquisas Paleontólógicas da Chapada do Araripe* (CPCA, Crato, Ceará, Brazil). The headcrest's soft tissue was examined using a scanning electron microscope (SEM). Elemental mapping was carried out using synchrotron radiation-micro X-ray fluorescence (SR-μXRF). The molecular content was examined using Raman spectroscopy (RS) and high-performance liquid chromatography (HPLC). The latter technique was performed to quantitate melanin degradation products, PTCA, PDCA, and PTeCA after treatment by alkaline hydrogen peroxide oxidation of demineralized samples of CPCA 3590[5,41]. To confirm the identification of PTCA and PTeCA, LC-MS of extracts of oxidation products was performed according to previously described methods (see Glass *et al.* 3). Following the image acquisition using SEM, melanosomes and minerals were measured using ImageJ[72], and statistical analysis was performed using Past 3.06[73]. SR-μXRF mapping was processed using PyMCA 5.1.1 software and Raman spectra were processed using Renishaw Wire 4.1 and Wire 4.4, and Origin 9.6.0.172. Analyses were performed at the Duke University Chemistry Department Mass Spectrometry Facility, Brazilian Synchrotron Light Laboratory (LNLS) and Institute of Chemistry of the University of São Paulo (IQ-USP). See SOM2 for details on material and methods.

Data availability

No datasets were generated or analyzed during the current study.

Received: 13 June 2019; Accepted: 11 October 2019;
Published online: 04 November 2019

References

1. Briggs, D. E. G. & Summons, R. E. Ancient biomolecules: Their origins, fossilization, and role in revealing the history of life. *BioEssays* **36**, 482–490 (2014).
2. Parry, L. A. *et al.* Soft-Bodied Fossils Are Not Simply Rotten Carcasses – Toward a Holistic Understanding of Exceptional Fossil Preservation: Exceptional Fossil Preservation Is Complex and Involves the Interplay of Numerous Biological and Geological Processes. *BioEssays* **40**, 1–11 (2018).
3. Glass, K. E. *et al.* Direct chemical evidence for eumelanin pigment from the Jurassic period. *Proc. Natl. Acad. Sci.* **109**, 10218–10223 (2012).
4. Lindgren, J. *et al.* Molecular preservation of the pigment melanin in fossil melanosomes. *Nat. Commun.* **3**, 824 (2012).
5. Ito, S., Wakamatsu, K., Glass, K. E. & Simon, J. D. High-performance liquid chromatography estimation of cross-linking of dihydroxyindole moiety in eumelanin. *Anal. Biochem.* **434**, 221–225 (2013).
6. Slominski, A., Tobin, D. J., Shibahara, S. & Wortsman, J. Melanin pigmentation in mammalian skin and its hormonal regulation. *Physiol. Rev.* **84**, 1155–1228 (2004).
7. Slominski, A., Zmijewski, M. A. & Pawelek, J. L-tyrosine and L-dihydroxyphenylalanine as hormone-like regulators of melanocyte functions. *Pigment Cell Melanoma Res.* **25**, 14–27 (2012).
8. Roy, A., Pittman, M., Saitta, E. T., Kaye, T. G. & Xu, X. Recent advances in amniote palaeocolour reconstruction and a framework for future research. *Biol. Rev.* 1–29, https://doi.org/10.1111/brv.12552 (2019).
9. Dubey, S. & Roulin, A. Evolutionary and biomedical consequences of internal melanins. *Pigment Cell Melanoma Res.* **27**, 327–338 (2014).
10. Colleary, C. *et al.* Chemical, experimental, and morphological evidence for diagenetically altered melanin in exceptionally preserved fossils. *Proc. Natl. Acad. Sci.* **112**, 12592–12597 (2015).
11. Vinther, J. A guide to the field of palaeo colour: Melanin and other pigments can fossilise: Reconstructing colour patterns from ancient organisms can give new insights to ecology and behaviour. *BioEssays* **37**, 643–656 (2015).
12. Vinther, J. Fossil melanosomes or bacteria? A wealth of findings favours melanosomes. *BioEssays* **38**, 220–225 (2015).
13. Schweitzer, M. H., Lindgren, J. & Moyer, A. E. Melanosomes and ancient coloration re-examined: A response to Vinther 2015 (DOI 10.1002/bies.201500018). *BioEssays* **37**, 1174–1183 (2015).
14. Moyer, A. E. *et al.* Melanosomes or Microbes: Testing an Alternative Hypothesis for the Origin of Microbodies in Fossil Feathers. *Sci. Rep.* **4**, 4233 (2014).
15. Lindgren, J. *et al.* Interpreting melanin-based coloration through deep time: a critical review. *Proc. R. Soc. B Biol. Sci.* **282**, 20150614 (2015).
16. Lindgren, J. *et al.* Molecular composition and ultrastructure of Jurassic paravian feathers. *Sci. Rep.* **5**, 13520 (2015).

17. Iniesto, M. *et al.* Involvement of microbial mats in early fossilization by decay delay and formation of impressions and replicas of vertebrates and invertebrates. *Sci. Rep.* **6**, 25716 (2016).
18. Iniesto, M., Villalba, I., Buscalioni, A. D., Guerrero, M. C. & López-Archilla, A. I. The effect of microbial mats in the decay of anurans with implications for understanding taphonomic processes in the fossil record. *Sci. Rep.* **7**, 45160 (2017).
19. Pinheiro, F. L. & Rodrigues, T. Anhanguera taxonomy revisited: is our understanding of Santana Group pterosaur diversity biased by poor biological and stratigraphic control? *PeerJ* **3**, 1–29 (2017).
20. Wang, X. *et al.* Sexually Dimorphic Tridimensionally Preserved Pterosaurs and Their Eggs from China. *Curr. Biol.* **24**, 1323–1330 (2014).
21. Hone, D. W. E., Naish, D. & Cuthill, I. C. Does mutual sexual selection explain the evolution of head crests in pterosaurs and dinosaurs? *Lethaia* **45**, 139–156 (2012).
22. Knell, R. J., Naish, D., Tomkins, J. L. & Hone, D. W. E. Sexual selection in prehistoric animals: detection and implications. *Trends Ecol. Evol.* **28**, 38–47 (2013).
23. Heimhofer, U. *et al.* Deciphering the depositional environment of the laminated Crato fossil beds (Early Cretaceous, Araripe Basin, North-eastern Brazil). *Sedimentology* **57**, 677–694 (2010).
24. Huang, Z. *et al.* Raman spectroscopy of *in vivo* cutaneous melanin. *J. Biomed. Opt.* **9**, 1198 (2004).
25. Galván, I. *et al.* Raman spectroscopy as a non-invasive technique for the quantification of melanins in feathers and hairs. *Pigment Cell Melanoma Res.* **26**, 917–923 (2013).
26. Galván, I., Jorge, A., Solano, F. & Wakamatsu, K. Vibrational characterization of pheomelanin and trichochrome F by Raman spectroscopy. *Spectrochim. Acta Part A Mol. Biomol. Spectrosc.* **110**, 55–59 (2013).
27. Perna, G. Vibrational Characterization of Synthetic Eumelanin by Means of Raman and Surface Enhanced Raman Scattering. *Open Surf. Sci. J.* **5**, 1–8 (2013).
28. Galván, I. & Jorge, A. Dispersive Raman spectroscopy allows the identification and quantification of melanin types. *Ecol. Evol.* **5**, 1425–1431 (2015).
29. Perna, G., Lasalvia, M. & Capozzi, V. Vibrational spectroscopy of synthetic and natural eumelanin. *Polym. Int.* **65**, 1323–1330 (2016).
30. Galván, I., Cerezo, J., Jorge, A. & Wakamatsu, K. Molecular vibration as a novel explanatory mechanism for the expression of animal colouration. *Integr. Biol.* **10**, 464–473 (2018).
31. Galván, I., Araujo-Andrade, C., Marro, M., Loza-Alvarez, P. & Wakamatsu, K. Raman spectroscopy quantification of eumelanin subunits in natural unaltered pigments. *Pigment Cell Melanoma Res.* **31**, 673–682 (2018).
32. Hong, L., Liu, Y. & Simon, J. D. Binding of Metal Ions to Melanin and Their Effects on the Aerobic Reactivity. *Photochem. Photobiol.* **80**, 477 (2004).
33. Capozzi, V. *et al.* Raman and optical spectroscopy of eumelanin films. *J. Mol. Struct.* **744–747**, 717–721 (2005).
34. Jehlička, J., Urban, O. & Pokorný, J. Raman spectroscopy of carbon and solid bitumens in sedimentary and metamorphic rocks. *Spectrochim. Acta - Part A Mol. Biomol. Spectrosc.* **59**, 2341–2352 (2003).
35. Pinheiro, F. L., Horn, B. L. D., Schultz, C. L., Andrade, J. A. F. G. & Sucerquia, P. A. Fossilized bacteria in a Cretaceous pterosaur headcrest. *Lethaia* **45**, 495–499 (2012).
36. Wogelius, R. A. *et al.* Trace Metals as Biomarkers for Eumelanin Pigment in the Fossil Record. *Science (80-.).* **333**, 1622–1626 (2011).
37. Bergmann, U., Manning, P. L. & Wogelius, R. A. Chemical mapping of paleontological and archeological artifacts with synchrotron X-rays. *Annu. Rev. Anal. Chem. (Palo Alto. Calif).* **5**, 361–89 (2012).
38. Clements, T. *et al.* The eyes of Tullimonstrum reveal a vertebrate affinity. *Nature* **532**, 500–503 (2016).
39. Gabbott, S. E. *et al.* Pigmented anatomy in carboniferous cyclostomes and the evolution of the vertebrate eye. *Proc. R. Soc. B Biol. Sci.* **283**, (2016).
40. Brown, C. M. *et al.* An exceptionally preserved three-dimensional armored dinosaur reveals insights into coloration and Cretaceous predator-prey dynamics. *Curr. Biol.* **27**, 2514–2521.e3 (2017).
41. Ito, S. *et al.* Usefulness of alkaline hydrogen peroxide oxidation to analyze eumelanin and pheomelanin in various tissue samples: application to chemical analysis of human hair melanins. *Pigment Cell Melanoma Res.* **24**, 605–613 (2011).
42. Glass, K. *et al.* Impact of diagenesis and maturation on the survival of eumelanin in the fossil record. *Org. Geochem.* **64**, 29–37 (2013).
43. Vitek, N. S., Vinther, J., Schiffbauer, J. D., Briggs, D. E. G. & Prum, R. O. Exceptional three-dimensional preservation and coloration of an originally iridescent fossil feather from the Middle Eocene Messel Oil Shale. *Palaontologische Zeitschrift* **87**, 493–503 (2013).
44. Briggs, D. E. G., Moore, R. A., Shultz, J. W. & Schweigert, G. Mineralization of soft-part anatomy and invading microbes in the horseshoe crab Mesolimulus from the Upper Jurassic Lagerstätte of Nusplingen, Germany. *Proc. R. Soc. B Biol. Sci.* **272**, 627–632 (2005).
45. Barden, H. E. *et al.* Bacteria or melanosomes? A geochemical analysis of micro-bodies on a tadpole from the Oligocene Enspel Formation of Germany. *Palaeobiodiversity and Palaeoenvironments* **95**, 33–45 (2015).
46. Eagan, J. L. *et al.* Identification and modes of action of endogenous bacteria in taphonomy of embryos and larvae. *Palaios* **32**, 206–217 (2017).
47. Mcnamara, M. E. The taphonomy of colour in fossil insects and feathers. *Palaeontology* **56**, 557–575 (2013).
48. Edwards, N. P., Manning, P. L. & Wogelius, R. A. Pigments through time. *Pigment Cell Melanoma Res.* **27**, 684–685 (2014).
49. Briggs, D. E. G. & Kear, A. J. Fossilization of Soft Tissue in the Laboratory. *Science (80-.).* **259**, 1439–1442 (1993).
50. Wilby, P. R., Briggs, D. E. G., Bernier, P. & Gaillard, C. Role of microbial mats in the fossilization of soft tissues. *Geology* **24**, 787–790 (1996).
51. Alleon, J. *et al.* Molecular preservation of 1.88 Ga Gunflint organic microfossils as a function of temperature and mineralogy. *Nat. Commun.* **8**, 16147 (2017).
52. Alleon, J. *et al.* Early entombment within silica minimizes the molecular degradation of microorganisms during advanced diagenesis. *Chem. Geol.* **437**, 98–108 (2016).
53. Défarge, C. *et al.* Texture of microbial sediments revealed by cryo-scanning electron microscopy. *SEPM J. Sediment. Res.* **66**, 935–947 (1996).
54. Schultze-Lam, S., Fortin, D., Davis, B. S. & Beveridge, T. J. Mineralization of bacterial surfaces. *Chem. Geol.* **132**, 171–181 (1996).
55. Vinther, J., Briggs, D. E. G., Prum, R. O. & Saranathan, V. The colour of fossil feathers. *Biol. Lett.* **4**, 522–525 (2008).
56. Lazova, R., Klump, V. & Pawelek, J. Autophagy in cutaneous malignant melanoma. *J. Cutan. Pathol.* **37**, 256–268 (2010).
57. Plonka, P. M., Slominski, A. T., Pajak, S. & Urbanska, K. Transplantable melanomas in gerbils (meriones unguiculatus). II: Melanogenesis. *Exp. Dermatol.* **12**, 356–364 (2003).
58. McNamara, M. E. *et al.* Non-integumentary melanosomes can bias reconstructions of the colours of fossil vertebrates. *Nat. Commun.* **9**, 2878 (2018).
59. Li, Q. *et al.* Melanosome evolution indicates a key physiological shift within feathered dinosaurs. *Nature* **507**, 350–353 (2014).
60. Wolnicka-Glubisz, A., Pecio, A., Podkowa, D., Kolodziejczyk, L. M. & Plonka, P. M. Pheomelanin in the skin of Hymenochirus boettgeri (Amphibia: Anura: Pipidae). *Exp. Dermatol.* **21**, 537–540 (2012).
61. Yang, Z. *et al.* Pterosaur integumentary structures with complex feather-like branching. *Nat. Ecol. Evol.* **3**, 24–30 (2019).
62. Smithwick, F. M., Nicholls, R., Cuthill, I. C. & Vinther, J. Countershading and stripes in the theropod dinosaur Sinosauropteryx reveal heterogeneous habitats in the Early Cretaceous Jehol Biota. *Curr. Biol.* **27**, 3337–3343.e2 (2017).
63. Lindgren, J. *et al.* Soft-tissue evidence for homeothermy and crypsis in a Jurassic ichthyosaur. *Nature* **564**, 359–365 (2018).

64. Wiemann, J. *et al*. Fossilization transforms vertebrate hard tissue proteins into N-heterocyclic polymers. *Nat. Commun.* **9**, 4741 (2018).
65. Damsté, J. S. S. & Koopmans, M. P. The fate of carotenoids in sediments: An overview. *Pure Appl. Chem.* **69**, 2067–2074 (1997).
66. Marshall, C. P. *et al*. Carotenoid Analysis of Halophilic Archaea by Resonance Raman Spectroscopy. *Astrobiology* **7**, 631–643 (2007).
67. Zhang, F. *et al*. Fossilized melanosomes and the colour of Cretaceous dinosaurs and birds. *Nature* **463**, 1075–1078 (2010).
68. Li, Q. *et al*. Plumage color patterns of an extinct dinosaur. *Science (80-.).* **327**, 1369–1372 (2010).
69. Xu, X. *et al*. A bizarre Jurassic maniraptoran theropod with preserved evidence of membranous wings. *Nature* **521**, 70–73 (2015).
70. Vinther, J. *et al*. 3D Camouflage in an Ornithischian Dinosaur. *Curr. Biol.* **26**, 2456–2462 (2016).
71. Negro, J. J., Finlayson, C. & Galván, I. Melanins in fossil animals: Is it possible to infer life history traits from the coloration of extinct species? *Int. J. Mol. Sci.* **19**, 1–11 (2018).
72. Schneider, C. A., Rasband, W. S. & Eliceiri, K. W. NIH Image to ImageJ: 25 years of image analysis. *Nat. Methods* **9**, 671–5 (2012).
73. Hammer, Ø., Harper, D. A. T. & Ryan, P. D. PAST: Paleontological Statistics Software Package. *Palaeontol. Electron.* **4**, 1–9 (2001).

Acknowledgements
We thank Carlos A. Perez and Jackson L. Silva (LNLS-CNPEM) for assistance provided during experiments (CNPEM proposal number 20170713); Douglas Galante (LNLS-CNPEM), Gabriel L. Osés and Bruno B. Kerber (UFSCar), Cibele G. Voltani (IGc-USP) for discussions on the methodology employed herein; Evandro P. Silva (IQ-USP, IAG-USP) and Dalva L. F. A. Faria (IQ-USP) for support on the μRaman and FTRaman analysis. Suggestions made by two anonymous reviewers considerably improved the quality of this work. This study was partially funded by the Conselho Nacional de Desenvolvimento Científico e Tecnológico (CNPq process number 305758/2017-9 granted to FLP), the Coordenação de Aperfeiçoamento de Pessoal de Nível Superior (CAPES Finance Code 001 granted to GP) and by a Scholarship Donation (Fujita Health University) granted to KW.

Author contributions
F.L.P. designed the project; F.L.P., G.P., S.I., K.W., J.D.S., L.E.A., J.A.F.A., K.G. conducted the experiments; F.L.P., G.P., S.I., K.G. analyzed and interpreted the results; F.L.P., G.P. wrote the manuscript.

Competing interests
The authors declare no competing interests.

Additional information
Supplementary information is available for this paper at https://doi.org/10.1038/s41598-019-52318-y.

Correspondence and requests for materials should be addressed to F.L.P. or G.P.

Reprints and permissions information is available at www.nature.com/reprints.

Publisher's note Springer Nature remains neutral with regard to jurisdictional claims in published maps and institutional affiliations.

5.7. SUPPLEMENTARY INFORMATION

Chemical characterization of pterosaur melanin challenges color inferences in extinct animals

Felipe L. Pinheiro; Gustavo Prado; Shosuke Ito; John D. Simon; Kazumasa Wakamatsu; Luiz E. Anelli; José A. F. Andrade; Keely Glass

Felipe L. Pinheiro

Email: felipepinheiro@unipampa.edu.br

This PDF file includes:

Supporting methods

Figures S1 to S5

Tables S1 to S3

5.7.1. Supporting text

Geologic Setting

Within the geological succession of the Araripe Basin, Northeastern Brazil (Fig. S1, A), the Crato Formation is one of the four Lower Cretaceous units of the Santana Group [1], the others being the Barbalha, Ipubi and Romualdo formations [2]. The Crato Formation is limited to the N-SE portions of the basin, more conspicuously in the Cariri Valley, Ceará State. Lithologically (Fig. S1, B), this unit consists of laminated limestones and greenish shales sequences with virtually the same thickness, which are also interbedded by sandstones and, occasionally, by thin layers of evaporitic minerals, predominantly gypsum.

The Crato Formation limestone is composed of fine-grained calcite crystals (micrite and spate), with varying content of amorphous organic matter and siliciclastic minerals [3–5]. According to some authors, the carbonate-siliciclastic sequences were deposited in a protected lacustrine environment, with a strong chemocline gradient, especially with respect to salinity and oxygen concentrations [3,6]. Other authors however argue that only the lowermost beds of the Crato Formation (i.e., Nova Olinda member sensu (6), which is the thicker carbonate sequence, can be considered as lacustrine [2]. All other sedimentary series may represent a palaeolake with direct contact with seawater, Sabkha or lagoon environment [2]. The presence of marine bivalves at the top of Crato Formation succession seems to support this interpretation [8].

Independent of the environment, the genesis of the Crato Formation limestones is related to authigenic precipitation of low-Mg calcite. Crystals were precipitated following seasonal phyto- and picoplankton blooms[5], seasonal salinity fluctuations caused by evaporation [7], and/or induced by bacteria from microbial mats and stromatolites [9,10]. This is supported by the presence of fossilized calcified bacteria reported in the region (see 9 and 10) as well as components that are directly associated with the microbial activity, such as honeycomb-like structures and pseudomorphs of pyrite [11,12]. Therefore, these microorganisms are considered a determinant for exceptional preservation of Crato Formation fossils [13]. Different diagenetic processes occurred in the different facies in which fossils are confined. Non-recalcitrant tissues were replaced by iron sulphides at beige facies,

whilst kerogen and calcium phosphates predominate in the greyish facies [11,14,15]. The abundance of fresh water parautochthonous fauna (as Ephemeroptera larvae and anurans) in association to halite pseudomorphs indicates fresh shallow waters at the top, with a putatively episodic hypersaline bottom [5,7,10]. Similarly, the absence of benthic fauna and bioturbated sediments indicate that deep waters were anoxic [7].

Statistical analysis

A statistical survey of size distribution indicates that 11.5% (n=38) of melanosomes lengths are around 576 nm, whereas 15.7% (n=52) of the diameter falls around 442 nm. The aspect ratio distribution indicates that 16% (n=53) are concentrated around 1.1, suggesting that most melanosomes are more oblate than cylindrical. These results considerably contrast with descriptive values, such as mean, standard deviation and median (Table S1). As expected, the size distribution does not correspond to mean values, since the latter only indicate the mean value of the whole population. Ergo, and despite the low variance (CV=0.2 to axes, and CV=0.3 to ratio), the calculated values may not represent the true nature of microbody dimensions, casting doubt of the general aspects used in statistical comparisons.

Performed scatter plot analysis shows a weak correlation between length and diameter (Fig. S2, A; r=0.4084; R^2=0.1668), and One-Way ANOVA results showed to be statistically significant (p<0.001), indicating that both axes are indeed independent variables. This interpretation is also supported by the ratio frequency (Fig. S2, B), which exhibits a mean of 1.5 ± 0.4, while 74.3% of the total ratio occurs between 1.1 to 1.7 frequencies. This result is expected, since these units are usually considered independent variables, and the low correlation and frequency values indicate that CPCA 3590 melanosomes are predominantly oblate/oval. We performed a principal component analysis (PCA) using both CPCA 3590 and the database provided by Li et al. [16] (Fig. S2, C). As a result, the CPCA 3590 microbodies are placed close to melanosomes from brown and penguin colours (i.e., dark black). Size correction does not have a significant impact on this relationship but, at 20%, it brings much closer to penguin (blackish) coloration. On the other hand, melanosomes are close to brownish hue in the bulk data.

Synchrotron Radiation X-Ray Fluorescence (SR-μXRF)

Despite general scepticism of the usefulness SR-μXRF for melanin characterization (cf. 2), we performed an elemental mapping of small samples of CPCA 3590 (Fig. S3). This method aimed to identify elemental distribution throughout the specimen and relate the presence of particular ions (e.g., sulphur) to the process of fossilization and melanogenesis [18]. Albeit different regions were examined, and other elements were found, these results served as a complement to the EDS spectra published in Pinheiro et al. (24: Fig. 3). As a result, the elemental mapping of CPCA 3590 exhibits the presence of As, Ca, Cu, Fe, Mn, Sr, and Zn in headcrest tissue in varying intensities (Fig. S3). For instance, Ca and Mn display a more pronounced and spatially limited occurrence, whereas As, Cu, Fe, Sr, and Zn are less intense and more disperse, reflecting their possible minor concentration in the sample.

Several works have demonstrated the usefulness of SR-μXRF on the elemental mapping of fossils [20–23], even when elements are present in trace amounts [24–27]. In addition, this method has proved its usefulness for the identification of metals associated with melanin preservation [20,28]. A recent study was able to positively identify the distribution of trace elements allegedly reminiscent of melanins in extant feathers [28]. Despite being recognized in trace amounts, we were able to identify elemental distribution in CPCA 3590 samples. Following the analyses, we examined possible sources for the identified elements in *T. imperator* headcrest.

The intense presence of calcium is considered here as being mainly derived from matrix carbonate. Moreover, it is also possible that lower concentrations might be derived from the fossil itself since this ion can be found in apatite [29] or incorporated into melanin [30]. On the other hand, the source of manganese might be allochthonous, as this mineral is usually found in its oxidized pyrolusite (MnO_2) form [31]. Indeed, this mineral has already been reported in the Crato beds as a component of dendritic habits that are sometimes associated with fossils [7]. Since copper, iron, and zinc are essential to some physiological processes, the presence of these elements is often considered as autochthonous (or parautochthonous in the case of Fe), is derived from the animal itself or its environment [21]. Some authors also suggest that, because Cu, Zn, and S have high affinity to melanin, these elements may form organic chelates which in turn may serve as markers for this pigment [32]. However, sulphur

was not identified in our SR-µXRF analysis, and Cu and Zn can be also incorporated by microbial activity or during diagenesis.

We note that some of these interpretations are merely speculative since experiments to recognize element oxidation states, such as X-ray absorption near edge structure (XANES) are still needed. As such, these elements could be also derived from the environment, from the preserved organic matter, or eumelanin. We acknowledge that at least three possible causes might explain the presence of the trace metals, as follow: (i) endogenously derived, since they are involved in physiological processes; (ii) accumulation during the lifespan, implying that the animal lived close to areas with elevated amounts of the recognized trace metals; or (iii) derived from diagenetic processes. Some of the identified elements, such as Ca, Cu, Fe, and Zn, are indeed involved in physiological processes and, thus, may be truly endogenous. The diagenesis, led by the lithostatic pressure, could result in migration of fluids to lesser pressured beds, and ions may have become chelated with the organic matter [21,31]. Moreover, some could also replace others with similar atomic radius, as is the case, for instance, of Rare Earth Elements, as well as Sr and Ca. For instance, some Rare Earth Elements can substitute Ca in apatite and calcite during diagenesis, where these elements mainly occupy the Ca I and Ca II sites [25,33].

Raman Spectroscopy

According to our results, the CPCA 3590 headcrest is mainly composed of calcium phosphate and eumelanin. These compounds were identified by diagnostic peaks among examined regions, which varied in their intensities. For instance, the PO_4^{3+} bands occur at ca. 965 cm^{-1} [29], whereas the eumelanin between 1300 cm^{-1} and 1600 cm^{-1} [34]. Furthermore, the phosphate spectra also exhibit bands of HCO_3^- (from calcium carbonate), which usually occur between 1085 cm^{-1} and 1092 cm^{-1} [35]. Thus, the overall spectra of the headcrest tissue consist of 282, 965, 1086 cm^{-1} bands (Fig. 2; Fig. S4), which are here assigned to the v_1 and v_3 vibrations of PO_4^{3+} and CO_3, respectively. Both compounds exhibit different peak intensities, and, for carbonate, bands are strong and narrow, whereas for phosphate they are weak and narrow. This feature is indicative of an ordered crystalline lattice, and the difference in intensity may suggest a stronger influence of the overlying matrix, which may mask PO_4^{3+}

scattering. The comparative analysis indicates that CPCA 3590 sample spectra are more related to hydroxyapatite due to the presence of 318 cm^{-1} and 1077 cm^{-1} bands.

The typical Raman spectrum of melanin is generally characterized by double and broad bands centred between ca. 1380 and 1585 cm^{-1} [36–38]. According to peak position, it can be assigned to different molecular bonds, such as out of plane deformation of O—H, C—OH from phenols, C—N stretching from pyrroles or indoles, among others (for details, see 17 and 22 and references therein). The broadness and relative intensity of bands may be caused by the irregular (less crystalline) arrangement of their carbon bonds [40]. In CPCA 3590, Raman peaks are assigned to plane vibrations of C—C bonds, as well as stretching of C—OH (from COOH), C—N from pyrrole rings, and C—O from the phenolic group, as well as from indole ring vibration [34,36–40].

At the soft tissue, Raman spectra also exhibit two broad bands between ca. 1200 to 1650 cm^{-1} (Fig. 2, C; Fig. S4, B), and their identification varies largely among examined regions (Fig. S4, C and D). We kept the laser power at a minimum to avoid sample damaging, as a higher power or prolonged exposure time can produce, by blazing, the D and G bands of carbonaceous compounds, which are common for organic matter decomposition. This procedure also ensured that peaks between 1300 to 1600 cm^{-1} are not artefactual and are indeed derived from the original compound.

The fitting procedure performed using Gaussian function (R^2=0.9539) revealed the exact position of the two bands (Fig. S4, B), which are centred at ca. 1336 cm^{-1} and 1567 cm^{-1} (Tab. S2). Although the signal is generally low as melanin is in trace amounts, these results strongly suggest that the spectra of CPCA 3590 are indeed derived from the vibration of eumelanin units.

In conclusion, the presence of peaks of carbonate indicates that the matrix has a significant contribution to the overall RS spectra; and this may be more pronounced in the melanin bands, which are broad and less intense. As a result, this influence could suggest that: (a) the laser beam has a deeper penetration than expected, and during the excitation, it gathers information from both fossil and the underlying matrix; and (b) melanin is present in low concentrations (trace amounts), possibly distributed in thin layers that are exceeded by the beam, which reaches the underlying matrix. Nevertheless, the identification of

carbonates and phosphates strongly support the interpretation that microbodies were preserved by phosphatization as suggested previously [19]. Therefore, the two broad bands observed unequivocally indicate that dark bands of *T. imperator* are composed of eumelanin.

5.7.2. Detailed Methods

Synchrotron Radiation µX-Ray Fluorescence

Examinations were performed at the UVX synchrotron light source of the Brazilian Synchrotron Light Laboratory from the Brazilian Centre for Research in Energy and Materials (LNLS-CNPEM), at the SR-µXRF beamline under the XRF-20170713 proposal. The experiment was performed using the white-beam mode with Iron (III) foil filters, the collimator of 3 mm, and the microbeam was provided by the KB system that produced a beam size of approximately 12 X 25 µm. Samples were placed onto aluminium sample-holders tilted 45° from the detector distant 20 cm. Examinations of small regions (ca. 1.0 to 5.2 mm) were carried out using the flyscan mode under 40 or 50 µm of step-size with an accumulation time of 0.1 seconds/point, with varying deadtime. The analysis generated various EDF and HDF archives, which were latter normalized and fitted, and its elements identified using the PyMCA software. Spectral and elemental maps were produced and saved as JPG and PNG, and further graphical processing was performed using Inkscape version 0.92.3 (2405546, 2018-03-11).

Identification of PTCA and PTeCA

To confirm the identification of PTCA and PTeCA in the alkaline peroxide oxidation mixture from CPCA 3590, the mixture was extracted with diethyl ether, dried as described previously [41]. A 25 µL injection of CPCA 3590 at a concentration of 60-80 µM in a 75:25 mixture of LC grade methanol and water solution was injected onto an Agilent 1200 Series high-performance liquid chromatography system (HPLC, Agilent Technologies Inc.) and separated using a Ascentis Express 5 cm x 2.1 mm x 2.7 µm C18 column (Supelco Analytical) with a column temperature of 35°C. The HPLC was connected with a standard ESI interface to an Agilent Technologies 6224 MS-TOF to obtain high-resolution exact mass measurements. The LC-MS-TOF was operated at a flow rate of 0.17 mL/min using a linear gradient of 0.3% formic

acid, 98% water, and 2% methanol (A) and 0.3% formic acid, 98% acetonitrile, and 2% water (B) as the mobile phase. The gradient program is provided in the table below (Table S3). The MS used an electrospray ionization (ESI) source in the negative mode. The results are shown in Figure S5.

Raman Spectroscopy

Prior to the Raman analysis, in order to eliminate modern contaminants during transport, the small fragment was washed in ethanol and left to dry inside a partially closed petri dish at ambient temperature and humidity. The sample was handled using disposable powder-free gloves. This washing procedure was repeated three times before the fragment was placed onto sterile glass slides in the confocal micro-Raman In Via Renishaw equipped with, He-Ne monochromatic lasers with 633 and 785 nm, detector CCD and spectral resolution of 4 cm^{-1}. Spectra were collected with a spectral range between 200-2000 cm^{-1}, with 0.05 to 1% laser power and an exposure time from 1 to 10 seconds, with an average of 20 accumulations. The analysis was made both in mapping and point-and-shoot modes, and examinations were carried out with sample devoid of any type of coating. In order to distinguish the materials, the spectrum was obtained using WiRE 4.1 and using Origin 8 (OriginLab). Spectra were normalized, and smoothing processing was performed using the Savitzky-Golay filter. Subtract baseline was performed using Fityk 0.9.8 [42], and deconvolutions were carried out using the Gaussian function with a spectral range between 1200 to 1700 cm^{-1}, where only correlation values below R^2=0.98 were considered. For spectra comparison, we examined the synthetic melanin from the oxidation of tyrosinase by hydrogen peroxide (M8631) and natural melanins from Sepia officinalis (M2649) purchased from Sigma-Aldrich Co. (Saint Louis - MO, USA). We also used the standard mineral spectra from the database of the RRUFF Project [43]. The RS equipment (FAPESP 2012/18936-0) is housed in the Research Unit of Astrobiology of the University of São Paulo (NAP/Astrobio, PRP-USP) currently at the TGM beamline (Toroidal Grating Monochromator) of the Brazilian Synchrotron Light Laboratory (LNLS) of the National Centre for Energy and Materials Research.

5.7.3. Cited References

1. Coimbra, J. C., Arai, M. & Carreño, A. L. Biostratigraphy of Lower Cretaceous microfossils from the Araripe basin, northeastern Brazil. Geobios 35, 687–698 (2002).
2. Assine, M. L. et al. Sequências deposicionais do Andar Alagoas da Bacia do Araripe, Nordeste do Brasil. Bol. Geociencias da Petrobras 22, 3–28 (2014).
3. Neumann, V. H. M. L. & Cabrera, L. Características Hidrogeológicas gerais, mudanças de salinidade e caráter endorréico do sistema lacustre Cretáceo do Araripe, NE Brasil. Rev. Geol. 15, 43–54 (2002).
4. Neumann, V. H., Borrego, A. G., Cabrera, L. & Dino, R. Organic matter composition and distribution through the Aptian-Albian lacustrine sequences of the Araripe Basin, northeastern Brazil. Int. J. Coal Geol. 54, 21–40 (2003).
5. Heimhofer, U. et al. Deciphering the depositional environment of the laminated Crato fossil beds (Early Cretaceous, Araripe Basin, North-eastern Brazil). Sedimentology 57, 677–694 (2010).
6. Neumann, V. H. & Cabrera, L. Significance and genetic interpretation of the sequential organization of the Aptian-Albian. An. Acad. Bras. Cienc. 72, 607–608 (2000).
7. Heimhofer, U. & Martill, D. M. The sedimentology and depositional environment of the Crato Formation. in The Crato Fossil Beds of Brazil: Window into an Ancient World (eds. Martill, D. M., Bechly, G. & Loveridge, R. F.) 44–62 (Cambridge University Press, 2007). doi:10.1017/CBO9780511535512.005
8. Silva, V. R. et al. First record of Neithea from the Aptian Crato Formation, Araripe Basin, Brazil, and it's significance. in Boletim de resumos do XXV Congresso Brasileiro de Paleontologia 320–320 (Sociedade Brasileira de Paleontologia, 2017).
9. Catto, B., Jahnert, R. J., Warren, L. V., Varejão, F. G. & Assine, M. L. The microbial nature of laminated limestones: Lessons from the Upper Aptian, Araripe Basin, Brazil. Sediment. Geol. 341, 304–315 (2016).
10. Warren, L. V. et al. Stromatolites from the Aptian Crato Formation, a hypersaline lake system in the Araripe Basin, northeastern Brazil. Facies 63, 1–19 (2017).

11. Osés, G. L. et al. Deciphering pyritization-kerogenization gradient for fish soft-tissue preservation. Sci. Rep. 7, (2017).
12. Osés, G. L. et al. Deciphering the preservation of fossil insects: a case study from the Crato Member, Early Cretaceous of Brazil. PeerJ 4, e2756 (2016).
13. Varejão, F. G. et al. Exceptional preservation of soft tissues by microbial entombment: Insights into the taphonomy of the Crato Konservat-Lagerstätte. Palaios 34, 331–348 (2019).
14. Pinheiro, F. L., Horn, B. L. D., Schultz, C. L., Andrade, J. A. F. G. & Sucerquia, P. A. Fossilized bacteria in a Cretaceous pterosaur headcrest. Lethaia 45, 495–499 (2012).
15. Prado, G. M. E. M., Anelli, L. E., Petri, S. & Romero, G. R. New occurrences of fossilized feathers: systematics and taphonomy of the Santana Formation of the Araripe Basin (Cretaceous), NE, Brazil. PeerJ 4, e1916 (2016).
16. Li, Q. et al. Reconstruction of Microraptor and the Evolution of Iridescent Plumage. Science (80-.). 335, 1215–1219 (2012).
17. Schweitzer, M. H., Lindgren, J. & Moyer, A. E. Melanosomes and ancient coloration re-examined: A response to Vinther 2015 (DOI 10.1002/bies.201500018). BioEssays 37, 1174–1183 (2015).
18. Solano, F. Melanins: Skin Pigments and Much More—Types, Structural Models, Biological Functions, and Formation Routes. New J. Sci. 2014, 1–28 (2014).
19. Pinheiro, F. L., Fortier, D. C., Schultz, C. L., Andrade, J. A. F. G. & Bantim, R. A. M. New information on the pterosaur Tupandactylus imperator, with comments on the relationships of Tapejaridae. Acta Palaeontol. Pol. 56, 567–580 (2011).
20. Wogelius, R. A. et al. Trace Metals as Biomarkers for Eumelanin Pigment in the Fossil Record. Science (80-.). 333, 1622–1626 (2011).
21. Bergmann, U. et al. Archaeopteryx feathers and bone chemistry fully revealed via synchrotron imaging. Proc. Natl. Acad. Sci. 107, 9060–9065 (2010).
22. Bergmann, U., Manning, P. L. & Wogelius, R. A. Chemical mapping of paleontological and archeological artifacts with synchrotron X-rays. Annu. Rev. Anal. Chem. (Palo Alto. Calif). 5, 361–89 (2012).

23. Edwards, N. P. et al. Mapping prehistoric ghosts in the synchrotron. Appl. Phys. A Mater. Sci. Process. 111, 147–155 (2013).
24. Gueriau, P. et al. Trace Elemental Imaging of Rare Earth Elements Discriminates Tissues at Microscale in Flat Fossils. PLoS One 9, e86946 (2014).
25. Gueriau, P. & Bertrand, L. Deciphering Exceptional Preservation of Fossils Through Trace Elemental Imaging. Micros. Today 23, 20–25 (2015).
26. Gueriau, P., Jauvion, C. & Mocuta, C. Show me your yttrium, and I will tell you who you are: implications for fossil imaging. Palaeontology 61, 981–990 (2018).
27. Gueriau, P., Bernard, S. & Bertrand, L. Advanced Synchrotron Characterization of Paleontological Specimens. Elements 12, 45–50 (2016).
28. Edwards, N. P. et al. Elemental characterisation of melanin in feathers via synchrotron X-ray imaging and absorption spectroscopy. Sci. Rep. 6, 1–10 (2016).
29. Morris, M. D. & Mandair, G. S. Raman assessment of bone quality. Clin. Orthop. Relat. Res. 469, 2160–2169 (2011).
30. Hong, L., Liu, Y. & Simon, J. D. Binding of Metal Ions to Melanin and Their Effects on the Aerobic Reactivity. Photochem. Photobiol. 80, 477 (2004).
31. Egerton, V. M. et al. The mapping and differentiation of biological and environmental elemental signatures in the fossil remains of a 50 million year old bird. J. Anal. At. Spectrom. 30, 627–634 (2015).
32. Manning, P. L. et al. Synchrotron-based chemical imaging reveals plumage patterns in a 150 million year old early bird. J. Anal. At. Spectrom. 28, 1024–1030 (2013).
33. Chen, H. & Stimets, R. W. Fluorescence of trivalent neodymium in various materials excited by a 785 nm laser. Am. Mineral. 99, 332–342 (2014).
34. Perna, G., Lasalvia, M. & Capozzi, V. Vibrational spectroscopy of synthetic and natural eumelanin. Polym. Int. 65, 1323–1330 (2016).
35. Gunasekaran, S., Anbalagan, G. & Pandi, S. Raman and infrared spectra of carbonates of calcite structure. J. Raman Spectrosc. 37, 892–899 (2006).
36. Huang, Z. et al. Raman spectroscopy of in vivo cutaneous melanin. J. Biomed. Opt. 9, 1198 (2004).

37. Galván, I. et al. Raman spectroscopy as a non-invasive technique for the quantification of melanins in feathers and hairs. Pigment Cell Melanoma Res. 26, 917–923 (2013).
38. Galván, I., Jorge, A., Solano, F. & Wakamatsu, K. Vibrational characterization of pheomelanin and trichochrome F by Raman spectroscopy. Spectrochim. Acta Part A Mol. Biomol. Spectrosc. 110, 55–59 (2013).
39. Perna, G. Vibrational Characterization of Synthetic Eumelanin by Means of Raman and Surface Enhanced Raman Scattering. Open Surf. Sci. J. 5, 1–8 (2013).
40. Galván, I. & Jorge, A. Dispersive Raman spectroscopy allows the identification and quantification of melanin types. Ecol. Evol. 5, 1425–1431 (2015).
41. Glass, K. E. et al. Direct chemical evidence for eumelanin pigment from the Jurassic period. Proc. Natl. Acad. Sci. 109, 10218–10223 (2012).
42. Wojdyr, M. Fityk : a general-purpose peak fitting program. J. Appl. Crystallogr. 43, 1126–1128 (2010).
43. Lafuente, B., Downs, R. T., Yang, H. & Stone, N. The power of databases: The RRUFF project. Highlights in Mineralogical Crystallography (2016). doi:10.1515/9783110417104-003
44. Clarke, J. A. et al. Fossil evidence for evolution of the shape and color of penguin feathers. Science (80-.). 330, 954–957 (2010).

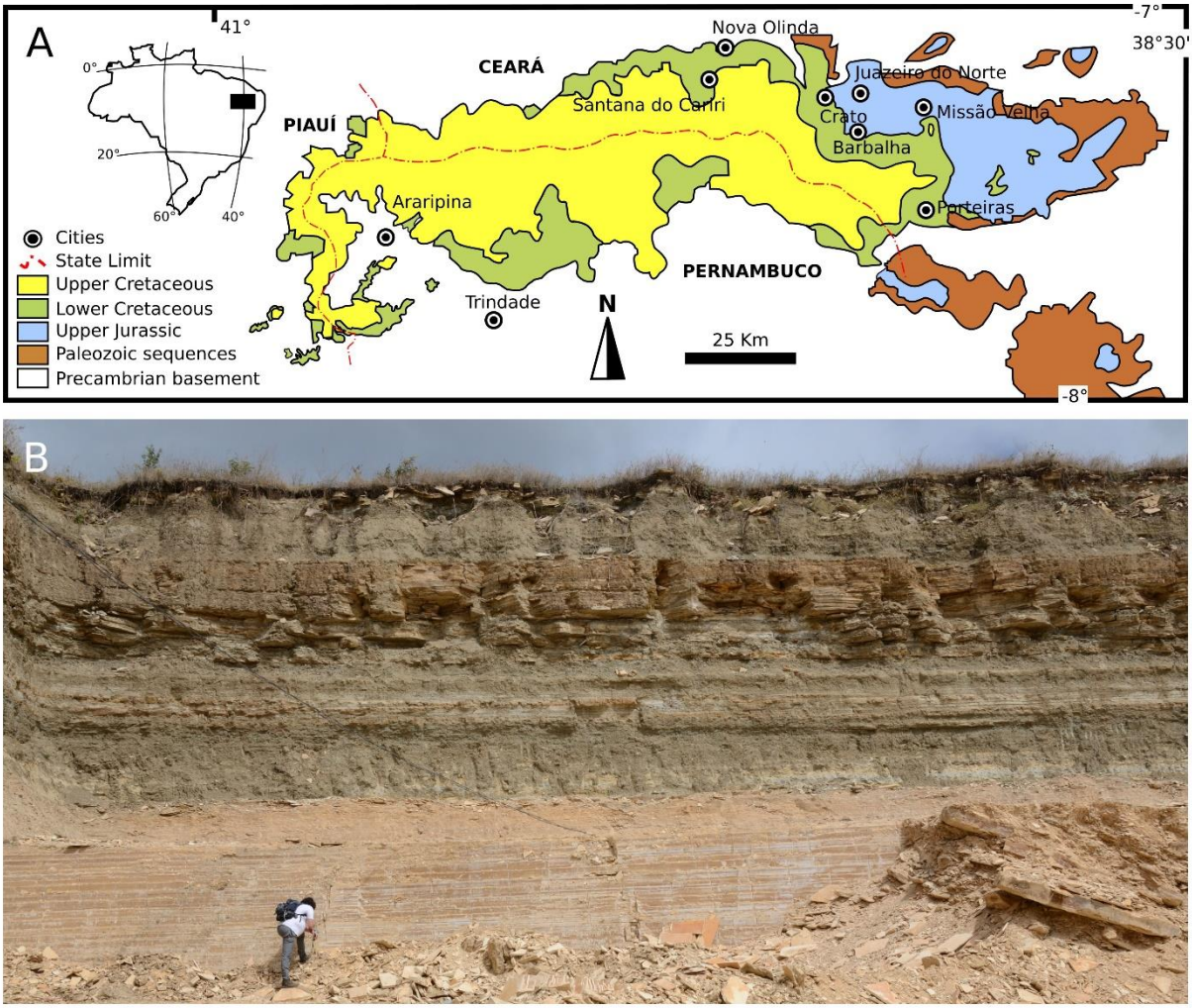

Figure S1. Araripe Basin and Crato Formation. (**A**) Location of the Araripe Basin, showing the sedimentary sequences distribution, in which the Crato Formation occur at N-SE part of the green limit. (**B**) Crato Formation outcrop, exhibiting thick sequences of laminated limestones interbedded by greenish shales and sandstones of the Nova Olinda member at the Triunfo Quarry located between Crato and Santana do Cariri cities.

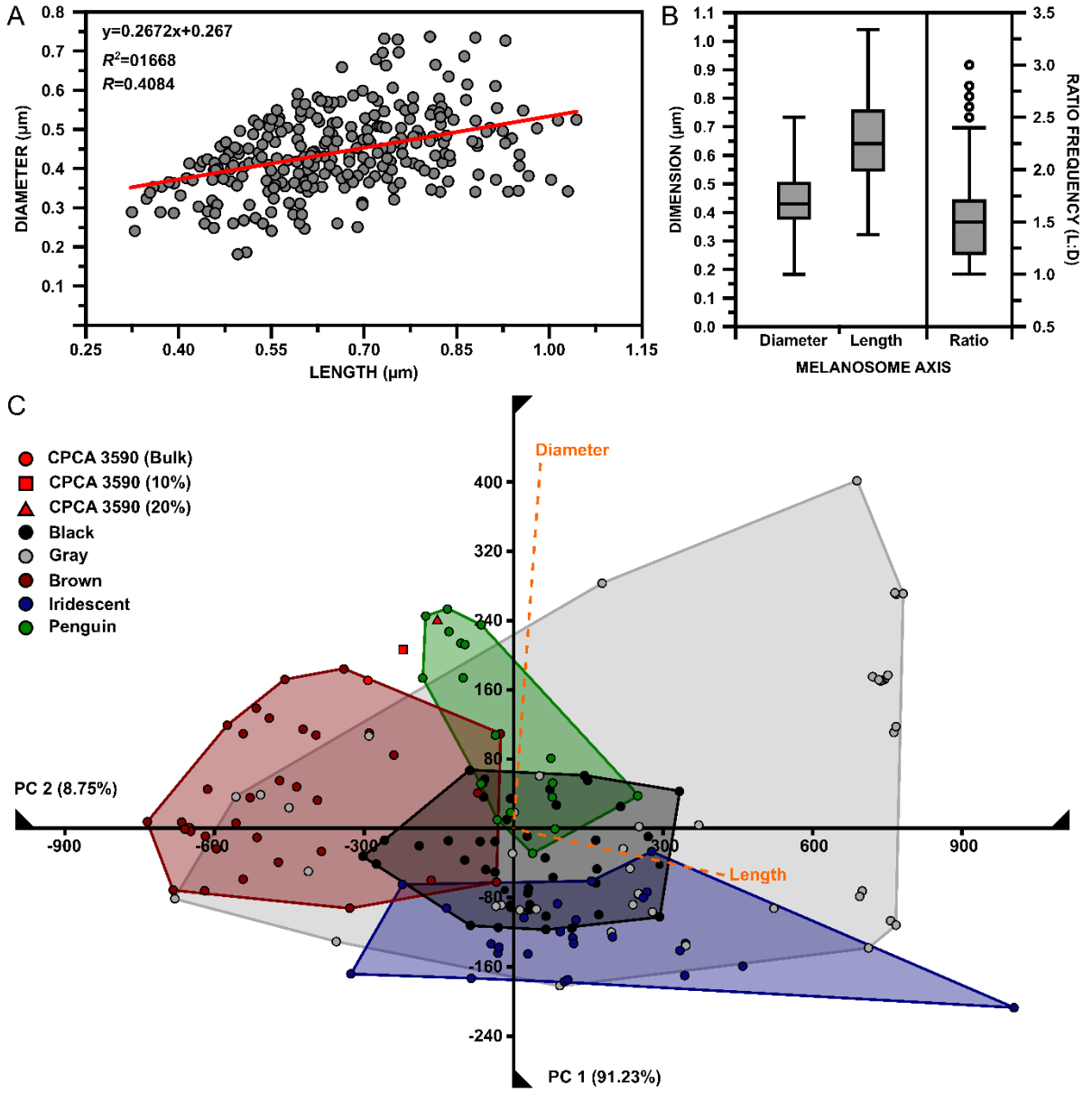

Figure S2. Statistical analysis of CPCA 3590 melanosomes (n=331). (**A**) Scatter plot and (**B**) boxplot of the melanosome axes (length and diameter) exhibiting a weak correlation (r=0.4084; R^2=0.1668) and the overall dimension of the melanosomes. Mean sizes that fall at around 441 nm in diameter, 652 µm in length and 1.5 in ratio. (**C**) Principal component analysis of the Li et al. [16] database (melanosome shape/colour) showing that diameter and length place the T. imperator microbodies close to melanosomes of brown and penguin colours (i.e., blue, and black hues, see Clarke et al. [44].

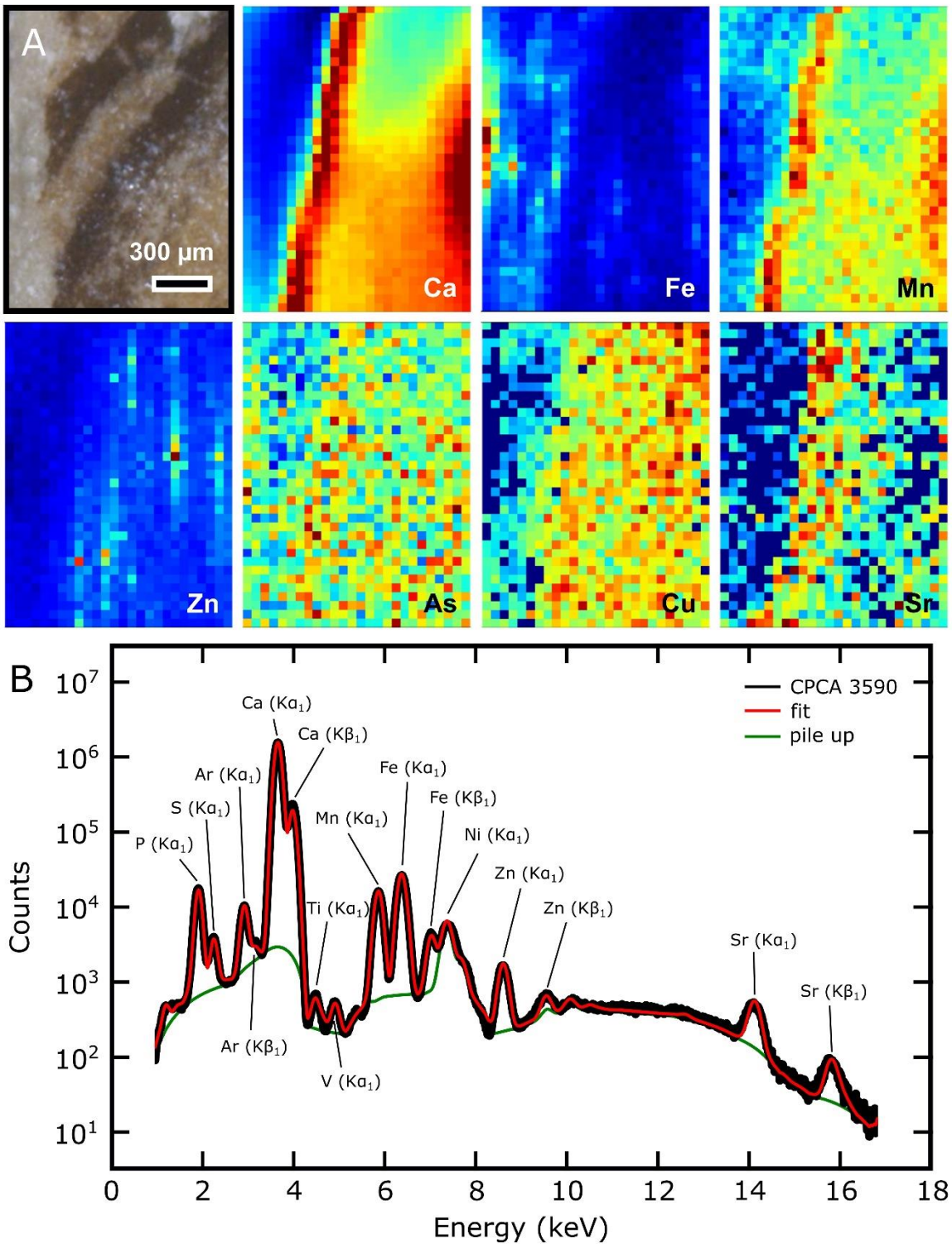

Figure S3. SR-µXRF elemental analysis of CPCA 3590 tissue. (**A**) SR-µXRF map of the headcrest tissue showing elements with good spatial correlation. Colors indicate the relative intensity, where the higher are shown in red while the lower in blue. (**B**) The fitted spectra of the region in (A) exhibiting the presence of other elements that occur without significant intensity and spatial correlation.

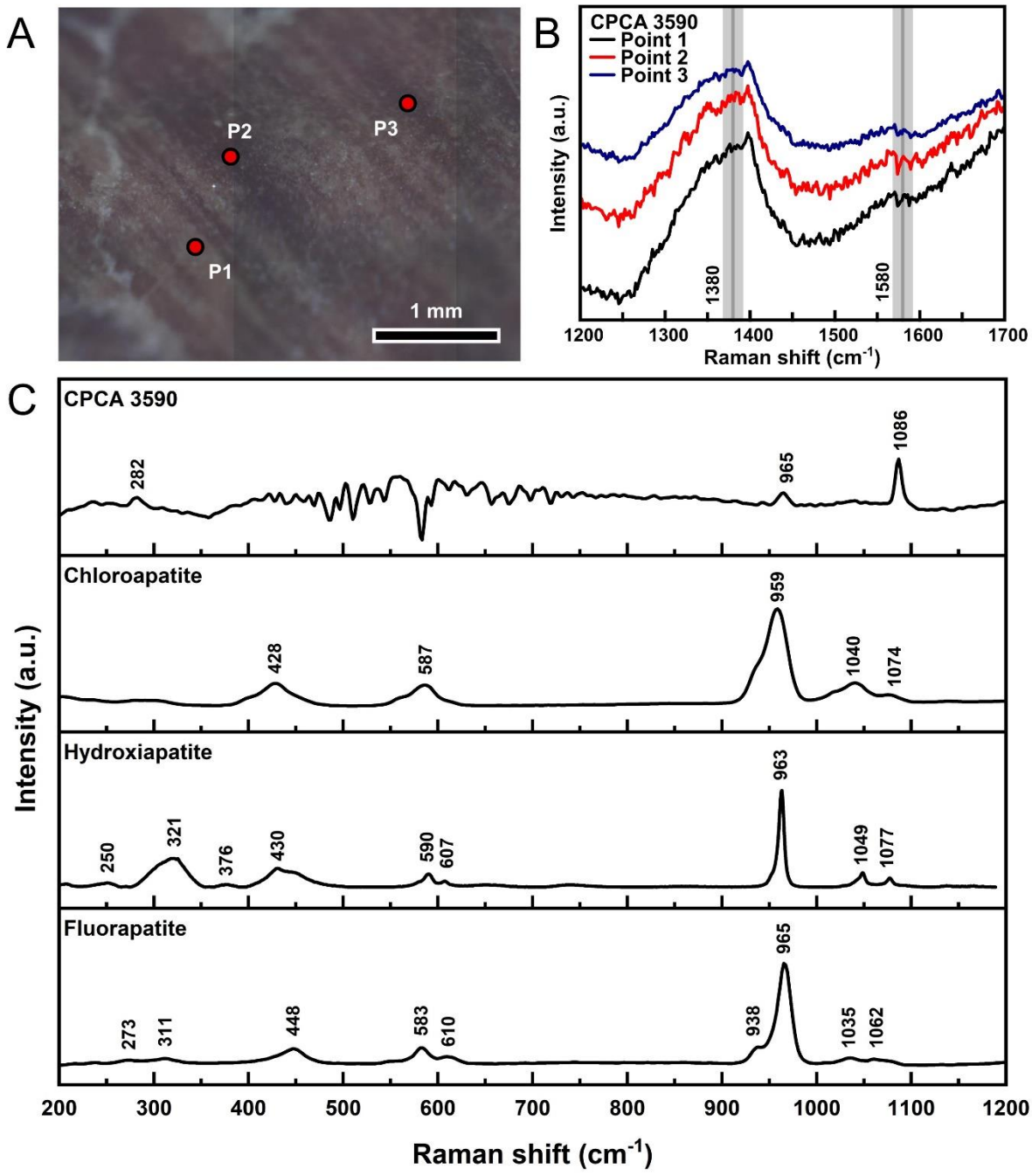

Figure S4. Raman spectra of *Tupandactylus imperator* headcrest. (**A**) Spectra from the banded tissue showing the three points analysed, where the P1 was carried out at the lighter portion, whereas P2 and P3 measures were taken from darker spots. (**B**) Spectra from the three points seen in (A) exhibiting the two bands of different intensities indicating melanin's presence; the first band centred at about 1380 cm^{-1} is pronounced, whereas the second band (ca. 1580 cm^{-1}) is almost undetectable. Grey lines and shadows represent the expected bands of eumelanin and ±10 cm^{-1} range, respectively. (**C**) FTRaman spectra from the bony part of the headcrest showing similar bands with standard calcium phosphates from the RRUFF project.

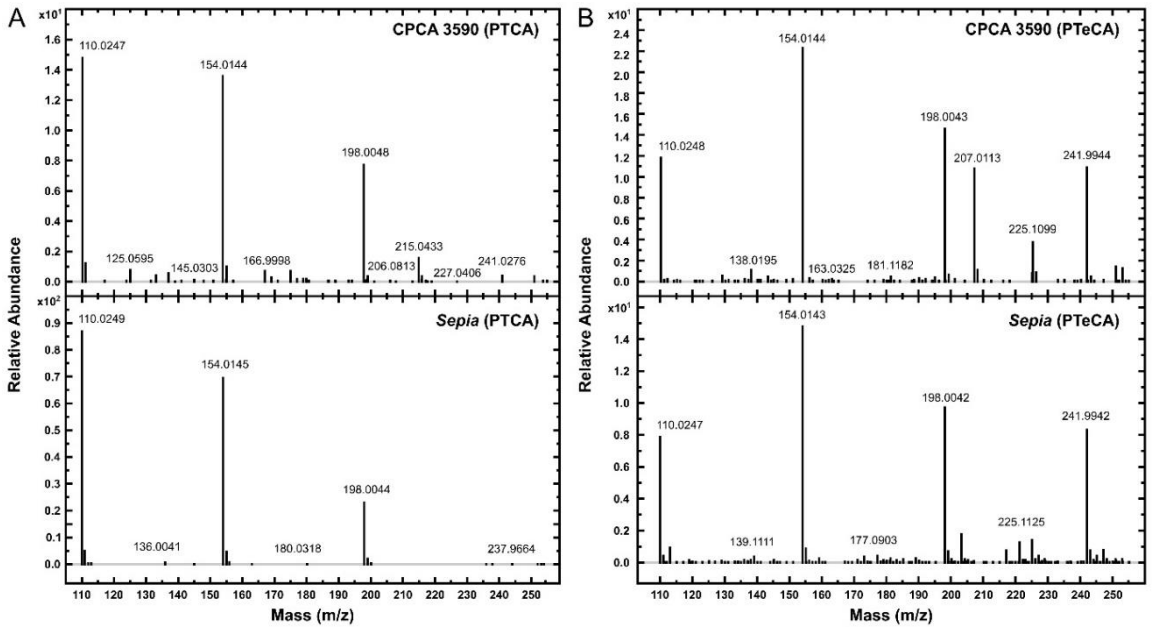

Figure S5. Mass spectra of the degradation products of the CPCA 3590 and Sepia melanin, where's (A) is from PTCA and (B) from PTeCA. Structures associated with the peaks of the fragments formed from the parent ion, the ion with the greatest mass in each of the spectrum above, are indicated.

Table S1. Average numbers of the measures (n=331) of entire melanosomes microbodies of CPCA 3590 specimen, with 10% and 20% corrected values. The diameter, length, and standard deviation (SD) variables are all in nm.

CPCA 3590	*Length ± SD*	*Length CV*	*Length Skew*	*Diameter ± SD*	*Diameter CV*	*Diameter Skew*	*Ratio*	*Ratio CV*	*Ratio Skew*	*Density*
Bulk	652.937 ± 147.513	0.2	0.2	441.420 ± 96.499	0.2	0.4	1.52	0.3	1.0	4.0
10%	718.284 ± 162.278	0.2	0.2	485.589 ± 106.161						
20%	783.553 ± 177.008	0.2	0.2	529.737 ± 115.811						

Table S2. Results of fitting using a Gaussian function for the headcrest tissue. DF - degrees of freedom; RCS - reduced chi-squared; A-R^2 – Adjusted R-Square.

Band	*Area*	*Center*	*FWHM*	*DF*	*R^2*	*RCS*	*A-R^2*
Band 1	69167.71	940.85	83.82	658	0.9852	69206.60921	0.9847
Band 2	223739.21	1140.59	193.61				
Band 3	398184.71	1327.88	80.02				
Band 4	526396.02	1407.33	227.12				
Band 5	866003.25	1573.35	112.53				
Band 6	8592.32	1693.57	15.58				
Band 7	278276.99	1780.72	352.63				
Band 8	17204.12	1892.48	54.00				

Table S3. Gradient program for LC-MS-TOF analysis of CPCA 3590.

Time (min)	*%A*	*%B*
0	100	0
4	100	0
12	85	15
18	40	60
22	40	60
28	100	0
29	100	0

ANNEX B – LIST OF ABSTRACTS

1. Silva, R.P.D., Prado, G.M.E.M., Anelli, L.E. (2019). The anurofauna of the Crato Formation (Cretaceous, Araripe Basin, NE Brazil): Taphonomic and pigment aspects. In: 27° SIICUSP. Instituto de Geociências, Universidade de São Paulo.

2. Prado, G. Salvato, R.C.J.P.S. (2022). A chemical view of a fossil melanin. In: XXVII Congresso Brasileiro de Paleontologia. Cuiabá, Mato Grosso, UFMT.

3. Prado, G., Lino, L.M., Quiroz-Valle, F., Casati, R., Becker-Kerber, B. (2021). A day in the (after)life: Spectroscopic investigation on a Cretaceous beetle. In: PALEO MG. (2021). Ituiutaba, Minas Gerais.

4. Prado, G., Muniz, F.P., Onary, S., Osés, G.L., Domingues, R.P., Pinheiro F.L., Becker-Kerber, B., Anelli, L.E. (2019). A diversidade de anuros da Formação Crato (Bacia do Araripe, NE Brasil) e suas implicações bioestratinômicas, paleoecológicas e taxonômicas. 2019. (Congresso). In: XXVI Congresso Brasileiro de Paleontologia. Uberlândia, Minas Gerais. Boletim de Resumos, 1 : 71 72.

5. Prado, G., Arthuzzi, J.C.L., Mello, J.V.T., Osés, G.L., Becker-Kerber, B., Alves, A., Galante, D. (2019). Different areas, same objectives: Synchrotron light source as a tool in Geosciences. In: XXVI Congresso Brasileiro de Paleontologia. Uberlândia, Minas Gerais. Boletim de Resumos, 1 : 72 73.

6. Prado, G.M.E.M., Anelli, L.E. (2018). Remarks on the presence of fish melanosomes from the Cretaceous Crato Formation (Araripe Basin, NE Brazil). In: 1° Simpósio da Pós Graduação do Instituto de Geociências da USP. São Paulo, São Paulo.

7. Prado, G.M.E.M., Pinheiro, F.L., Anelli, L.E. (2018). Preliminary assessments of the colour patterns of Tapejarid pterosaurs from the Cretaceous Crato Formation (Araripe Basin, NE Brazil). In: 1° Simpósio da Pós Graduação do Instituto de Geociências da USP. São Paulo, São Paulo.

8. Osés, G.L., Galante, D., Rizzutto, M.A., Prado, G.M.E.M., Becker-Kerber, B., Romero, G.R., Rodrigues, F., Petri, S., Pacheco, M.L.A.F. (2018). Investigation of fossil preservation at the SR XRF. In: 28th RAU Annual Users Meeting, 2018, Campinas, SP. 28th RAU Annual Users Meeting Abstract Book, p. 129 129.

9. Kerber, P.B., Becker-Kerber, B., Osés, G.L., Galante, D., Prado, G.M.E.M., Pacheco, M.L.A.F. (2018). Elemental and molecular investigation of anatase (TiO_2) at the Brazilian

synchrotron light laboratory? Defining a possible biosignature. In: 28th RAU Annual Users Meeting, 2018, Campinas, SP. 28th RAU Annual Users Meeting Abstracts 53, 53.

10. Osés, G.L., Petri, S., Prado, G.M.E.M., Becker-Kerber, B., Galante, D., Voltani, C.G., Romero, G.R., Rizzutto, M.A., Rodrigues, F., Pacheco, M.L.A.F. (2018). Widespread pyritization at the Crato Formation (Upper Aptian), Brazil: patterns and possible explanations. In: International Palaeontological Congress, Paris: France. 5th International Paleontological Congress Abstract Book, 1 : 502 502.

11. Pinheiro, F., Glass, K., Prado, G.M.E.M., Ito, S. (2018). Direct chemical characterization of eumelanin in a pterosaur headcrest In: Figueiredo, A.E.Q., Oliveira, P.V. (eds.). XI Simpósio Brasileiro de Paleontologia de Vertebrados. Teresina PI: Paleontologia em Destaque, 1, 86.

12. Elesbão, M.E.T.S., Santos, M.A.C., BRuno, J., Prado, G.M.E.M., Voltani, C.G., Pinheiro, F.L. (2018). Um Dastilbe iria bem em meu aquátio? Análise da coloração de um peixe fóssil. In: Figueiredo, A.E.Q., Oliveira, P.V. (eds.). XI Simpósio Brasileiro de Paleontologia de Vertebrados. Teresina PI: Paleontologia em Destaque, 1, 43.

13. Osés, G.L., Petri, S., Rizzutto, M.A., Galante, D., Becker-Kerber, B., Romero, G.R., Voltani, C.G., Prado, G.M.E.M., Rudnitzki, I.D., Rodrigues, F., Silva, E.P., Silva, T.F., Curado, J.F., Rangel, E.C., Ribeiro, R.P., Sucerquia, P.A., Pacheco, M.L.A.F. (2017). Mecanismos de piritização de insetos e peixes da Formação Crato, Aptiano. In: XXV Congresso Brasileiro de Paleontologia. Ribeirão Preto SP: Paleontologia em Destaque, 1, 238.

ANNEX C – LIST OF UNRELATED PUBLISHED MANUSCRIPTS

Paper 01
Title: *Uma vida repleta de causos.*
Authors: Gabriel L. Osés, **Gustavo M.E.M. Prado**.
Journal: *Setembrino Petri: Do Proterozóico ao Holoceno.*
Impact Factor: N/A.
Year: 2018.
DOI: 9788599198186.
Status: Published.
Brief Commentary: In this book chapter, Gabriel L. Osés and I were invited by the organizers to participate with a chapter concerning the earliest geological and palaeontological experiences of the Professor Setembrino Petri (IGc-USP).

Paper 02
Title: *Paleometry as a key tool to deal with paleobiological and astrobiological issues: some contributions and reflections on the Brazilian fossil record.*
Authors: Amanda L.S. Gomes, Bruno Becker-Kerber, Gabriel L. Osés, **Gustavo Prado**, Pedro Becker Kerber, Gabriel E.B. de Barros, Douglas Galante, Elidiane Rangel, Pidassa Bidola, Julia Herzen, Franz Pfeiffer, Márcia A. Rizzutto, Mírian L.A.F. Pacheco.
Journal: *International Journal of Astrobiology.*
Impact Factor: 1.358.
Year: 2019.
DOI: 10.1017/S1473550418000538.
Status: Published.
Brief Commentary: My contribution was on chemical analysis (especially SR-µXRF and Raman Spectroscopy). I also contributed to discussion, figures, and writing the manuscript.

Paper 03
Title: *The oldest record of Ediacaran macrofossils in Gondwana (~563 Ma, Itajaí Basin, Brazil)*
Authors: Bruno Becker-Kerber, Paulo S.G. Paim, Farid Chemale Junior, Tiago J. Girelli, Ana Lucia Z. Rosa, Abderrazak El Albani, G.L. Osés, **Gustavo M.E.M. Prado**, Milene Figueiredo, Luiz Sérgio A. Simões, Mírian L.A.F. Pacheco.
Journal: *Gondwana Research.*
Impact Factor: 6.151.
Year: 2020.
DOI: 10.1016/j.gr.2020.03.007.
Status: Published.
Brief Commentary: My contribution on this paper was mainly on performing experiments, especially SR-µXRF and XANES (which was not used). I also contributed with discussions, preparation of figures, and writing the manuscript.

Paper 04
Title: *The role of volcanic-derived clays in the preservation of Ediacaran biota from the Itajaí Basin (ca. 563 Ma, Brazil).*

Authors: Bruno Becker-Kerber, Abderrazak El Albani, Kurt Konhauser, Ahmed Abd Elmola, Claude Fontaine, Paulo S.G. Paim, Arnaud Mazurier, **Gustavo M.E.M. Prado**, Douglas Galante, Pedro B. Kerber, Ana Lucia Z. Rosa, Thomas. R. Fairchild, Alain Meunier, Mírian L.A.F. Pacheco.
Journal: *Scientific Reports.*
Impact Factor: 4.996.
Year: 2021.
DOI: 10.1038/s41598-021-84433-0.
Status: Published.
Brief Commentary: Similar to the former paper, my contribution on this paper was mainly on performing experiments, SR-µXRF and XANES (which was not used). I also contributed with discussions, preparation of figures, and writing the manuscript.

Paper 05
Title: *In situ filamentous communities from the Ediacaran (approx. 563 Ma) of Brazil.*
Authors: Bruno Becker-Kerber, Gabriel E.B. Barros, Paulo S.G. Paim, **Gustavo M.E.M. Prado**, Ana Lucia Z. Rosa, Abderrazak El Albani, Marc Laflamme.
Journal: *Proceedings of the Royal Society B.*
Impact Factor: 5.530.
Year: 2021.
DOI: 10.1098/rspb.2020.2618.
Status: Published.
Brief Commentary: My contribution on this paper was mainly on carried out experiments, such as SEM, EDS, and SR-µXRF. I also contributed with discussions, preparation of figures, and writing the manuscript.

Paper 06
Title: *Synchrotron radiation in palaeontological investigations: Examples from Brazilian fossils and its potential to South American palaeontology.*
Authors: Gustavo Prado, Jorge C.K. Arthuzzi, Gabriel L. Osés, Flávia Callefo, Lara Maldanis, Paula Sucerquia, Bruno Becker-Kerber, Guilherme R. Romero, Francy R. Quiroz-Valle, Douglas Galante.
Journal: *Journal of South American Earth Sciences.*
Impact Factor: 2.453.
Year: 2021.
DOI: 10.1016/j.jsames.2020.102973.
Status: Published.
Brief Commentary: In this paper, I designed the study, reviewed the bibliography on this subject, wrote the manuscript prepared the figures, submitted, reviewed, etc.

Paper 07
Title: *Clay templates in Ediacara vendotaeniaceans: Implications for the taphonomy of carbonaceous fossils.*
Authors: Bruno Becker-Kerber, Ahmed Abd Elmola, A. Zhuravlev, Claudio Gaucher, Marcelo G. Simões, **Gustavo M.E.M. Prado**, José A.G. Vintaned, Claude Fontaine, Lucas M. Lino, Dario F. Sanchez, D. Galante, Paulo S.G. Paim, Flávia Callefo, G. Kerber, Alain Meunier, Abderrazak El Albani.
Journal: *GSA Bulletin.*

Impact Factor: 5.410.
Year: 2022.
DOI: 10.1130/B36033.1.
Status: Published.
Brief Commentary: My contribution on this paper was mainly on carried out experiments, with discussions, preparation of figures, and writing the manuscript.

Paper 08
Title: *Diverse vase-shaped microfossils within a Cryogenian glacial setting in the Urucum Formation (Brazil).*
Authors: Luana Morais, Bernardo T. Freitas, Thomas R. Fairchild, Thiago F. Toniolo, Marcelo D.R. Campos, **Gustavo M.E.M. Prado**, Pedro A.S. Silva, Isaac D. Rudnitzki, Daniel J.G. Lahr, Juliana M. Leme, Pascal Philippot, Michel Lopez, Ricardo I.F. Trindade.
Journal: *Precambrian Research.*
Impact Factor: 4.261.
Year: 2021.
DOI: 10.1016/j.precamres.2021.106470.
Status: Published.
Brief Commentary: I contributed with the Raman spectroscopy analysis, where I processed the data, interpreted the results, identified the bands, prepared the figures, and contributed with discussions and writing the manuscript.

Paper 09
Title: *Ediacaran Corumbella has a cataphract calcareous skeleton with controlled biomineralization.*
Authors: Gabriel L. Osés, Rachel Wood, Guilherme Romero, **Gustavo Prado**, Pidassa Bidola, Julia Herzen, Franz Pfeiffer, Sérgio Stampar, Mírian Pacheco.
Journal: *iScience.*
Impact Factor: 6.107.
Year: 2022.
DOI: 10.1016/j.isci.2022.105676.
Status: Published.
Brief Commentary: In this paper I thoroughly contributed to the Raman spectroscopy, processing the all the data, interpreted the results, prepared the figures, and contributed with discussions and writing the manuscript.

Paper 10
Title: *Paleovolcanology, geochemistry, and zircon U-Pb-Hf isotopes of the volcano-sedimentary sequences from the Ediacaran Campo Alegre-Corupá Basin, southern Brazil: linking volcanism and tectonics during Western Gondwana consolidation.*
Authors: Francy R. Quiroz-Valle, Lucas M. Lino, Sérgio B. Citroni, Miguel A. S. Basei, M. Hueck, Silvio R. F. Vlach, Bruno Becker-Kerber, **Gustavo M.E.M. Prado.**
Journal: *Gondwana Research.*
Impact Factor: 6.151.
Year: 2022.
DOI: 10.1016/j.gr.2022.12.003.
Status: Published.

Brief Commentary: In this paper, I contributed with discussions about the subjects regarding of palaeontology, in addition to also assisted in writing the manuscript.

Paper 11
Title: *Taphonomy of fish, invertebrates and plant remains in the first Tethyan-South Atlantic marine ingression along Cretaceous rift systems in NE-Brazil.*
Authors: Cibele Voltani, Gabriel L. Osés, Bernardo T. Freitas, **Gustavo M. E. M. Prado**, Rosemarie Rohn, Mírian L.A.F. Pacheco, Luiz E. Anelli, Renato P. Almeida, Marcelo G. Simões, Ludmila A.C. Prado, Rilda V.C. Araripe, Douglas Galante, Elidiane C. Rangel.
Journal: Cretaceous Research.
Impact Factor: 2.432.
Year: 2023.
DOI: 10.1016/j.cretres.2023.105508.
Status: Published.
Brief Commentary: In the document, I designed and performed the experiments, processed the data, prepared the figures, and contributed to the manuscript.

Paper 12
Title: *Tectographs from the Itajaí Basin (~563 Ma): a cautionary tale from the Precambrian.*
Authors: Bruno Becker-Kerber, Lucas M. Lino, Francy R. Quiroz-Valle, **Gustavo M.E.M. Prado**
Journal: Terra Nova (expected).
Impact Factor: 3.271.
Year: N/A.
DOI: N/A.
Status: Under review.
Brief Commentary: In this paper I helped in the petrographic and chemical analysis designed and performed the experiments and contributed with text of the manuscript.

Paper 13
Title: *Mayfly larvae preservation from the Early Cretaceous of Brazilian Gondwana: Analogies with modern and Lagerstätten deposits*
Authors: Jaime J. Dias, Ismar de Souza Carvalho, Ângela Delgado Buscalioni, Raman Umamaheswaran, Ana Isabel López-Archilla, **Gustavo M.E.M. Prado**, José Artur Ferreira Gomes de Andrade.
Journal: Gondwana Research (expected).
Impact Factor: 6.151.
Year: N/A.
DOI: N/A.
Status: Under review.
Brief Commentary: In this paper, I contributed with discussions about the subjects regarding the taphonomy of Crato Formation fossils and reviewed/contributed the manuscript.